# Simulating Gauge Theories on Quantum Computers

by Edison Murongani Murairi

B.S. in Physics, May 2020, New York University Abu Dhabi
M.Phil. in Physics, January 2024, The George Washington University

A Dissertation submitted to

The Faculty of
The Columbian College of Arts and Sciences
of The George Washington University
in partial fulfillment of the requirements
for the degree of Doctor of Philosophy

August 31, 2024

Dissertation directed by

Andrei Alexandru
Professor of Physics

The Columbian College of Arts and Sciences of The George Washington University certifies that Edison Murongani Murairi has passed the Final Examination for the degree of Doctor of Philosophy as of May 6th, 2024. This is the final and approved form of the dissertation.

Simulating Gauge Theories on Quantum Computers

Edison Murongani Murairi

Dissertation Research Committee:

Andrei Alexandru, Professor of Physics, Dissertation Director

Andrei Afanasev, Professor of Physics, Committee Member

Frank X. Lee, Professor of Physics, Committee Member

**Acknowledgments**

This academic journey has been supported by many, and I am profoundly grateful to each one. My deepest thanks go to my advisors, Prof. Andrei Alexandru and Paulo Bedaque, for their invaluable guidance and profound impact on my work. Dr. Henry Lamm deserves special appreciation for welcoming me into his research group and the enriching experience at the Fermilab summer school. I also extend my gratitude to Dr. Andrea Carosso and Dr. Michael Cervia for their steadfast support in both scientific and technical matters. My family—my parents for their unconditional support and my siblings for their joyous distractions—have been my cornerstone, and Emily Shutz, in particular, for her patience and encouragement through my daily endeavors. The unwavering support and belief of my friends have immensely bolstered my confidence and perseverance. I am thankful for everyone mentioned and those in the background, for smoothing the path of this significant chapter in my life.

**Abstract of Dissertation**

Simulating Gauge Theories on Quantum Computers

Despite remarkable success in the last decades, numerical simulations of lattice gauge theories still have significant challenges. The Hilbert space of a quantum system grows exponentially fast with the number of degrees of freedom, making direct real-time evolution of quantum field theories intractable on a classical computer. Secondly, Mote Carlo simulations for thermal field theories suffer from the sign problem at finite fermion density. Quantum computers are promising candidates to address both challenges. However, at least two requirements must be met. First, the degrees of freedom of the theory must be mapped efficiently onto the qubits. Secondly, low-cost quantum circuits must be constructed to perform the time evolution. This thesis addresses both issues. That is, I present an algorithm designed to construct efficient quantum circuits for the time evolution of arbitrary Hamiltonians and demonstrate its performance on some quantum field theories. Then, I will present a lattice gauge theory truncation method and construct its time evolution quantum circuit.

## Table of Contents

**Acknowledgments** . . . . . **iii**

**Abstract of Dissertation** . . . . . **iv**

**List of Figures** . . . . . **vii**

**List of Tables** . . . . . **ix**

**Chapter 1: Introduction** . . . . . **1**
Chapter 1.1: Overview . . . . . 1
Chapter 1.2: Introduction to Quantum Computation . . . . . 2
Chapter 1.2.1: Preliminaries . . . . . 2
Chapter 1.2.2: Quantum Bits, Quantum Gates and Quantum Circuits . . . . 4
Chapter 1.2.3: Measures of Quantum Circuit Complexity . . . . . 8
Chapter 1.2.4: A Note on Quantum Error Correction and Fault Tolerance . . 9
Chapter 1.3: Introduction to Gauge Theory . . . . . 11
Chapter 1.3.1: Gauge Theory in the Continuum . . . . . 11
Chapter 1.3.2: Lattice Gauge Theory . . . . . 13
Chapter 1.4: Hilbert Space Truncation . . . . . 18
Chapter 1.5: General Method for Hamiltonian Time Evolution . . . . . 20
Chapter 1.5.1: Trotterization Method . . . . . 20
Chapter 1.5.2: Hamiltonian in Pauli Basis . . . . . 22
Chapter 1.5.3: Trotterization based on Pauli operators . . . . . 23
Chapter 1.6: Summary of Results . . . . . 24

**Chapter 2: Quantum Algorithm for Simultaneous Diagonalization of Commuting Pauli Operators** . . . . . **27**
Chapter 2.1: Introduction . . . . . 27
Chapter 2.2: Review of Tableau Representation . . . . . 29
Chapter 2.2.1: Clifford Gates and the Symplectic Group . . . . . 30
Chapter 2.2.2: Statement of the problem . . . . . 32
Chapter 2.3: Qubitwise Diagonalization Algorithm . . . . . 33
Chapter 2.3.1: Approach . . . . . 33
Chapter 2.3.2: The Algorithm . . . . . 35
Chapter 2.3.3: Accommodating Qubit Connectivity . . . . . 38
Chapter 2.4: Analysis of the Algorithm . . . . . 39
Chapter 2.4.1: Preliminaries . . . . . 40
Chapter 2.4.2: Circuit Depth . . . . . 42
Chapter 2.4.3: CNOT Gate Count . . . . . 43
Chapter 2.5: Examples . . . . . 46
Chapter 2.5.1: Random Sets of Commuting Pauli Operators . . . . . 46
Chapter 2.5.2: Molecular Hamiltonians . . . . . 48
Chapter 2.5.3: Linear Qubit Connectivity . . . . . 50

Chapter 2.6: Conclusions . . . 51

**Chapter 3: Quantum Circuits of Diagonal Unitaries . . . 53**
Chapter 3.1: Introduction . . . 53
Chapter 3.2: The compilation method . . . 55
Chapter 3.3: Examples . . . 66
Chapter 3.3.1: Random Diagonal Hamiltonians . . . 66
Chapter 3.3.2: $\mathbb{Z}_2$ Gauge Theory . . . 68
Chapter 3.4: Qubitization of Non-Abelian Gauge Theories . . . 70
Chapter 3.4.1: $N = 4$ (spinor) irrep . . . 72
Chapter 3.4.2: $N = 5$ (fundamental) irrep . . . 73
Chapter 3.5: Discussion . . . 76
Chapter 3.6: Acknowledgements . . . 78
Chapter 3.7: Appendix . . . 78
Chapter 3.7.1: CNOT-cost lower bound of simulating Pauli strings . . . 78
Chapter 3.7.2: CNOT gate count for a diagonal Hamiltonian with $\mathcal{N} = 2^n$ Pauli Strings . . . 80

**Chapter 4: Fuzzy Gauge Theory . . . 82**
Chapter 4.1: Introduction . . . 82
Chapter 4.2: Lattice gauge theory in the hamiltonian formalism . . . 86
Chapter 4.3: Fuzzy lattice gauge theory . . . 90
Chapter 4.4: The continuum limit of fuzzy theories . . . 97
Chapter 4.4.1: The continuum limit of fuzzy theories . . . 98
Chapter 4.4.2: Gauge Theory . . . 105
Chapter 4.5: Quantum Circuitry . . . 109
Chapter 4.6: Conclusions . . . 112
Appendix . . . 114
Appendix I: A Generalization To $U(N)$ Gauge Groups . . . 114
Appendix II: Compiling Quantum Circuits for a Fuzzy Gauge Theory . . . 117

**Chapter 5: Conclusion . . . 120**

**References . . . 122**

## List of Figures


1 Example of a Quantum Circuit . . . . . 6

2 Action of a local gauge transformation operator $\exp\{i\omega^a G^a(x)\}$ with group element $g = \exp\{i\omega^a T^a\}$ at a site $x$. . . . . 16

3 The plaquette $P \equiv U_{\mu\nu}(x)$ at site $x$ and in directions $\mu$ and $\nu$. . . . . 17

4 Quantum circuit structure from Eq. 37. . . . . 24

5 Number of CNOT conjugations involved in diagonalizing $n$ commuting Pauli operators acting on $n$ qubits . . . . . 47

6 Number of CNOT conjugations obtained in diagonalizing a set of $r$ independent commuting Pauli operators acting on $n = 15$ . . . . . 49

7 Diagonalization circuits of a large commuting sub-Hamiltonian of a H4 chain 51

8 Operator $V$ diagonalizing the Hamiltonian $H = IXX + ZYZ + XXI$ . . . . . 61

9 Quantum circuit implementing the factor $\exp(-ic_j ZZZ\delta t)$ . . . . . 62

10 Tree representation of $IIZ + IZI + IZZ + ZZZ$ . . . . . 64

11 Circuit simulating one Trotterized time step with the Hamiltonian $H = IIZ + IZI + IZZ + ZZZ$ . . . . . 65

12 The average CNOT gate count required to simulate a diagonal Hamiltonian as function of the number of Pauli strings for $n = 8$ qubits . . . . . 68

13 Quantum circuit approximately simulating one time step for a $\mathbb{Z}_2$ gauge theory with staggered fermions in 1 + 1 dimensions for $L = 4$ lattice sites without a periodic boundary condition . . . . . 70

14 Quantum circuit simulating a time step for the kinetic term K as encoded in Eq. (76) . . . . . 75

15 Comparison of the energy gaps in the fuzzy $\sigma$-model with those of the $\ell max$ truncation strategy for $\ell max = 1, 2$. . . . . 104

16 Behavior of the perturbative coefficient of $g^6$ in $\mathsf{a}\Delta E$ for the fuzzy $\sigma$-model. 105

17 Energy gaps in the *physical* subspace of qubitized $SU(2)$ gauge theories for a single-plaquette system. . . . . 107

18 Expectation value of the plaquette operator $\mathcal{O} = \square$ with respect to the evolved state $|\Psi(t)\rangle = \exp(-it\mathcal{H})\,|\Psi(0)\rangle$. . . . . 111

## List of Tables

1 Results of qubitwise diagonalization of molecular Hamiltonians . . . . . 50

# Chapter 1: Introduction

## Chapter 1.1: Overview

In the last decades, numerical simulations of gauge theories on classical computers have been used with remarkable success in studying hadronic properties. However, classical computers still face significant challenges in simulating gauge theories. To begin, the Hilbert space of a quantum theory grows exponentially with the number of degrees of freedom. For example, the Hilbert space describing only a system of $N$ spin half-particles has dimension $2^N$, making direct diagonalization of the Hamiltonian of the system an intractable problem as $N$ increases.

This challenge in performing direct time evolution of large quantum systems on classical computers is typically circumvented by employing Monte Carlo methods in Euclidean time. In this approach, the usual Path Integral formalism of Quantum Field theory (QFT) is turned into a statistical mechanics problem where expectation values of desired observables can be computed via importance sampling techniques, e.g. Metropolis-Hastings algorithm [142, 98]. However, this approach fails when we are interested in the properties of matter at high pressure and/or finite density due to the sign problem [76, 5, 111]. That is, the Boltzmann factor $e^{-S[\Phi]}$ is complex and therefore cannot be interpreted as the "unnormalized" probability of the field configuration $\Phi$.

The effect of the sign problem is that an exponentially large number of operations (e.g. Monte Carlo steps) is needed to calculate an observable to a desired accuracy as we increase the volume. Accordingly, solving the sign problem means finding an efficient (polynomial time) algorithm for calculating an observable to an arbitrary accuracy[1]. However, this problem is known to be NP-Hard for certain systems. A *generic* solution for the sign problem for all systems would provide polynomial-time solution to an NP-hard problem, which is unlikely.

Quantum computers are expected to address both issues. For the first issue, the dimension

[1] Ref. [180] provides a precise definition of efficient algorithm in this context.

of the Hilbert space described by a set of quantum bits (qubits) also grows exponentially with the number of qubits, suggesting that the time evolution on a quantum computer may be feasible. In addition, performing the time evolution directly on a quantum computer circumvents the sign problem encountered in Monte Carlo simulations. Moreover, quantum computers provide access to the real-time dynamics of a system. That is, we can calculate the time evolution of a physical observable.

Simulating gauge theories on quantum computers comes with its own set of challenges. First, the degrees of freedom of the theory must be mapped to qubit states. Then, given this mapping, efficient algorithms must be developed to perform the time evolution and extract the quantities of interest. My research aimed at addressing both issues. More specifically, I have studied different methods to map a gauge theory to a quantum computer, and I have developed algorithms to perform the time evolution on a quantum computer.

The rest of the introduction will provide a background to the problem. That is, I will first give an overview of quantum computation and quantum information theory. Secondly, I will review the relevant aspects of gauge theories with an emphasis on the Hamiltonian formulation of SU($N$) lattice gauge theory. The Hamiltonian lattice gauge theory formulation is natural to simulation on quantum computers. Next, I will discuss in more depth the problem of encoding gauge theories on quantum computers. Finally, I will conclude the introduction with a general strategy to construct a quantum circuit of the time evolution of an arbitrary Hamiltonian. Then, the rest of this dissertation will be from my co-authored articles Refs. [145, 144, 8].

## Chapter 1.2: Introduction to Quantum Computation

### Chapter 1.2.1: Preliminaries

Quantum computers are devices that process information in a fundamentally different way from current computers, which I will refer to as classical computers. The theoretical basis underlying such new machines is called quantum information theory. The motivation

behind developing this new method of computing comes from the realization that processing information with quantum phenomena may drastically speed up certain computations.

A few years after the proposals of quantum computers by e.g. P. Benioff in Ref. [20] and R. Feynmann in Ref. [69], researchers began to find problems that are significantly less complex on quantum computers than on classical computers. For example, Deutsch and Jozsa found a problem that requires $O(n)$[2] operations on classical computers while it required only $O(1)$ operations on quantum computers where $n$ is the problem size [62, 63]. This result is remarkable because it means that, unlike a classical computer, a quantum computer will solve the problem with the same number of operations regardless of how large the size of the problem is. This trend continues with, for example, the Bernstein-Varizani problem, which also required $O(1)$ operations on a quantum computer but $O(n)$ on a classical computer [23].

Both the Deutsch-Jozsa and Bernstein-Vazirani algorithms are polynomial improvements from classical computers to quantum computers. In 1994, Simon showed an example of an exponential improvement in using quantum computers. In Ref. [169], Simon showed a problem that required $\Omega(2^{n/2})$[3] on a classical computer while a quantum computer needs only $O(n)$. Perhaps, the most celebrated example of the power of quantum computers is Shor's algorithm, which can factor integers in $O(n)$[4] operations on a quantum computer [168].The difficulty of integers factoring on classical computers is the basis for modern cryptography, see the RSA protocol [164]. By factoring integers, Shor's algorithm showed that a full-scale quantum computer can break RSA-based cryptographic systems. In fact several quantum-safe cryptographic protocols have been proposed in the last decade (see e.g. Refs [30, 66, 72]) to better protect information.

Given several examples of problems where quantum computers offer a significant

[2] $O$ is referred to as the 'Big O'. It indicates an upper bound of the worst-case scenario.

[3] Unlike the 'Big O', the 'Big Omega' ($\Omega$) indicates a lower bound of the worst-case scenario

[4] In this case, $n$ is the number of bits required to represent an integer.

speed-up over classical computers, it is natural to ask whether Hamiltonian time evolution can be done efficiently on a quantum computer. Such an idea is the original motivation by R. Feynmann (Ref. [69]) in his proposal of quantum computers and is one of the most anticipated applications of quantum computing. Theoretical studies suggest that the time evolution of local Hamiltonians, which we encounter in physical systems, have properties that can be exploited to simulate their time evolution efficiently on quantum computers [24, 25, 26]. My thesis will focus on exploiting these properties for Hamiltonians of gauge theories. Before I proceed, I will describe how to encode information on a quantum computer, and what types of operations can be performed. An excellent reference for the material in the next section is Ref. [149, 113].

**Chapter 1.2.2: Quantum Bits, Quantum Gates and Quantum Circuits**

Quantum bit (qubit) is the unit of information on a quantum computer, as is the bit on a classical computer. Formally, a quantum bit is a two-level quantum state or a vector in a two-dimensional complex Hilbert space. In analogy to the (classical) bit, the two levels are traditionally denoted by $|0\rangle$ and $|1\rangle$. They form an orthonormal basis of a two-dimensional complex Hilbert space $\mathcal{H}$. Therefore, a generic quantum state can be written as

$$|\Psi\rangle = \alpha\,|0\rangle + \beta\,|1\rangle \tag{1}$$

where $\alpha$ and $\beta$ are complex coefficients. A single qubit may be used, for example, to represent an object that has two independent states. For instance, one can use a single qubit to represent a coin where the state $|0\rangle$ may represent "Head" and the state $|1\rangle$ may represent "Tail". Later on, I will explain how a quantum computer with a single qubit can be used to perform a coin toss with an arbitrary probability of the outcome being "Head" or "Tail". To encode a more complex system than, for example, a coin, more qubits may be necessary. Fortunately, the generalization of a single qubit state to multiple qubit states is straightforward. When a system has two or more qubits, the total Hilbert space is the

tensor product of the individual Hilbert space. That is, for an $n$-qubits system, $\mathcal{H} = \bigotimes_{q=1}^{n} \mathcal{H}_q$, and the dimension of the total Hilbert space is $\dim\mathcal{H} = 2^n$.

A basis for the total Hilbert space can be obtained simply by concatenating the basis of individual spaces. For example, the Hilbert space of two qubits may be written as $\mathcal{H} = \text{span}\{|0\rangle \otimes |0\rangle, |0\rangle \otimes |1\rangle, |1\rangle \otimes |0\rangle, |1\rangle \otimes |1\rangle\}$. It is customary to drop the $\otimes$ symbol and join the state labels. For example, we would write instead $\mathcal{H} = \text{span}\{|00\rangle, |01\rangle, |10\rangle, |11\rangle\}$. The process generalizes straightforwardly for an arbitrary number of qubits.

After encoding information into qubit states, a quantum computer operates by manipulating qubit states. Typically, two types of operations are used on a quantum computer – unitary gates and measurements. Unitary operations, which we call unitary gates are the main operations used to manipulate information on a quantum computer. They are generally classified by the number of qubits they act on. For example, single-qubit gates act on one qubit at a time while multiple-qubit gates act on more than one qubit. One important result of quantum information theory is that any unitary operator can be expressed as a product of only single-qubit gates and two-qubit gates (see e.g. Ref. [149]). Therefore, I will simplify the discussion by focusing only on single-qubit gates and two-qubit gates.

It is convenient to define quantum circuits before discussing different types of quantum gates. A quantum gate circuit is a diagram representing qubits and a collection of quantum gates applied to them. Each qubit is represented by a wire, and each gate is represented by its symbol. A quantum circuit is read from left to right. In the example Fig. 1, the circuit has three qubits $q_0$, $q_1$ and $q_2$. A single-qubit gate $U_1$ is applied on $q_0$, followed by a two-qubit gate $U_2$ on $q_1$ and $q_2$. Not that the two gates $U_1$ and $U_2$ could be applied at the same time.

The first single-qubit gates I will consider are the Pauli matrices $X$, $Y$, and $Z$. They are unitary and Hermitian. In the computational basis ($|0\rangle$, $|1\rangle$), their matrix representations

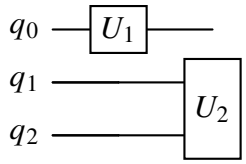


Figure 1: Example of a Quantum Circuit

are

$$X = \begin{pmatrix} 0 & 1 \\ 1 & 0 \end{pmatrix} \qquad Y = \begin{pmatrix} 0 & -\mathrm{i} \\ \mathrm{i} & 0 \end{pmatrix} \qquad Z = \begin{pmatrix} 1 & 0 \\ 0 & -1 \end{pmatrix} \tag{2}$$

In a quantum circuit, these gates are represented by the symbols $X$, $Y$, and $Z$ respectively. The $X$ gate is also referred to as Not gate due to its action $X|0\rangle = |1\rangle$ and $X|1\rangle = |0\rangle$. Three other single-qubit gates are commonly used. These are the Hadamard gate $H$, the phase gate $S$, and the $T$ gate. The Hadamard gate implements a basis transformation between the computational basis and the eigenbasis of the $X$ gate, denoted by $|\pm\rangle = \frac{1}{\sqrt{2}}(|0\rangle \pm |1\rangle)$. More specifically, the action of the Hadamard gate is given by $H|0\rangle = |+\rangle$ and $H|1\rangle = |-\rangle$. On the other hand, the $S$ gate is the principal square root of the $Z$ gate. Finally, the $T$ gate is the principal square root of the $S$ gate. In the computational basis, their matrix representations are

$$H = \frac{1}{\sqrt{2}} \begin{pmatrix} 1 & 1 \\ 1 & -1 \end{pmatrix} \qquad S = \begin{pmatrix} 1 & 0 \\ 0 & \mathrm{i} \end{pmatrix} \qquad T = \begin{pmatrix} 1 & 0 \\ 0 & e^{\mathrm{i}\frac{\pi}{4}} \end{pmatrix} \tag{3}$$

The last three common single-qubit gates I will discuss are the rotation gates represented by $R_{\mathrm{i}}(\theta)$ where $i \in \{x, y, z\}$. They are defined as $R_{\mathrm{i}}(\theta) = e^{-\mathrm{i}\theta\sigma_{\mathrm{i}}/2}$ where $\sigma_{\mathrm{i}}$ ($i \in \{x, y, z\}$) is a Pauli matrix. Finally, a global phase gate, sometimes denoted by $K(\phi)$ is given by $e^{\mathrm{i}\phi}\,\mathbb{1}\!\mathrm{l}$ where $\phi \in \mathbb{R}$ and $\mathbb{1}\!\mathrm{l}$ is the identity matrix. It is noteworthy that the rotation gates along with the global phase gate form a universal set for single-qubit gates. That is, any single-qubit gate can be decomposed as a product of a phase gate and rotation gates. One

realization of this decomposition is the ZYZ Euler angles decomposition.

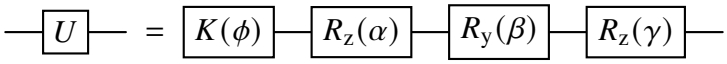


(4)

where $\phi$, $\alpha$, $\beta$ and $\gamma$ are suitable real numbers.

Now that I have discussed universal single-qubit gates, it is time to discuss two-qubit gates. A major distinction between classical information and quantum information is the possibility of entanglement in classical information. That is, a quantum correlation between two or more different qubits. One quantum gate that induces entanglement is the Controlled-X gate (or Controlled-Not) gate abbreviated by CNOT. This gate is a two-qubit gate, one of which is the control qubit while the other is the target. Its action is to apply the $X$ gate if and only if the state of the control qubit is $|1\rangle$. In a quantum circuit, this gate is represented by a dot on the control qubit and a $\oplus$ on the target qubit. Equation 5 shows a CNOT gate where the top qubit is the control while the second qubit is the target. The matrix representation is in the computational basis.

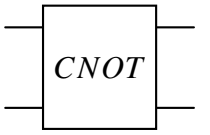


$$= \begin{pmatrix} 1 & 0 & 0 & 0 \\ 0 & 1 & 0 & 0 \\ 0 & 0 & 0 & 1 \\ 0 & 0 & 1 & 0 \end{pmatrix} \tag{5}$$

Importantly, the $CNOT$ gate along with the single-qubit rotation gates form a *universal* gate set. In other words, any unitary operator can be implemented exactly or to an arbitrary precision only with these gates. Another universal gate set is composed of the $H$, $S$, $CNOT$ and $T$ gates. The first three of these gates are generators of the Clifford group[5]. Remarkably, it is known that a set composed of the whole Clifford group and any one non-Clifford element is a universal set. Therefore, there exist several universal gates, and different ones are used depending on the application. Throughout this work, I will mostly

[5]The Clifford group will be defined later in this work.

use the universal set $\{H, S, CNOT, R_z\}$.

The final type of operation is the measurement. Measurement is typically used as the final operation to extract the result of a computation even though there are complex algorithms that use them as an integral part. According to the measurement postulate of quantum mechanics, measuring an observable results in the collapse of the wave function $|\psi\rangle$ to one of its eigenstate $|e\rangle$ with probability $|\langle e|\psi\rangle|^2$. For example, suppose a qubit state is given by $|\psi\rangle = \alpha\,|0\rangle + \beta\,|1\rangle$. A Pauli $Z$ measurement (also called computational basis measurement) results in $|\psi\rangle$ collapsing to $|0\rangle$ with probability $|\alpha|^2$ and similarly for $|1\rangle$. To illustrate a simple quantum computation, I will describe how to simulate coin toss on a quantum computer as I promised. Suppose the initial state $|\psi\rangle = |0\rangle$. Applying a Hadamard gate (Eq. 3) results in

$$|\psi\rangle = \frac{1}{\sqrt{2}}\left(|0\rangle + |1\rangle\right) \tag{6}$$

Clearly, a $Z$-measurement will result in $|0\rangle$ or $|1\rangle$ with equal probabilities 0.5. To construct a coin toss with arbitrary outcome probabilities, one may start with the initial state $|\psi\rangle = |0\rangle$. The application of the $R_y(\theta)$ rotation will result in

$$|\psi\rangle = \cos\theta\,|0\rangle + \sin\theta\,|1\rangle \tag{7}$$

so that the outcomes $|0\rangle$ and $|1\rangle$ have probabilities $\cos^2\theta$ and $\sin^2\theta$, respectively. Simulating a coin toss is simple but also gives a clear example of how qubit states can be used to store and manipulate information.

**Chapter 1.2.3: Measures of Quantum Circuit Complexity**

One trivial measure of the cost/complexity of a quantum circuit is the total number of gates. However, due to the possibility of applying some gates in parallel, one can see that there is a better measure of the cost of running a quantum circuit. For better illustration,

consider the example circuit in Fig. 1. In this circuit, the computer does not need to wait until $U_1$ is performed to perform $U_2$ since they act on different qubits. Since the two gates can be performed simultaneously, the circuit in Fig. 1 can be executed in a single time step. Consequently, the complexity of a quantum circuit can be measured by the number of time steps required to execute the circuit; this number is called the circuit depth [113].

The goal of optimizing quantum circuits may be formulated as optimizing its depth. One upper bound to the circuit depth is the number of gates. One argument is that in the worst-case scenario where all the gates involve the same qubit, the depth will be identical to the gate count. Therefore, sometimes only the gate count complexity is reported instead of the circuit depth since the former is easier to compute analytically.

Another consideration for measuring quantum circuit complexity is that current quantum computers have a limited number of qubits, reaching 1000 qubits only recently at the time of writing. Moreover, these qubits are error-prone with $\sim 10^{-3}$ gate-error rate and from $\sim 10^{-3}$ to as large as $10^{-1}$ readout error rate[6], earning them their names Noisy-Intermediate Scale Quantum (NISQ) hardware [158]. With error rates above 0.1 for some hardware, two-qubit gates are the major source of noise in quantum circuits. Even worse, for a quantum computer with limited connectivity, several swap gates[7], each requiring an overhead of three two-qubit gates, may need to be performed before performing the intended two-qubit gate. Due to its large cost, the number of CNOT gates is generally considered a good measure of the circuit complexity for NISQ hardware.

**Chapter 1.2.4: A Note on Quantum Error Correction and Fault Tolerance**

In the previous section, I discussed that errors may occur while performing quantum gates and while reading out measurement results. The theory of quantum error correction, formulated in Ref. [120], is an effort to find ways to encode quantum information such that an error may be detected and corrected. The overarching idea is to introduce redundancies

[6]See for example IBM's Eagle processor released in November 2021

[7]The swap gate is a two-qubit operation that interchanges the states of two qubits.

that may be employed to recover quantum information after errors have occurred. To illustrate this method, consider probably the simplest code – the three-qubit code. The code uses three qubits to encode one qubit with the map

$$\begin{aligned} |0\rangle &\mapsto |000\rangle \\ |1\rangle &\mapsto |111\rangle \end{aligned} \tag{8}$$

Then, an arbitrary qubit state is encoded as

$$|\psi\rangle = \alpha\,|0\rangle + \beta\,|1\rangle \mapsto \alpha\,|000\rangle + \beta\,|111\rangle \tag{9}$$

It is easy to see that this code protects against a single bit-flip error. Whenever one bit-flip error has occurred, it is possible to detect it and reverse it. Conversely, it is also easy to see that whenever two bits are flipped at once, the code will detect an error but will always wrongly correct it. Finally, if all three bits are flipped, the code will fail to detect that there was an error. The field of quantum error correction is well studied, and there exist several families of codes that are more powerful, see e.g. Refs. [84, 115]. An important question is whether it is possible to find codes that allow a quantum computer to function with arbitrary accuracy. The answer, also known as the threshold theorem, is affirmative [84].[8]. A quantum computer that produces arbitrarily accurate results even in the presence of noise is said to be fault-tolerant.

Unfortunately, fault tolerance requires an overhead in the number of qubits and the number of gates, see Footnote 8. Current estimates for existing codes suggest that more qubits with lower error rates are needed to achieve fault tolerance.

To conclude the discussion of fault tolerance, I will mention in passing that after the qubits

[8]The content of the theorem is: Suppose there are a threshold error $p_{\mathrm{T}}$ and local errors occurring with probability $p < p_{\mathrm{T}}$. Then, for any quantum circuit $C$ and $\varepsilon > 0$, there exists a circuit $C'$ consisting of $O\left(\mathrm{polylog}(|C|/\varepsilon)\,|C|\right)$ gates and $O\left(\mathrm{polylog}(|C|/\varepsilon)\,q\right)$ qubits such that the output of $C'$ in the presence of noise is a distance $\varepsilon$ apart from the output of $C$ in the absence of noise. The numbers $q$ and $|C|$ are respectively the number of qubits and the number of gates in $C$ [84].

have been encoded in logical qubits, the quantum gates also need to be encoded correctly in logical operators. A desirable encoding is the transversal encoding[9]. An important challenge to this encoding is the result known as the Eastin-Knill theorem (Ref. [67]), stating that not every gate in a universal gate set can be encoded transversally in any quantum error correcting code. Given this limitation, there is always at least one gate in the universal gate set that will have a more costly implementation, for example, through a technique called magic state distillation [140, 31]. In some implementations, for instance, the Steane code, the $T$ gate is the gate implemented non-transversally. Therefore, the number of $T$ gates is considered a measure of circuit complexity. I will report the number of $T$ gates when discussing fault-tolerant quantum circuits later.

## Chapter 1.3: Introduction to Gauge Theory

### Chapter 1.3.1: Gauge Theory in the Continuum

I begin by providing a brief introduction to gauge theories. The content of this section can be found in e.g. Refs [156, 15]. A convenient place to start this introduction is to consider the earliest of such theories, the so-called Quantum Electrodynamics (QED). The QED Lagrange density can be written as

$$\mathscr{L} = \bar{\psi}(\mathrm{i}\gamma^{\mu}\partial_{\mu} - m)\psi - \frac{1}{4}F_{\mu\nu}F^{\mu\nu} - q\bar{\psi}\gamma^{\mu}\psi A_{\mu}(x) \tag{10}$$

where $\psi$ are Dirac fields and $\gamma^{\mu}$ are the Dirac $\gamma$ matrices, $A^{\mu}$ represents the electromagnetic field and finally $F^{\mu\nu}$ is the electromagnetic tensor given by $F^{\mu\nu} = \partial^{\mu}A^{\nu} - \partial^{\nu}A^{\mu}$. The Lagrangian density (Eq. 10) is invariant under local U(1) transformation

$$\psi(x) \mapsto e^{-\mathrm{iq}\Lambda(\mathrm{x})}\psi(x) \quad \text{and} \quad A_{\mu} \mapsto .A_{\mu} + \partial_{\mu}\Lambda. \tag{11}$$

[9] A gate $G$ is encoded on $n$ physical qubits as $G \mapsto G'_1 \otimes G'_2 \otimes ... \otimes G'_{\mathrm{n}}$. This way, each $G'_{\mathrm{i}}$ acts locally on each qubit, and therefore does not propagate potential errors from one qubit to another.

We therefore say that QED is a U(1) gauge theory. It is important to note that QED is described by an Abelian gauge theory because the group U(1) is Abelian. A generalization of gauge theories to non-abelian groups is known as Yang-Mills theory based on SU(N) groups [189]. The Lagrangian density is given by

$$\mathscr{L} = \bar{\psi}(\mathrm{i}\gamma^\mu D_\mu - m)\psi - \frac{1}{4}F^{\mathrm{a}}_{\mu\nu}F_{\mathrm{a}}^{\mu\nu} \tag{12}$$

where the covariant derivative, $D^\mu$, is given by $D^\mu\psi = (\partial^\mu + \mathrm{i}gT_{\mathrm{a}}\,A^\mu_{\mathrm{a}})\psi$ with a sum over the repeated index $a$ assumed. The matrices $T_{\mathrm{a}}$ are the generators of the group algebra in an appropriate representation. The field-strength tensor is given by $F^{\mu\nu} = \partial^\mu A^\nu - \partial^\nu A^\mu + \mathrm{i}g[A^\mu, A^\nu]$. The theory is invariant under local gauge transformation

$$\psi(x) \mapsto e^{-\mathrm{igT_a\Lambda(x)_a}}\psi(x) \quad \text{and} \quad A^\mu_{\mathrm{a}} \mapsto A^\mu_{\mathrm{a}} + \partial^\mu\Lambda_{\mathrm{a}} + g\,f_{\mathrm{abc}}\Lambda_{\mathrm{b}}A^\mu_{\mathrm{c}} \tag{13}$$

where $f_{\mathrm{abc}}$ are the SU($N$) structure constants.

If the symmetry group is SU(3) for example, we obtain Quantum Chromodynamics (QCD), the theory of the strong interaction. More precisely, QCD is the theory of the strong interaction between quarks, an interaction mediated by a massless vector boson called gluon. This interaction couples to the so-called color charge carried by both quarks and gluons. The fact that even gluons carry color charges leads to non-trivial self-interaction of gluons (even in the absence of quarks).

Quarks occur in six flavors. From lightest to heaviest, these flavors are called up, down, charm, strange, top and bottom. Quarks are building blocks of hadrons. Hadrons are typically classified according to the number of quarks in their composition. For instance, baryons are composed of three quarks. An example of a baryon is the proton with two up quarks and one down quark. On the other hand, mesons are hadrons composed of one quark and one anti-quark. Examples of mesons are the pions $\pi^{0,\pm}$.

An important feature of QCD is the so-called asymptotic freedom. That is, the coupling

factor decreases with increasing energy. Consequently, the theory is perturbative at high energy but not at low energy. This phenomenon means that it is crucial to derive non-perturbative methods to study such a theory at all energy scales. In the next chapter, I will discuss lattice gauge theory, a method addressing this challenge.

**Chapter 1.3.2: Lattice Gauge Theory**

As noted earlier, the lattice formulation provides a non-perturbative approach to gauge theories. In the Lagrangian language, the spacetime continuum is replaced with a lattice with spacing $a$ and $N$ lattice points. Importantly, this discretization is also a regularization scheme to quantum field theories by providing an ultraviolet cut-off $1/a$ [75]. The continuum theory can be recovered by performing the limit $a \to 0$ and $N \to \infty$ to the critical point where the correlation length diverges. This result is possible due to universality arguments (see e.g. Refs. [77, 124, 75]). In the Hamiltonian language, which is commonly used in quantum computation, only the spatial components are discretized. For quantum computation, I will then only focus on the Hamiltonian formulation. An in-depth discussion of the Lagrangian counterpart can be found in e.g. Ref. [75, 61].
As noted earlier, we replace the spatial components of the spacetime continuum with a lattice, $\Lambda$. A typical gauge theory, e.g. QCD, may contain fermionic fields and gauge fields. In the Hamiltonian formulation, each lattice site is associated with a Hilbert space acted on by fermionic operators while each link ('space' between two adjacent lattice sites) is associated with a Hilbert space acted on by gauge fields operators, which have bosonic commutation relations. Since fermionic operators anti-commute, the Hilbert space at each site is finite-dimensional. In-kind, encoding their Hilbert space on a quantum computer requires a finite number of qubits per site. Moreover, there exists a mapping between fermion-raising and -lowering operators to operators acting on qubits [106, 32, 46]. The link Hilbert space, however, is infinite-dimensional since gauge fields have bosonic commutation relations. Therefore, encoding the link Hilbert spaces on a quantum computer is more challenging and here I will focus on this problem.

Consequently, I will mostly discuss gauge theories without fermions and only include them whenever appropriate.

For the rest of this discussion, I will adopt a common notation where a $x \in \Lambda$ represents the site of the lattice $\Lambda$ and $(x, x+\mu)$ denotes a directed link from site $x$ to the adjacent site in the $\mu$-direction. Moreover, I will focus the discussion on the case of a gauge theory with group $G = \mathrm{SU(N)}$ group for the moment, and I will include other cases when needed.

$\mathrm{SU}(N)$ is a compact Lie group, whose associated Lie algebra $su(N)$ has $N^2 - 1$ generators $T^{\mathrm{a}}$, satisfying the relation

$$\left[T^{\mathrm{a}}, T^{\mathrm{b}}\right] = \mathrm{i} f^{\mathrm{abc}} T^{\mathrm{c}} \tag{14}$$

where $f^{\mathrm{abc}}$ are called structure constants. A $D$-dimensional representation of the $su(N)$ algebra is a realization of the commutation relation above by $D \times D$ matrices. We call the $N$-dimensional representation the defining representation of the $su(N)$ algebra, and we reserve the symbol $T^{\mathrm{a}}$ for the generators of this representation. For any group element, $g \in \mathrm{SU(N)}$, there exists a parametrization $g = \exp\{\mathrm{i}\omega^{\mathrm{a}} T^{\mathrm{a}}\}$.

At each link, we associate a Hilbert space with an orthonormal basis $|g\rangle$ where $g \in \mathrm{G}$:

$$\langle g', g\rangle = \delta(g', g) \quad \text{and} \quad \int dg\, |g\rangle \langle g| = 1 \tag{15}$$

A state in such a Hilbert space can therefore be written as $|\psi\rangle = \int dg \psi(g) |g\rangle$. The function $\psi(g)$ is a square-integrable function on the group manifold with respect to the Haar measure. Hence, the Hilbert space at each link is the space of square-integrable functions on the group, $\psi(g) \in L^2(\mathrm{G})$. It is clear from this construction that the Hilbert space at each link for a gauge theory of a Lie group is infinite-dimensional.

To construct gauge transformations, it is convenient to define two translation operators

called left and right translations as follows:

$$L(g)\,|h\rangle = |gh\rangle \quad \text{and} \quad R(g)\,|h\rangle = \left|hg^{-1}\right\rangle . \tag{16}$$

These translations are group representations because they are group homomorphisms (Eq. 17). They are also called (left and right) regular representations of the group due to their central role in representation theory and Fourier analysis.

$$\begin{aligned} L(g')L(g)\,|h\rangle &= L(g')\,|gh\rangle = |g'gh\rangle = L(g'g)\,|h\rangle \\ R(g')R(g)\,|h\rangle &= R(g')\left|hg^{-1}\right\rangle = \left|hg^{-1}g'^{-1}\right\rangle = \left|h(g'g)^{-1}\right\rangle = R(g'g)\,|h\rangle . \end{aligned} \tag{17}$$

Therefore, they can be parametrized as $L(g) = \exp\{\mathrm{i}\omega^{\mathrm{a}}\mathbb{T}^{\mathrm{a}}_{\mathrm{L}}\}$ and $R(g) = \exp\{\mathrm{i}\omega^{\mathrm{a}}\mathbb{T}^{\mathrm{a}}_{\mathrm{R}}\}$ where $\mathbb{T}^{\mathrm{a}}_{\mathrm{L}}$ and $\mathbb{T}^{\mathrm{a}}_{\mathrm{R}}$ are generators satisfying the group algebra

$$\left[\mathbb{T}^{\mathrm{a}}_{\mathrm{L}}, \mathbb{T}^{\mathrm{b}}_{\mathrm{L}}\right] = \mathrm{i}f^{\mathrm{abc}}\mathbb{T}^{\mathrm{c}}_{\mathrm{L}} \quad \text{and} \quad \left[\mathbb{T}^{\mathrm{a}}_{\mathrm{R}}, \mathbb{T}^{\mathrm{b}}_{\mathrm{R}}\right] = \mathrm{i}f^{\mathrm{abc}}\mathbb{T}^{\mathrm{c}}_{\mathrm{R}}. \tag{18}$$

Moreover, it is easily verified that the left and right translations commute, implying

$$[\mathbb{T}^{\mathrm{a}}_{\mathrm{L}}, \mathbb{T}^{\mathrm{b}}_{\mathrm{R}}] = 0. \tag{19}$$

Now, a gauge transformation at each site can be defined in a straightforward manner using the Gauss operator given by

$$G^{\mathrm{a}}_{\mathrm{x}} \equiv \sum_{\mu=1}^{\mathrm{d}} \left\{\mathbb{T}^{\mathrm{a}}_{\mathrm{L}}(x,\mu) + \mathbb{T}^{\mathrm{a}}_{\mathrm{R}}(x-\mu,\mu)\right\} . \tag{20}$$

The Gauss operator is the generator of the gauge transformation. That is, a gauge transformation with a group element $g$ at site $x$ acts as $\exp\{\mathrm{i}\omega^{\mathrm{a}}G^{\mathrm{a}}(x)\}$. The action of this transformation is that each link with an arrow from the site $x$ is left-translated while each

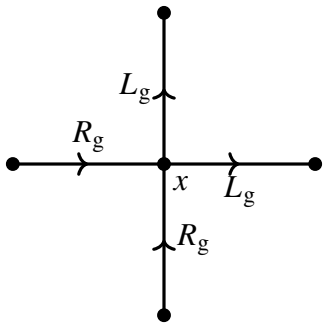


Figure 2: Action of a local gauge transformation operator $\exp\{i\omega^a G^a(x)\}$ with group element $g = \exp\{i\omega^a T^a\}$ at a site $x$. The outgoing links from the site $x$ are acted on by the left translation $L_g$ while the incoming links are acted on by the right translation $R_g$.

link with an arrow towards the site $x$ is right-translated, see Figure 2.

The definition of gauge invariance also follows similarly. A state is gauge invariant if it is unchanged after any gauge transformation. It is easily verified that this condition is equivalent to

$$G^a(x)\,|\psi\rangle = 0. \tag{21}$$

We say that physical space is the space of gauge invariant states, $\mathcal{H}_{\text{phys}} \subseteq \mathcal{H}$. Physical observables, on the other hand, correspond to gauge invariant operators. These are operators that are unchanged after any gauge transformation. In turn, this condition corresponds to saying that an observable $O$ is gauge invariant if and only if

$$\left[G^a_x, O\right] = 0 \tag{22}$$

Presently, we are ready to construct the Hamiltonian describing the theory. This procedure was first presented in Ref. [122]. The most straightforward term to choose is a gauge invariant term that only acts on each link separately. Arguably, the simplest choice is the Casimir operators $\mathbb{T}^2 \equiv \mathbb{T}^a_L \mathbb{T}^a_L + \mathbb{T}^a_R \mathbb{T}^a_R$ constructed out of the generators of the left and right translations, respectively, and we assumed summation over the repeated index $a$.

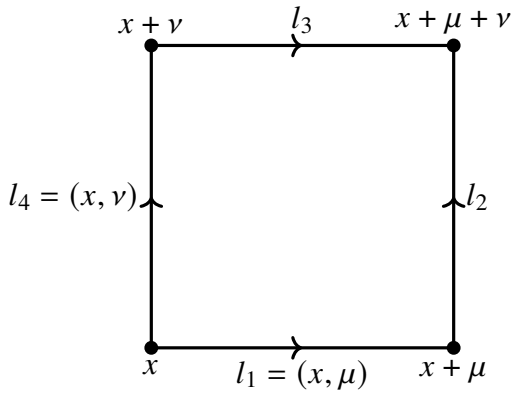


Figure 3: The plaquette $P \equiv U_{\mu\nu}(x)$ at site $x$ and in directions $\mu$ and $\nu$.

This term is usually referred to as the kinetic term.

Having built a kinetic term, we proceed to construct an interaction term between different links. The first step is to define the group position operators as $\hat{U}^{\mathrm{j}}_{\mathrm{mn}}$ by the action $\hat{U}^{\mathrm{j}}_{\mathrm{mn}} |g\rangle = D^{\mathrm{j}}_{\mathrm{mn}}(g) |g\rangle$ where $D^{\mathrm{j}}(g)$ is a group representation with normalized generators $\lambda^{\mathrm{a}}$, $D^{\mathrm{j}}(g) = \exp\{\mathrm{i}\omega^{\mathrm{a}}\lambda^{\mathrm{a}})\}$. Moreover, $m$ and $n$ are integers from $-j$ to $j$, $-j \leq m, n \leq j$. It can then be verified in a straightforward way that the commutation relations between $\hat{U}^{\mathrm{j}}_{\mathrm{mn}}$ and the $\mathbb{T}^{\mathrm{a}}_{\mathrm{L,R}}$ are given by

$$\left[\hat{U}^{\mathrm{j}}_{\mathrm{mn}}, \mathbb{T}^{\mathrm{a}}_{\mathrm{L}}\right] = \lambda^{\mathrm{a}}_{\mathrm{mm'}} \hat{U}^{\mathrm{j}}_{\mathrm{m'n}} \quad \text{and} \quad \left[\hat{U}^{\mathrm{j}}_{\mathrm{mn}}, \mathbb{T}^{\mathrm{a}}_{\mathrm{R}}\right] = -\lambda^{\mathrm{a}}_{\mathrm{mm'}} \hat{U}^{\mathrm{j}}_{\mathrm{m'n}}. \tag{23}$$

The simplest nontrivial interaction term is known as the plaquette (see Figure 3). Analogously to the Lagrangian formulation (see e.g. Ref. [61, 75]), the plaquette operator will be defined as

$$\begin{aligned} \hat{\square}(P) &\equiv \hat{U}_{\mathrm{ij}}(l_1)\, \hat{U}_{\mathrm{jk}}(l_2)\, \left[\hat{U}(l_3)^{\dagger}\right]_{\mathrm{kl}} \left[\hat{U}(l_4)^{\dagger}\right]_{\mathrm{li}} \\ &= \mathrm{Tr}\left[\hat{U}(l_1)\, \hat{U}(l_2)\, \hat{U}(l_3)^{\dagger}\, \hat{U}(l_4)^{\dagger}\right]. \end{aligned} \tag{24}$$

where $P$ denotes a plaquette and $l_{\mathrm{i}}$ denotes a link. The gauge invariance of the plaquette operator can be verified explicitly by considering how a gauge transformation at a given

site acts on the links attached. Having both terms, a Hamiltonian can be written as

$$H = \frac{g^2}{2a} \sum_{\mathrm{l}} \mathbb{T}^2_{\mathrm{l}} - \frac{1}{4ag^2} \sum_{\mathrm{P}} \left( \square(P) + \square^\dagger(P) \right). \tag{25}$$

The operator $\square^\dagger$ has been included to ensure the Hamiltonian is Hermitian, and $g$ is a coupling constant. This Hamiltonian was first constructed in Ref. [122] and derived directly from Wilson's action in Ref. [55]. The purpose of performing Hamiltonian time evolutions of lattice gauge theory on a quantum computer is to encode the unitary time evolution of this Hamiltonian on a quantum computer.

First, it is important to remember that this Hamiltonian acts on an infinite-dimensional Hilbert space[10]. Encoding the time evolution of this Hamiltonian on a quantum computer therefore requires a truncation scheme on the Hilbert space. The next section provides a brief review to this challenge.

**Chapter 1.4: Hilbert Space Truncation**

Perhaps the simplest method to truncate the link Hilbert space of a SU(N) gauge theory is by imposing a limit in the representation basis, see e.g. Refs. [130, 192, 42]. The construction is straightforward. Recall that the Hilbert space at each link can be identified with $\mathcal{L}^2(G)$, the space of the square-integrable functions over the group. From Peter-Weyl theorem (e.g. Refs. [51, 74]), the irreducible representations form a complete basis of $\mathcal{L}^2(G)$. SU($N$), being a compact Lie group, all its irreducible representations are finite-dimensional. For simplicity, I will restrict this short discussion to the case of SU(2) whose irreducible representations are labeled by $j = 0, 1/2, 1, ....$ We can identify each matrix element of an irreducible representation with a ket $|j, m', m\rangle$ where $m'$ and $m$ ($m', m \in \{-j, -j+1, ..., j\}$) denote a matrix element. These states are related to the states

[10]The space of square-integrable functions on the SU($N$) manifold.

$|g\rangle$ by

$$\langle g|j,m',m\rangle = \sqrt{\frac{(2j+1)}{8\pi^2}} D^{\mathrm{j}}_{\mathrm{m'm}}(g). \tag{26}$$

The next task will be to write the Hamiltonian (Eq. 25) in this basis, see for example Refs. [192, 42]. Now, notice that a simple truncation scheme is to impose a limit $j_{\max}$. This way, the Hilbert space at each link has dimension

$$\mathcal{H}_\ell = \sum_{\mathrm{j}=0,1/2,\ldots,\mathrm{j}_{\max}} (2j+1)^2 = \frac{(4j_{\mathrm{j}_{\max}}+3)(2j_{\max}+1)(j_{\max}+1)}{3} = O(j^3_{\max}), \tag{27}$$

requiring $n_\ell = O\left(\log\left(j_{\max}\right)\right)$ qubits per link. In this strategy, calculations are performed with a fixed $j_{\max}$, and $j_{\max}$ is increased until the results converge. This strategy is particularly appealing since the number of qubits only grows logarithmically with the truncation $j_{\max}$. However, as we will argue later, the cost of the time evolution for even $j_{\max} = 1/2$ can be prohibitive for near-term quantum computers.

The issue with the approach above is that one needs to increase the complexity of the problem (by increasing $j_{\max}$.) A remedy to this issue is to formulate the gauge theory directly in a finite-dimensional Hilbert space such that the theory is in the right universality class. That is, the finite-dimensional theory has a critical point in the universality class of the original theory. We call such a formulation a *qubitization* of the original theory. Finite-dimensional formulations of gauge theory have been studied in the literature. For example, the author of Ref. [100] constructed a $SU(2)$ gauge theory where each link Hilbert space is five-dimensional. A generalization to SU($N$), however, was not obtained due to a spurious U(1) symmetry. Later on, this approach was pursued by the authors of Ref. [151] who found a series of finite-dimensional formulations of $SU(2)$ gauge theories, the smallest of which being four-dimensional. In Ref. [37], the authors provided a formulation, which could be extended to an arbitrary $SU(N)$.

An important consideration is whether a particular formulation is in the universality class

of the target theory. Moreover, a practical consideration is that of the cost of each theory on the quantum computer. A large cost will negate the potential advantage of using a quantum computer in the first place. With these considerations in mind, I will present a finite-dimensional formulation of gauge theory, the Fuzzy gauge theory that shows evidence of being a valid *qubitization*. In addition, I will argue that this formulation is practical on current quantum devices, at least for a single plaquette and for short time evolution.To end this note on Hilbert space truncation, I also note that another promising strategy pursued in Refs. [90, 89, 11] is to replace a SU($N$) group with a discrete finite subgroup.

**Chapter 1.5: General Method for Hamiltonian Time Evolution**

The problem of Hamiltonian Time evolution on a quantum computer is to find a quantum circuit approximating the unitary time evolution operator $U(t) = \exp\{-\mathrm{i}Ht\}$. It is immediately clear why this problem is difficult. Even though the Hamiltonian may be sparse, as is the case for local systems, it is exponentially large. To approximate $U(t)$, a popular technique used is called Trotterization, see e.g. Refs [179, 173, 174, 47].

**Chapter 1.5.1: Trotterization Method**

The main idea is to split an otherwise complex problem into simpler sub-problems that may be solved independently and combined to yield the solution to the original problem. Trotterization, in particular, relies on the Trotter formula (Ref. [179, 173, 174]): for two operators $A$ and $B$,

$$e^{-\mathrm{i(A+B)}\Delta\mathrm{T}} = e^{-\mathrm{i\,A}\,\Delta\mathrm{T}}\, e^{-\mathrm{i\,B}\,\Delta\mathrm{T}} + \mathcal{O}(\Delta T^2) \tag{28}$$

with the equality holding only if $A$ and $B$ commute. Eq. 28 is generally referred to as the First-order Trotter formula. Eq. 28 implies that for an arbitrary time $T$ the time evolution $U(T)$ can be approximated by splitting $T$ into $k$ time steps such that $T = k\Delta T$, incurring an

overall error $O(\Delta T)$. A second order approximation (Ref. [174]) is given in Eq. 29.

$$e^{-\mathrm{i(A+B)\Delta T}} = e^{-\mathrm{i\,A\,\Delta T/2}}\, e^{-\mathrm{i\,B\,\Delta T}} e^{-\mathrm{i\,A\,\Delta T/2}} + O(\Delta T^3). \tag{29}$$

The second order formula (Eq. 29) improves the overall error at the cost of a larger quantum circuit. I will mostly focus on the first-order approximation, and the arguments presented here can be straightforwardly generalized to higher orders.

There is a straightforward scheme to apply the first-order Trotterization on the Hamiltonian (Eq. 25). First, notice that each operator $\mathbb{T}^2_1$ acts on each link separately, and each interaction term acts on one plaquette as well. The main idea is therefore to split the Hamiltonian into plaquette Hamiltonians. In addition, the Hamiltonian of two plaquettes commute if the two plaquettes do not share a link. In a two-dimensional lattice for example, we can divide the plaquettes into two groups such that the plaquettes in each group do not share a link. Let's call one group the even plaquettes (E) and the other the odd plaquettes (O). Now, the Hamiltonian (Eq. 25) can be written as $H = H_\mathrm{E} + H_\mathrm{O}$ where $H_\mathrm{E}$ is the Hamiltonian acting only on the even plaquettes while $H_\mathrm{O}$ acts on the odd plaquettes:

$$H_\mathrm{E} = \sum_{\mathrm{P}\in\mathrm{E}} H_\mathrm{P} \qquad\qquad H_\mathrm{O} = \sum_{\mathrm{P}\in\mathrm{O}} H_\mathrm{P} \tag{30}$$

and one time step of the time evolution operator is

$$U(\Delta T) = e^{-\mathrm{iH_E\Delta T}}\, e^{-\mathrm{iH_O\Delta T}} + O(\Delta T^2), \tag{31}$$

noting that $H_\mathrm{E}$ and $H_\mathrm{O}$ do not necessarily commute. Finally, $H_\mathrm{E}$ and $H_\mathrm{O}$ can be further Trotterized by considering only one plaquette. In other words, we have reduced the whole original problem to that of a single plaquette with the caveat that we need to take several small steps $\Delta T$. Therefore, I have focused on the quantum circuits of a single plaquette in my work.

### Chapter 1.5.2: Hamiltonian in Pauli Basis

The purpose of this section is to discuss how to write a Hamiltonian as a linear combination of Pauli operators, a convenient starting point in implementing the Hamiltonian time evolution in quantum circuits. The first step is to notice that the $2 \times 2$ identity matrix along with the Pauli matrices $X$, $Y$, and $Z$ form a basis for $2 \times 2$ matrices. Moreover, for Hermitian matrices, the coefficients are all real. We call this basis the Pauli basis.

The task now is to generalize the idea of Pauli basis to $2^n \times 2^n$ matrices. We may begin by defining the $n$-qubits Pauli group $\mathcal{P}_n$ as

$$\mathcal{P}_n = \{c\, \sigma_1 \otimes \sigma_2 \otimes ... \otimes \sigma_n\} \tag{32}$$

such that $c \in \{\pm 1, \pm i\}$ and $\sigma_i \in \{1, X, Y, Z\}$. $\mathcal{P}_n$ is a group under multiplication with $4^{n+1}$ elements. Fixing $c = 1$, yields the subgroup $P_n = \{\sigma_1 \otimes \sigma_2 \otimes ... \otimes \sigma_n\}$ with only $4^n$ elements. $P_n$ is the subgroup that I will use for the rest of this discussion.

Choosing an inner product as $\langle a, b \rangle = \mathrm{Tr}\left[a^\dagger b\right]$, it is easy to see that every two operators $\frac{1}{\sqrt{2^n}} p_i$ and $\frac{1}{\sqrt{2^n}} p_j$ for all $p_i, p_j \in P_n$ are orthonormal. Moreover, since $2^n \times 2^n$ matrices also have $4^n$ free parameters, the normalized Pauli operators also form a basis for $2^n \times 2^n$ matrices. Finally, for Hermitian matrices, all the coefficients are real. Then, any Hamiltonian can be written as

$$H = \sum_i c_i\, p_i \tag{33}$$

where $p_i \in P_n$ and $c_i = \mathrm{Tr}\left[p_i H\right] / 2^n$. The expansion above is the Pauli basis expansion of a Hamiltonian. Each $p_i$ is called a Pauli operator. To end, it is customary to use the symbol $I$ to denote the identity matrix and to drop the $\otimes$ symbols for brevity. Consequently, a Pauli operator is typically written as a string of Pauli matrices $I$, $X$, $Y$, and

$Z$, and is therefore also called a Pauli string. For example for $n = 3$, one example of a Pauli string (Pauli operator) is $XIZ = X \otimes 1 \otimes Z$.

**Chapter 1.5.3: Trotterization based on Pauli operators**

Suppose a Hamiltonian, for example, a single plaquette Hamiltonian in our case, is given in Pauli basis (Eq. 33). The commutation relations of Pauli operators suggest a natural method to Trotterize the Hamiltonian. For $n = 1$, it is clear that a Pauli string ($X$, $Y$, or $Z$) commutes only with the identity Pauli string ($I$). However, for $n > 1$, it is possible for two Pauli strings to commute. One example is that the Pauli strings $XX$, $YY$ commute. Later, I will explain how to verify in $O(n)$ operations whether two Pauli strings commute or not (without performing any matrix multiplication).

Given that it is efficient to verify Pauli strings commutation, a convenient Trotterization strategy is to divide the Pauli strings into clusters so that two Pauli strings can be in the same cluster if and only if they commute. In other words, we write the Hamiltonian as

$$H = \sum_{\mathrm{i}} c_{\mathrm{i}}\, p_{\mathrm{i}} \tag{34}$$

$$= \sum_{\mathrm{C}} H_{\mathrm{C}} \tag{35}$$

where each $H_{\mathrm{C}}$ is a linear combination of commuting Pauli strings. The one-step time evolution operator can then be approximated

$$U(\Delta T) \approx \prod_{\mathrm{c}} e^{-\mathrm{i}H_{\mathrm{C}}\Delta \mathrm{T}}. \tag{36}$$

Now, we are ready to present a general strategy to construct a quantum circuit approximating $U(\Delta T)$. Because each $H_{\mathrm{C}}$ consists of commuting Pauli strings, it can diagonalized simply by finding a basis that simultaneously diagonalizes all the Pauli strings. Let $V_{\mathrm{C}}$ be such a unitary operator and $D_{\mathrm{C}}$ be the resulting diagonal matrix,

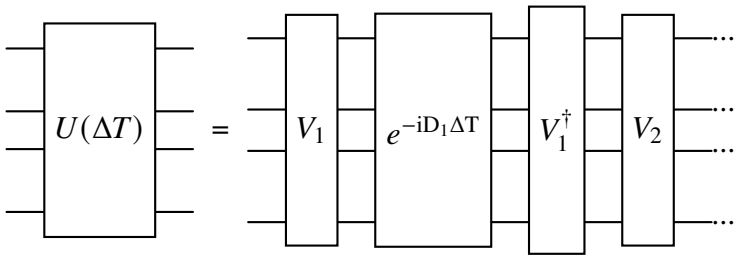


Figure 4: Quantum circuit structure from Eq. 37.

$H_C = V_C D_C V_C^\dagger$. Eq. 36 becomes

$$U(\Delta T) \approx \prod_C V_C \; e^{-i\, D_C\, \Delta T}\; V_C^\dagger. \tag{37}$$

Now, the problem of finding $U(\Delta T)$ for a single plaquette is reduced to that of finding quantum circuit implementations of $V_C$ and diagonal unitary matrices. The generic structure of this construction is shown in Figure 4. I have solved this problem throughout my research. In the next chapter, I will describe the general algorithm I developed to find $V_C$, noting that it is the best-known solution to the problem at the time of writing. The content of the chapter is from the article Ref. [144]. Next, I will describe the asymptotically optimal algorithm I developed to find a quantum circuit of diagonal unitaries. The content of this chapter is from article Ref. [145]. Finally, I will discuss a truncation method of lattice gauge theories, and evaluate its quantum circuit cost, see article Ref. [8].

**Chapter 1.6: Summary of Results**

The content of the next three chapters is from my co-authored articles Refs. [145, 144, 8] to address the challenges presented in this introduction. This chapter will summarize the main results of these articles.

In article Ref. [144], I designed an algorithm to find a circuit diagonalizing any set of commuting Pauli operators. An important aspect of this algorithm is that it is recursive. That is, it proceeds with at most $n$ (the number qubits) steps so that after each step, all the

Pauli matrices acting on a particular qubit are transformed into $Z$ or $I$. This way, after at most $n$ steps, each entire Pauli operator will be diagonalized. This recursive structure has several advantages. One advantage is that optimizing the algorithm reduces to simply optimizing each step. Moreover, analytical studies of the algorithm's performance become straightforward. In other words, we can calculate upper bounds on the number of gates and the circuit depth. Notably, the algorithm guarantees a circuit depth of $n \log r$, the best-known result for this problem. In addition, the algorithm generalizes very well to devices with limited connectivity. In particular, it is shown that for linear connectivity, the algorithm significantly outperforms previously known results.

The article Ref. [145] provides an algorithm to construct a quantum circuit to perform the exact time evolution of a diagonal Hamiltonian. The Pauli operators in a diagonal Hamiltonian contain only Pauli matrices $I$ and $Z$. As such, the Hamiltonian can be stored naturally in a binary tree. The algorithm performs a tree traversal to efficiently read the Pauli matrices $Z$ or $I$ and write quantum gates accordingly. An advantage of using a tree structure is that reading the binary tree is classically more efficient than reading each Pauli string one after another. Secondly, the structure of the quantum circuit is amenable to analytical studies. In kind, it can be shown analytically that the algorithm is optimal when the Hamiltonian has all the possible diagonal Pauli operators.

Moreover, benchmarking the algorithm against randomly generated diagonal Hamiltonian showed that it performed equally well or better than existing methods. This algorithm, along with the Pauli operator diagonalization algorithm can be used to construct efficient quantum circuits for an arbitrary Hamiltonian. We can therefore use them to measure the cost of simulating different theories. In Chapter 1.4: Hilbert Space Truncation, I have shown a simple approach to truncating the link Hilbert space. Moreover, I have argued that this truncation approaches the true theory as the cut-off is increased. However, the quantum circuit construction algorithm showed that in the case of $\sigma$-models for instance, the quantum gate cost grows so fast that this truncation method may be impractical on

near-term quantum devices [9]. This result demonstrates that it is crucial to find valid qubitizations to enable efficient simulations on quantum computers.

Finally, article Ref. [8] presents a finite-dimensional formulation of gauge theory, which we call Fuzzy gauge theory. The article provides a specific construction for SU(2) gauge theory as well as a generalization of U($N$) gauge theory. In the case of non-linear O(3) $\sigma$-models, it was shown in Ref. [9] that the fuzzy construction led to a valid qubitization of the theory, suggesting that this strategy may also yield valid truncations for gauge theories. Importantly, we have given arguments that this is indeed plausible. Finally, applying the quantum circuit constructions in Ref. [145, 144] yields a relatively low cost, manageable by current devices at least for a sinngle plaquette and for short time evolution.

## Chapter 2: Quantum Algorithm for Simultaneous Diagonalization of Commuting Pauli Operators

**Abstract**

A variety of quantum algorithms employ Pauli operators as a convenient basis for studying the spectrum or evolution of Hamiltonians or measuring multi-body observables. One strategy to reduce circuit depth in such algorithms involves simultaneous diagonalization of Pauli operators generating unitary evolution operators or observables of interest. We propose an algorithm yielding quantum circuits with depths $O(n \log r)$ diagonalizing $n$-qubit operators generated by $r$ Pauli operators. Moreover, as our algorithm iteratively diagonalizes all operators on at least one qubit per step, it is well suited to maintain low circuit depth even on hardware with limited qubit connectivity. We observe that our algorithm performs favorably in producing quantum circuits diagonalizing randomly generated Hamiltonians as well as molecular Hamiltonians with short depths and low two-qubit gate counts.

### Chapter 2.1: Introduction

Quantum simulations [135, 21, 70, 71, 133, 147, 186] are frequently cited as one of the most promising classes of quantum algorithms to see a practical quantum advantage [57], in an era where analog quantum simulators and universal quantum computers are becoming viable for many-body systems of size $O(50)$. In the case of qubit hardware, it is frequently convenient to decompose one's Hamiltonian into Pauli operators, also known as "multi-qubit Pauli matrices," i.e., Pauli matrices on individual qubits strung together [147]. In fact, this convenience carries over to other algorithms implementing the action of a Hamiltonian on qubits, such as in a quantum Lanczos algorithm suggested by Ref. [114]. Moreover, for a yet wider collection of quantum algorithms, efficient measurement schemes must be devised to estimate the value of physical observables with respect to a given prepared state, even where direct simulation of time evolution is not

required, such as in variational quantum eigensolvers [155] and quantum tomography [68, 104, 152, 52, 147]. Due to the qubitwise nature of measuring prepared quantum states, it is already natural to consider Pauli operators as a basis for measurements of observables in these many algorithms [68, 152, 147, 155].

In practical implementations of such algorithms, one finds that the number of Pauli operators involved, i.e., in decomposing one's Hamiltonian to be simulated or physical observables to be measured, may grow polynomially or even exponentially in system size. This growth can have troublesome consequences for the circuit depth involved in such computations [145]. In particular, one finds larger errors will be introduced into computations due to the decoherence of qubits associated with two-qubit gates (with entangling power) in near-term hardware.

As such, one would like to augment these algorithms with strategies to minimize such costs. One such strategy involves simultaneous diagonalization of commuting Pauli operators [182], offering a reduction of the problem at hand to only the diagonal Pauli basis (i.e., strings of identity and $Z$ Pauli matrices). Generally speaking, for measurement schemes on universal quantum computers, one must already perform a sort of diagonalization for each of the Pauli operators generating an observable of interest (since one typically measures in a $Z$ basis as well), so the suggestion of simultaneous diagonalization [53] is a natural choice to reduce the number of measurements entailed. However, simultaneous diagonalization for measurements of Pauli operators may entail two-qubit gates that would otherwise be unnecessary in the state preparation or measurements of individual Pauli operators. Therefore, it is additionally important to minimize the number of such gates involved in simultaneous diagonalization to find the strategy advantageous. Conveniently, such a strategy can be used in tandem with other procedures to efficiently perform state tomography, such as randomized measurement protocols, e.g., in Ref. [36].

In what follows, we present a method to exactly and efficiently diagonalize a commuting

set of Pauli operators. To provide context, we give a brief introduction and review to the mathematical language of stabilizer theory typically used to solve this problem in Chapter 2.2: Review of Tableau Representation. We present our algorithm in Chapter 2.3: Qubitwise Diagonalization Algorithm and illustrate how it may be used to accommodate quantum hardware with limited connectivity. Furthermore, we provide estimates of worst-case circuit costs in Chapter 2.4: Analysis of the Algorithm. Additionally, we benchmark the resource costs of our algorithm in Chapter 2.5: Examples by considering randomized sets of Pauli operators as well as molecular Hamiltonians, again taking limited qubit connectivity into account. Finally, we summarize our findings and discuss future avenues for exploring circuit costs with our algorithm in Chapter 2.6: Conclusions.

**Chapter 2.2: Review of Tableau Representation**

Before we propose our algorithm, let us review language frequently used to pose the problem of efficient diagonalization of Pauli operators. Specifically, we briefly introduce here the tableau representation of Pauli operators, in particular, using the notation in Refs. [182, 145]. We discuss the unitary operations on these Pauli operators in Chapter 2.2.1: Clifford Gates and the Symplectic Group and pose the problem of diagonalization in Chapter 2.2.2: Statement of the problem.

Suppose we have $N$ commuting Pauli operators acting on $n$ qubits, e.g., generating an evolution operator, $U = \exp\left(\mathrm{i} \sum_{\mathrm{i}=1}^{\mathrm{N}} c_{\mathrm{i}} P_{\mathrm{i}}\right)$, or physical observables that we would like to measure, $\{O = \sum_{\mathrm{i}=1}^{\mathrm{N}} c_{\mathrm{i}} P_{\mathrm{i}}\}$. The tableau corresponding to this collection of Pauli operators $\mathcal{P} = \{P_1, \ldots, P_{\mathrm{N}}\}$ is composed of three arrays: $\mathcal{X}$, $\mathcal{Z}$, and $\mathcal{S}$. The arrays $\mathcal{X}$ and $\mathcal{Z}$ each have dimensions $N \times n$, while the $\mathcal{S}$ array is a column vector with $N$ rows. For a given Pauli operator $P_{\mathrm{i}}$ with relative phase factor $c_{\mathrm{i}}/|c_{\mathrm{i}}| = \pm 1$, the entries of the three arrays are

given by

$$\mathcal{X}[i,j] = \begin{cases} 0 \text{ if the } j\text{th digit of } P_{\mathrm{i}} \text{ is } Z \text{ or } I \\ 1 \text{ otherwise} \end{cases},$$

$$\mathcal{Z}[i,j] = \begin{cases} 0 \text{ if the } j\text{th digit of } P_{\mathrm{i}} \text{ is } X \text{ or } I \\ 1 \text{ otherwise} \end{cases}, \tag{38}$$

$$\mathcal{S}[i] = \begin{cases} 0 \text{ if } c_{\mathrm{i}} > 0 \\ 1 \text{ otherwise} \end{cases}.$$

For the remainder of the article, we call the "tableau" of our Pauli operators the $N \times 2n$ block matrix $(\mathcal{X}|\mathcal{Z})$. Here, we neglect the relative phases tracked by the vector $\mathcal{S}$, as they are not necessary for developing a scheme to diagonalize the collection of commuting Pauli operators. Let us define the following notation for elements of these arrays: $\mathcal{X}_{\mathrm{i}}$ and $\mathcal{Z}_{\mathrm{i}}$ [with "lowered" indices] denote the $i$th column vectors of $\mathcal{X}$ and $\mathcal{Z}$, respectively. In kind, "raised" indices $\mathcal{X}^{\mathrm{i}}$ and $\mathcal{Z}^{\mathrm{i}}$ will denote the $i$th row vectors. Moreover, a row of the tableau $u = (\mathcal{X}^{\mathrm{j}}, \mathcal{Z}^{\mathrm{j}}) \in \mathbb{F}_2^{2\mathrm{n}}$ is said to "encode" a Pauli operator $P$ if $P = \bigotimes_{\mathrm{i}=1}^{\mathrm{n}} X^{\mathrm{u_i}} Z^{\mathrm{u_{n+i}}}$ up to an overall phase.

**Chapter 2.2.1: Clifford Gates and the Symplectic Group**

Since a diagonal Pauli operator may contain only factors $I$ and $Z$, the $\mathcal{X}$ array of diagonal Pauli operators is zero. Consequently, diagonalization of Pauli operators may be viewed as conjugation with unitary operators to reduce the $\mathcal{X}$ array to zero. Specifically, since we seek to transform Pauli operators into other Pauli operators, these unitary operators are Clifford gates, generated by the Hadamard (H), phase (S), and controlled-NOT (CNOT) gates [83].

Now, let $C$ be an arbitrary Clifford gate. Conjugating the Pauli operators of $\mathcal{P}$ with $C$ can equivalently be viewed as an action transforming each column $\mathcal{X}_{\mathrm{i}}$ and $\mathcal{Z}_{\mathrm{i}}$. We denote this

action by functions $f_i$ and $g_i$, written

$$\mathcal{X}_i \mapsto \mathcal{X}'_i = f_i\left(\mathcal{X}_1 \ldots \mathcal{X}_N, \mathcal{Z}_1 \ldots \mathcal{Z}_N\right) \tag{39}$$

$$\mathcal{Z}_i \mapsto \mathcal{Z}'_i = g_i\left(\mathcal{X}_1 \ldots \mathcal{X}_N, \mathcal{Z}_1 \ldots \mathcal{Z}_N\right) \tag{40}$$

which we will show are necessarily linear:

$$f_i(\mathcal{X}, \mathcal{Z}) = \sum_{j=1}^{n} a_i^j \mathcal{X}_j + b_i^j \mathcal{Z}_j, \tag{41}$$

$$g_i(\mathcal{X}, \mathcal{Z}) = \sum_{j=1}^{n} \tilde{a}_i^j \mathcal{X}_j + \tilde{b}_i^j \mathcal{Z}_j, \tag{42}$$

where $a_i^j, b_i^j, \tilde{a}_i^j, \tilde{b}_i^j \in \{0, 1\}$, or, more compactly,

$$f(\mathcal{X}, \mathcal{Z}) = \mathcal{X}A + \mathcal{Z}B, \tag{43}$$

$$g(\mathcal{X}, \mathcal{Z}) = \mathcal{X}\tilde{A} + \mathcal{Z}\tilde{B}, \tag{44}$$

for $A, B, \tilde{A}, \tilde{B} \in \mathbb{F}_2^{n \times n}$. We give the matrices corresponding to elementary Clifford gate conjugations here, derived from rules presented in, e.g., Refs. [2, 182]. First let $\mathbf{e}_i$ be the unit column vector with $i$th entry equal to 1. Then, we may summarize

(1) For a Hadamard gate conjugation on qubit $i$, $\mathrm{H}(i)$, we have corresponding matrices $B = \tilde{A} = \mathbf{e}_i \mathbf{e}_i^\top$ and $A = \tilde{B} = 1_{n \times n} - B$.

(2) For a phase gate conjugation on qubit $i$, $\mathrm{S}(i)$, we have corresponding matrices $A = \tilde{B} = 1_{n \times n}$, $B = 0_{n \times n}$, and $\tilde{A} = \mathbf{e}_i \mathbf{e}_i^\top$.

(3) For a conjugation with $\mathrm{CNOT}(i, j)$ gates controlled by qubit $i$ and targeting qubit $j$, we have corresponding matrices $A = \tilde{B}^\top = 1_{n \times n} + \mathbf{e}_i \mathbf{e}_j^\top$ and $B = \tilde{A} = 0_{n \times n}$.

Since these gates generate the Clifford group, and all compositions of linear functions are also linear, we conclude that all Clifford elements are linear, i.e., are given by some

$(A, B, \tilde{A}, \tilde{B})$. For example, conjugation with S on qubits 1 and 2 corresponds to $(1, 0, \mathbf{e}_1\mathbf{e}_1^\top + \mathbf{e}_2\mathbf{e}_2^\top, 1)$, and conjugation with H on qubit $i$ followed by CNOT$(i, j)$ corresponds to $(1 - \mathbf{e}_i\mathbf{e}_i^\top, \mathbf{e}_i\mathbf{e}_i^\top + \mathbf{e}_i\mathbf{e}_j^\top, \mathbf{e}_i\mathbf{e}_i^\top + \mathbf{e}_i\mathbf{e}_j^\top, 1 - \mathbf{e}_i\mathbf{e}_i^\top)$.

Furthermore, we note that the overall matrices

$$C = \begin{pmatrix} A & \tilde{A} \\ B & \tilde{B} \end{pmatrix} \tag{45}$$

for operations H$(i)$, S$(i)$, and CNOT$(i, j)$ each satisfy the identity

$$C\Lambda C^\top = \Lambda = \begin{pmatrix} 0_{n\times n} & 1_{n\times n} \\ 1_{n\times n} & 0_{n\times n} \end{pmatrix}. \tag{46}$$

Therefore, the same identity must immediately hold for all compositions of these gates. Thus, we explicitly see the connection of Clifford gates to the group of $2n \times 2n$ symplectic matrices on $\mathbb{F}_2$, Sp$(2n, \mathbb{F}_2)$, as noted in Refs. [160, 116, 121].

### Chapter 2.2.2: Statement of the problem

Let $n$ be the total number of qubits. Suppose we are given a set of $N$ commuting Pauli operators $\mathcal{P} = \{P_1, \ldots, P_N\}$. We would like to produce a unitary circuit with which we will conjugate the Pauli operators in this set in order to simultaneously diagonalize them. In the interest of simplifying applications to quantum hardware, we would like to reduce the overall circuit depth and the total number of two-qubit gates involved as well as enhance flexibility of diagonalization strategies to accommodate limited qubit connectivity.

It can be shown that such a set may be generated by at most $r \leq \min(n, N)$ Pauli operators. Let us call $T = \{t_1, ..., t_r\}$ a generating set of $\mathcal{P}$ if each element of $\mathcal{P}$ is a product of elements of $T$. That is, for each $P \in \mathcal{P}$, $P = \prod_{i=1}^{r} t_i^{\alpha_i}$ for some $\alpha_i \in \{0, 1\}$ up to an overall

phase. In addition, if no element of $T$ can be expressed as a product of other elements of $T$, we say that the elements of $T$ are independent.

Now, let $T$ be an independent generating set of $\mathcal{P}$. $T$ can be obtained by first constructing the tableau of $\mathcal{P}$ and row reducing the $\mathcal{X}$ and $\mathcal{Z}$ arrays. Importantly, a basis that diagonalizes $T$ will also diagonalize $\mathcal{P}$. Meanwhile, since $T$ is an independent set, it is more constrained than $\mathcal{P}$ is. Therefore, we may reduce our problem to finding a hardware-efficient diagonalization of $T$.

**Chapter 2.3: Qubitwise Diagonalization Algorithm**

In this section, we propose an algorithm for simultaneously diagonalizing Pauli operators generating a desired set. First, we outline the philosophy of the algorithm in Chapter 2.3.1: Approach. More technically, we outline precisely the recursive steps of the proposed algorithm in Chapter 2.3.2: The Algorithm. In kind, we explain how one can apply these steps in order to accommodate limited qubit connectivity in Chapter 2.3.3: Accommodating Qubit Connectivity.

**Chapter 2.3.1: Approach**

Our approach to diagonalize $T$ is to iteratively diagonalize all Pauli operators one qubit at a time. In terms of the tableau for $T$, $(\mathcal{X}|\mathcal{Z})$, for some qubit $i$ we solve the equation $\mathcal{X}'_i = \sum_{j=1}^{n} a_i^j \mathcal{X}_j + b_i^j \mathcal{Z}_j = 0$ for factors $a_i^j$ and $b_i^j$, which we will show prescribes a sequence of Clifford gates with which we conjugate the elements of $T$, rendering all operators diagonal on $i$. In matrix form,

$$\mathcal{X}'_i = \left(\mathcal{X} \,\middle|\, \mathcal{Z}\right) \begin{pmatrix} \boldsymbol{a}_i \\ \boldsymbol{b}_i \end{pmatrix} = 0, \tag{47}$$

where $\boldsymbol{a}_i$ denotes the column vector $\left(a_i^1, \ldots, a_i^n\right)^\top$ and similarly for $\boldsymbol{b}_i$. We may interpret this null vector as the constraint that certain columns in $\mathcal{X}$ or $\mathcal{Z}$ must sum to a zero vector, i.e., $\sum_{j=1}^{n} \mathcal{X}_j a_i^j + \mathcal{Z}_j b_i^j = 0$.

Equation (47) has a non-zero solution if the null space of $(\mathcal{X}|\mathcal{Z})$ is non-trivial. Since $T$ is an independent set of commuting Pauli operators, this tableau forms a matrix of rank $r \leq n$. Also, $(\mathcal{X}|\mathcal{Z})$ has at most $n$ rows but $2n$ columns. Therefore, this matrix must have a null space of dimension $2n - r \geq n$, and so such a vector $(\boldsymbol{a}_\mathrm{i}, \boldsymbol{b}_\mathrm{i})$ exists. We can then obtain a solution $(\boldsymbol{a}_\mathrm{i}, \boldsymbol{b}_\mathrm{i})$ for example by applying Gauss-Jordan elimination on the matrix $(\mathcal{X}|\mathcal{Z})$, as we will discuss more explicitly in Chapter 2.4.1: Preliminaries.

In fact, since the operators considered here are independent and commute, we have $\mathcal{X}^\mathrm{j} \cdot \mathcal{Z}^\mathrm{k} + \mathcal{Z}^\mathrm{j} \cdot \mathcal{X}^\mathrm{k} = 0$, implying that examples of such vectors in the null space include the $r$ rows of $(\mathcal{Z}|\mathcal{X}) = (\mathcal{X}|\mathcal{Z})\Lambda$. More generally, we can see that a vector $u \in \mathbb{F}_2^{2\mathrm{n}}$ is an element of the null space if and only if it encodes a Pauli operator that commutes with each Pauli operator encoded by $(\mathcal{Z}|\mathcal{X})$. (To see this fact, recall that a vector is in the null space when $(\mathcal{X}|\mathcal{Z})u = 0$, or equivalently $(\mathcal{Z}|\mathcal{X})\Lambda u = 0$. Writing out $u = (\boldsymbol{v}, \boldsymbol{w})$, where $\boldsymbol{v}, \boldsymbol{w} \in \mathbb{F}_2^\mathrm{n}$, it follows that $\mathcal{Z}^\mathrm{k} \cdot \boldsymbol{w} + \mathcal{X}^\mathrm{k} \cdot \boldsymbol{v} = 0$, implying $u$ commutes with the Pauli operator encoded by the row $k$ of the tableau $(\mathcal{Z}|\mathcal{X})$, for each $k = 1, \ldots, r$.) In terms of classical coding theory [147], we may view the tableau as a parity check matrix for a linear code spanned by these null vectors as code words.

One can embed this null vector $(\boldsymbol{a}_\mathrm{i}, \boldsymbol{b}_\mathrm{i})$ as the $i$th columns of matrices $A$ and $B$ encoding an overall unitary operation that renders all Pauli operators diagonal on qubit $i$.

Importantly, there is still plenty of freedom in the choices of Clifford operations to specify $\tilde{A}$ and $\tilde{B}$ as well as the other columns of $A$ and $B$. We exploit this freedom to prescribe the following instructions, which generate a particular choice of such matrices sending $\mathcal{X}_\mathrm{i} \mapsto 0$. Additionally, these degrees of freedom as well as the choice of a suitable null vector can be further exploited to make choices that maintain low circuit depth given a particular quantum device where qubit connectivity is not all-to-all. For completeness, we will also show how a suitable null vector can be chosen efficiently.

In short: an element of the tableau's null space indicates columns of $\mathcal{X}$ and $\mathcal{Z}$ that are dependent and therefore may be added to diagonalize operators along some qubit $i$ at each

stage. As we detail below, these addition operations imply a concrete list of simple one- and two-qubit gates on a diagonalizing circuit.

**Chapter 2.3.2: The Algorithm**

Now, we are ready to prescribe the instructions to perform iteratively at each stage. Let $\alpha = 1, \ldots, s \leq n$ be the stage where $n^{(\alpha)}$ digits are not yet diagonal for all Pauli operators. Moreover, $T^{(\alpha)}$ is the corresponding generating set of size $r^{(\alpha)} = |T^{(\alpha)}|$. Stage $\alpha = 1$ begins with the initial problem for our algorithm, i.e., $T^{(1)} = T$. At each stage $\alpha$, we construct the corresponding tableau $(\mathcal{X}^{(\alpha)}|\mathcal{Z}^{(\alpha)})$. Then, we select a vector $(\boldsymbol{v}^{(\alpha)}, \boldsymbol{w}^{(\alpha)})$ in the null space of $(\mathcal{X}^{(\alpha)}|\mathcal{Z}^{(\alpha)})$. Choose a qubit $i$ such that $v^{(\alpha)\mathrm{i}} = 1$ or $w^{(\alpha)\mathrm{i}} = 1$. Pauli operators will be diagonalized on this qubit in two steps by the procedure below:
(1) The first step consists of applying single-qubit Clifford gates to update each column $j = 1, \ldots, n^{(\alpha)}$: $\mathcal{X}^{(\alpha)}{}_{\mathrm{j}} \mapsto \mathcal{X}^{(\alpha)\prime}_{\mathrm{j}} = v^{(\alpha)\mathrm{j}}\mathcal{X}^{(\alpha)}{}_{\mathrm{j}} + w^{(\alpha)\mathrm{j}}\mathcal{Z}^{(\alpha)}{}_{\mathrm{j}}$, according to the rules relating $a$ and $b$ to corresponding single-qubit Clifford gates outlined in Chapter 2.2.1: Clifford Gates and the Symplectic Group.

(a) If $w^{(\alpha)\mathrm{j}} = 0$, then we simply apply the identity gate, i.e., we need not do anything for this $j$.

(b) If $v^{(\alpha)\mathrm{j}} = 0$ and $w^{(\alpha)\mathrm{j}} = 1$, perform a conjugation with the gate $\mathrm{H}(j)$.

(c) If $v^{(\alpha)\mathrm{j}} = 1$ and $w^{(\alpha)\mathrm{j}} = 1$, perform a conjugation with the gate $\mathrm{S}(j)$ followed by a conjugation with the gate $\mathrm{H}(j)$.

At the end of this step, we have

$$\mathcal{X}^{(\alpha)\prime}_{\mathrm{j}} = v^{(\alpha)\mathrm{j}}\mathcal{X}^{(\alpha)}_{\mathrm{j}} + w^{(\alpha)\mathrm{j}}\mathcal{Z}^{(\alpha)}_{\mathrm{j}} \tag{48}$$

with $v^{(\alpha)\mathrm{j}} = 1$ or $w^{(\alpha)\mathrm{j}} = 1$. This step essentially selects all of the columns of $\mathcal{X}^{(\alpha)}$ and $\mathcal{Z}^{(\alpha)}$ that are involved in reducing the column $\mathcal{X}^{(\alpha)}_{\mathrm{i}}$ to zero and stores them in $\mathcal{X}^{(\alpha)\prime}$.
(2) The final step is then to add all of these columns into $\mathcal{X}^{(\alpha)}_{\mathrm{i}}$. We carry out this step using

conjugations with CNOT gates. In particular, for each $j = 1, \ldots, n^{(\alpha)}$, if $v^{(\alpha)\mathrm{j}} = 1$ or $w^{(\alpha)\mathrm{j}} = 1$ and $j \neq i$, perform a conjugation with CNOT$(j, i)$. At the end of this step, the columns $\mathcal{X}^{(\alpha)\prime}_{\mathrm{j}}$ selected by having coefficients $v^{(\alpha)\mathrm{j}} = 1$ or $w^{(\alpha)\mathrm{j}} = 1$ are added to the column $\mathcal{X}^{(\alpha)\prime}_{\mathrm{i}}$. We therefore obtain

$$\mathcal{X}^{(\alpha)\prime\prime}_{\mathrm{i}} = \sum_{\mathrm{j}=1}^{\mathrm{n}} v^{(\alpha)\mathrm{j}} \mathcal{X}^{(\alpha)}_{\mathrm{j}} + w^{(\alpha)\mathrm{j}} \mathcal{Z}^{(\alpha)}_{\mathrm{j}} = 0,$$

which is guaranteed to equal zero as desired since $(\boldsymbol{v}^{(\alpha)}, \boldsymbol{w}^{(\alpha)})$ is in the null space of $(\mathcal{X}^{(\alpha)}|\mathcal{Z}^{(\alpha)})$; see Eq. (47) and the discussion below it.

Thus concludes stage $\alpha$. After we have diagonalized the Pauli matrices acting on qubit $i$ with unitary operations, the Pauli operators acting on the remaining qubits must also commute. Therefore, we can diagonalize the remaining qubits in recursive stages. After stage $\alpha$ is complete, we have $n^{(\alpha+1)} \leq n^{(\alpha)} - 1$. Note $n^{(\alpha+1)}$ is not necessarily $n^{(\alpha)} - 1$, as other qubits beside $i$ may have been diagonalized in the process. Proceeding to the next stage, to obtain $T^{(\alpha+1)}$, we exclude all the qubits that are acted upon only by $I$ or $Z$. Consequently, note that $r^{(\alpha+1)} \leq r^{(\alpha)}$, as the number of distinct generators may decrease after reducing the number of qubits still in consideration. Then, we repeat the above process for $T^{(\alpha+1)}$. At a stage $\alpha = s$ where $n^{(\mathrm{s})} = 1$, $r^{(\mathrm{s})} = 1$ and the step 1 of the procedure above is sufficient to diagonalize the qubit. Thus, the recursion indeed terminates. The complete algorithm is summarized below in pseudocode.

**Algorithm 1** Qubitwise diagonalization

**Input:** A set of commuting Pauli operators acting on $n$ qubits.
**Output:** A circuit simultaneously diagonalizing the set.

1: $\alpha \leftarrow 1$
2: Discard all the qubits on which all Paulis are already diagonal.
3: $n^{(\alpha)} \leftarrow$ Number of remaining qubits
4: **if** $n^{(\alpha)} = 0$ **then**
5: Exit ▷ The diagonalization is complete.
6: **end if**
7: Find independent Pauli operators $T^{(\alpha)}$ ▷ See Chapter 2.2.2: Statement of the problem.
8: $\mathcal{M}^{(\alpha)} \leftarrow \left(\mathcal{X}^{(\alpha)} \middle| \mathcal{Z}^{(\alpha)}\right)$ ▷ Tableau encoding of $T^{(\alpha)}$
9: Find the null space of $\mathcal{M}^{(\alpha)}$
10: Select a vector $(\boldsymbol{v}, \boldsymbol{w})$ in the null space of $\mathcal{M}^{(\alpha)}$
11: Select $i$ such that $v^{\mathrm{i}} = 1$ or $w^{\mathrm{i}} = 1$ ▷ qubit $i$ on which all Paulis will be diagonalized
12: **for** $j = 1$ to $j = n^{(\alpha)}$ **do**
13: **if** $v^{\mathrm{j}} = 0$ AND $w^{\mathrm{j}} = 1$ **then**
14: Perform a conjugation with H $(j)$
15: **end if**
16: **if** $v^{\mathrm{j}} = 1$ AND $w^{\mathrm{j}} = 1$ **then**
17: Perform a conjugation with S $(j)$
18: Perform a conjugation with H $(j)$
19: **end if**
20: **end for**
21: **for** $j = 1$ to $j = n^{(\alpha)}$ **do**
22: **if** ($v^{\mathrm{j}} = 1$ or $w^{\mathrm{j}} = 1$) AND $i \neq j$ **then**
23: Perform a conjugation with CNOT$(j, i)$
24: **end if**
25: **end for**
26: $\alpha \leftarrow \alpha + 1$
27: Go to Line 2.

Note that the example of a simple construction for step 2 above provides a circuit with depth linear with the number of CNOT gates at each stage, assuming hardware on which commuting CNOT gates that share qubits *cannot* be performed in parallel. In Section Chapter 2.4.2: Circuit Depth, we discuss another construction with circuit depth that grows only logarithmically with the number of CNOT gates at each stage. Via this latter construction we achieve the $O(n \log r)$ overall circuit depth advertised.

### Chapter 2.3.3: Accommodating Qubit Connectivity

We now turn our attention to discussing how this algorithm may be tailored to hardware with limited connectivity, in the sense that we would like it to involve relatively few SWAP gates. Suppose that the graph $G = (V, E)$ represents the hardware connectivity. That is, a qubit $q_i$ is represented by a vertex in $V$, and there is an edge $(q_i, q_j) \in E$ if qubits $q_i$ and $q_j$ are directly connected on the hardware (i.e., permitting a CNOT operation with either qubit as target or control and without SWAP operations).[11] Qualitatively, the strategy is to exploit the degrees of freedom still allowed by the algorithm described in the previous section, particularly in the choices of the null vector and the order of additions in tableau columns prescribed by this null vector. We elaborate on how these choices can be related and how they can be made with limited qubit connectivity in mind.

The first task is to choose a null space vector $(\boldsymbol{v}, \boldsymbol{w})$ that is compatible with the qubit connectivity of a given quantum device. However, we stress that the choice of this vector also entails a list of qubits, for pairs of which ($q_i$ and $q_j$) we add corresponding column vectors of the tableau, via CNOT gates (and potentially SWAP gates as well). We would like to choose qubit pairs whose paths involve relatively few SWAP gates to be realized. That is, for all $i$ such that $v^i = 1$ or $w^i = 1$ and $j$ such that $v^j = 1$ or $w^j = 1$, we desire a relatively short path between vertices $q_i$ and $q_j$ in the connectivity graph $G$. As such, we can choose a null vector for which the qubits $q_i$ and $q_j$ are relatively close to one another in $G$. Furthermore, we give below an explanation of how, given an arbitrary null space vector, we can choose pairs of qubits on which we will perform CNOT gates, in order to further accommodate limited connectivity.

Now given an arbitrarily chosen null vector, we can describe the problem of choosing how one adds columns as per step 2 for this null vector. (We may assume that step 1 of the algorithm is already completed, as it involves only one-qubit gates.) For step 2, let us

[11] One may also consider hardware with yet further limited connectivity such that a gate CNOT$(i, j)$ may be performed but not CNOT$(j, i)$. The remainder of this discussion below may be generalized to this case, however potentially requiring yet additional resources to accommodate such limitations.

denote the qubits where $(\boldsymbol{v}, \boldsymbol{w})$ is nonzero as $Q = \{q_1, q_2, q_3, \ldots\}$ and the columns $\mathcal{X}_{\mathrm{q}}$ with $q \in Q$ to be added using CNOT gate conjugations. In general, since the pairs $(q_{\mathrm{i}}, q_{\mathrm{j}}) \subseteq V$ may be disconnected on the hardware in consideration, we would need to perform appropriate conjugations with SWAP gates resulting in $q_{\mathrm{i}} \mapsto q'_{\mathrm{i}}$ and $q_{\mathrm{j}} \mapsto q'_{\mathrm{j}}$ such that $q'_{\mathrm{i}}$ and $q'_{\mathrm{j}}$ are connected on the hardware (i.e., share an edge in $E$). This transformation can be accomplished along any path in $G$ connecting $q_{\mathrm{i}}$ and $q_{\mathrm{j}}$, and the number of SWAP gates depends on the length of the path. As such, we seek to minimize the length of a path that traverses all of the qubits $q \in Q$. Our minimization problem is similar to the well-known traveling salesperson problem (TSP) [110]. However, in contrast with the TSP, which requires every node be visited exactly once, our problem requires only the nodes in $Q$ be visited once. That is, a node not in $Q$ may or may not be visited at all. This minimization problem naturally maps to the so-called shortest-path problem with specified nodes (SPPSN)[12] [185], where the specified nodes are the nodes in $Q$. This problem has been extensively studied, and several solutions are provided in, e.g., Refs. [185, 127, 65, 102]. Indeed, solving the SPPSN gives us a sequence of qubits $\{q_{\sigma 1}, q_{\sigma 2}, q_{\sigma 3}, ...\}$ along which the number of SWAP gates is minimized when performing step 2. Finally, we note that the choice of null vector essentially dictates which SPPSN we must solve.

As explained above, modifications in step 2 of our algorithm can allow for multiple avenues to reduce the SWAP gates required. Not only can we draw upon efficient solutions to the related generalization of a TSP (i.e., choose how to add columns of $\mathcal{X}'$), but also we are afforded a choice of which such problem we would like to solve (i.e., choose which columns of $\mathcal{X}'$ to be added according to $(\boldsymbol{v}, \boldsymbol{w})$). In Chapter 2.5.3: Linear Qubit Connectivity, we demonstrate how this strategy can be adapted to hardware with linear connectivity.

**Chapter 2.4: Analysis of the Algorithm**

Here, we estimate the size of quantum circuits produced by the algorithm presented in the

[12] In other words, the problem is to find the shortest path passing through a subset of vertices in a graph.

previous section. In particular, we focus on the overall circuit depth as well as the number of CNOT gates entailed. First, we explain in Chapter 2.4.1: Preliminaries how these qualities of the circuit are related to the null vectors introduced in Chapter 2.3.1: Approach. With this understanding in hand, we then can estimate the circuit depth (Chapter 2.4.2: Circuit Depth) and total two-qubit gate count (Chapter 2.4.3: CNOT Gate Count) required to implement the diagonalization circuits prescribed by our algorithm.

**Chapter 2.4.1: Preliminaries**

Before we proceed, it is helpful to recall the perspective that our algorithm essentially searches for $\mathcal{X}$ and $\mathcal{Z}$ columns that are dependent and adds them to diagonalize along some qubit $i$ at each stage. This interpretation is useful in estimating the cost.

**Definition 1** *The symplectic weight of a vector* $(v, w) \in \mathbb{F}_2^{2n}$ *is defined as*

$$\omega(\boldsymbol{v}, \boldsymbol{w}) = \left|\left\{i \mid (v^i, w^i) \neq (0,0)\right\}\right|. \tag{49}$$

In other words, the symplectic weight counts the number of digits not equal to $I$ in the corresponding Pauli operator (i.e., the operator's Hamming weight). We will also find $\omega(\boldsymbol{v}, \boldsymbol{w})$ of null space vectors helpful in estimating the number of CNOT gate conjugations.

**Lemma 1** *Given a vector* $(\boldsymbol{v}, \boldsymbol{w})$ *in the null space of* $(\mathcal{X}^{(\alpha)}|\mathcal{Z}^{(\alpha)})$*, our algorithm prescribes* $\omega(\boldsymbol{v}, \boldsymbol{w}) - 1$ *CNOT gate conjugations to diagonalize one qubit.*

Suppose qubit $i$ is to be diagonalized using the vector $(\boldsymbol{v}, \boldsymbol{w})$ through steps 1 and 2. By Definition 1, step 1 will update $\omega(\boldsymbol{v}, \boldsymbol{w})$ columns in $\mathcal{X}$. Then, step 2 will use $\omega(\boldsymbol{v}, \boldsymbol{w}) - 1$ CNOT conjugations, because there are $\omega(\boldsymbol{v}, \boldsymbol{w}) - 1$ columns in $\mathcal{X}$ to be added to column $\mathcal{X}_i$.

**Lemma 2** *The number of CNOT gate conjugations required to diagonalize a given qubit at stage* $\alpha$ *is at most* $r^{(\alpha)}$ *if* $n^{(\alpha)} > r^{(\alpha)}$*, and at most* $r^{(\alpha)} - 1$ *if* $n^{(\alpha)} = r^{(\alpha)}$.

We first consider the case $n^{(\alpha)} > r^{(\alpha)}$. At stage $\alpha$, the rank of $(\mathcal{X}^{(\alpha)}|\mathcal{Z}^{(\alpha)})$ is $r^{(\alpha)}$, implying that any collection of $r^{(\alpha)} + 1$ columns is a dependent set. Therefore, there exists a vector $(\boldsymbol{v}, \boldsymbol{w})$ in the null space of $(\mathcal{X}^{(\alpha)}|\mathcal{Z}^{(\alpha)})$ with weight $\omega(\boldsymbol{v}, \boldsymbol{w}) \leq r^{(\alpha)} + 1$. Consequently, using Lemma 1, we demand at most $r^{(\alpha)}$ CNOT gate conjugations at this stage.

For the case $n^{(\alpha)} = r^{(\alpha)}$, we know $\omega(\boldsymbol{v}, \boldsymbol{w}) \leq r^{(\alpha)}$ for all $(\boldsymbol{v}, \boldsymbol{w})$ in the null space, because there are only $r^{(\alpha)}$ qubits. Therefore, this case entails at most $r^{(\alpha)} - 1$ CNOT gate conjugations.

Finally, we stress that, in either case, such a null space vector can be produced efficiently. For example, we can find such a null space vector by finding a set of $\leq r^{(\alpha)} + 1$ columns adding to zero. To demonstrate this bound, we first transform the matrix $(\mathcal{X}^{(\alpha)}|\mathcal{Z}^{(\alpha)})$ to its reduced row-echelon form in polynomial complexity [196]. Then, up to a relabeling of qubits, our tableau can be written in the so-called standard form of a stabilizer code (see e.g. [147]):

$$\left(1_{\mathrm{r}^{(\alpha)}\times\mathrm{r}^{(\alpha)}} \quad \mathcal{A}_{\mathrm{r}^{(\alpha)}\times(\mathrm{n}^{(\alpha)}-\mathrm{r}^{(\alpha)})} \quad | \quad \mathcal{B}_{\mathrm{r}^{(\alpha)}\times\mathrm{n}^{(\alpha)}}\right) \tag{50}$$

where $\mathcal{A}$ and $\mathcal{B}$ are matrices over $\mathbb{F}_2$ with the indicated dimensions. In this form, any column of $\mathcal{A}$ or $\mathcal{B}$ is clearly a linear combination of the columns of 1; the $m$th column $c_{\mathrm{m}}$ ($r^{(\alpha)} < m \leq 2n$) of the transformed tableau above can be written as $c_{\mathrm{m}} = \sum_{\mathrm{i}=1}^{\mathrm{r}^{(\alpha)}} c_{\mathrm{m}}^{\mathrm{i}} \mathbf{e}_{\mathrm{i}}$. In other words, any column of $\mathcal{A}$ or $\mathcal{B}$ may be added with a subset of the columns of 1 to yield a zero vector, and so a vector encoding this sum would be a suitable null vector to start our algorithm of Chapter 2.3.2: The Algorithm. Explicitly, the collection of these columns to be summed corresponds to a null vector $u \in \mathbb{F}_2^{2\mathrm{n}^{(\alpha)}}$ with $u^{\mathrm{i}} = 1$ and $u^{\mathrm{m}} = 1$ only at $i$ and $m$ for which $c_{\mathrm{m}}^{\mathrm{i}} = 1$. In fact, one may choose the column $c$ of $\mathcal{A}$ or $\mathcal{B}$ with the lowest (Hamming) weight to reduce the weight of the corresponding null vector $\omega(u)$ as well as the gate cost that it entails (as per Lemma 1).

### Chapter 2.4.2: Circuit Depth

Now, we will analyze the overall circuit depth of the algorithm. Notably, on hardware where commuting CNOT gates can be performed in parallel, as discussed in e.g., Ref. [101], we in fact already have constant depth at each stage via the instructions provided in Chapter 2.3.2: The Algorithm, yielding overall depth $O(n)$. Remarkably, accommodating more generic hardware, we find that the circuit has depth $O(n \log r)$ in contrast with the number of gates, which we will show is $O(nr)$.

At each stage $\alpha$, we note that step 1 produces a circuit of depth at most two, because only single-qubit gates may be performed on each qubit. Meanwhile, as we shall argue below, the CNOT gates conjugations in step 2 can be performed with depth $O(\log r^{(\alpha)})$. Moreover, since there are at most $n$ recursive stages in the algorithm, the overall circuit has depth $O(n \log r)$.

Recall that step 1 modifies the columns involved in the diagonalization according to Eq. (48), and step 2 adds these $\mathcal{X}'$ columns. Without loss of generality, let us denote these columns by $\mathcal{X}'_1, \mathcal{X}'_2, ..., \mathcal{X}'_\omega$ where $\omega$ is the weight of the null space vector used for diagonalization. In step 2, we can add these columns in pairs sequentially (as described earlier in Chapter 2.3.2: The Algorithm), or alternatively we may form disjoint pairs to be added in parallel to the same end. That is, we can perform CNOT$(2j, 2j-1)$ resulting in $\mathcal{X}'_{2j-1} \leftarrow \mathcal{X}'_{2j-1} + \mathcal{X}'_{2j}$ for $j \in \{1, 2, \ldots, \lfloor \omega/2 \rfloor\}$. Note that all of these CNOT gates amount to depth 1, since they each act on totally different qubits. Now, we add these resulting columns $\mathcal{X}'_1, \mathcal{X}'_3, \ldots$ in the same fashion. This process repeats until we are left with only one $\mathcal{X}$ column, and each round of this pairwise addition process is a circuit with depth 1. We summarize this procedure in pseudocode in Algorithm 2, replacing lines 21–25 of the instructions given in Algorithm 1.

**Algorithm 2** Step 2 yielding logarithmic depth

**Input:** A null space vector $(\boldsymbol{v}, \boldsymbol{w})$.
**Output:** A modified step (2) of the algorithm.

$Q \leftarrow \{q = 1, \ldots, n^{(\alpha)} \mid v^{\mathrm{q}} = 1 \text{ or } w^{\mathrm{q}} = 1\}$
**while** $|Q| > 1$ **do**
  **for** $j = 1$ to $j = \lfloor |Q|/2 \rfloor$ **do**
    Perform a conjugation with $\mathrm{CNOT}(q_{2\mathrm{j}}, q_{2\mathrm{j}-1})$
  **end for**
  $Q \leftarrow Q \setminus \{q_{2\mathrm{j}} \mid j = 1, \ldots, \lfloor |Q|/2 \rfloor\}$
**end while**

Since each round of pairwise additions reduces the number of $X$ columns to be added by about one half, there are $O(\log_2 \omega)$ such rounds, each with depth 1. Using Lemma 2, we can choose $\omega \leq r^{(\alpha)} + 1$, and so each stage $\alpha$ involves a circuit with depth $O(\log r^{(\alpha)})$.

### Chapter 2.4.3: CNOT Gate Count

Having analyzed the circuit depth, we now turn our attention to discussing the total number of CNOT gates.

**Theorem 1** *The number of CNOT gate conjugations required by the algorithm (Chapter 2.3.2: The Algorithm) is at most* $n\,r - \frac{r(r+1)}{2}$.

To establish this bound, we will use Lemma 2 to count the number of CNOT gate conjugations at each stage. The first stage, $\alpha = 1$, requires at most $r^{(1)} = r$ CNOT gate conjugations. For the subsequent stage, $\alpha = 2$, if $n^{(2)} \geq r$, the number of independent generators at $r^{(2)}$ may remain $r$. Consequently, for all stages $\alpha$ such that $n^{(\alpha)} > r$, the inequality $r^{(\alpha)} \leq r$ holds. There are at most $(n - r)$ such stages, amounting to at most $(n - r)\,r$ CNOT gate conjugations. Once we reach a stage $s$ such that $n^{(\mathrm{s})} = r$, the stage $\alpha = s + j$ has $r^{(\mathrm{s+j})} \leq n^{(\mathrm{s+j})} \leq r - j$, because each stage diagonalizes on at least one qubit. The number of CNOT gate conjugations in these stages is therefore at most $\sum_{\mathrm{j}=0}^{\mathrm{r}-1}(r - j - 1) = r(r-1)/2$. Putting both CNOT gate conjugation counts together, we obtain $n\,r - r(r+1)/2$.

This bound is also derived for a different algorithm in Ref. [53]. Notably, in the limiting

case $r = n$, this bound reduces to the known result $n(n-1)/2$ (see, e.g., Refs. [182, 143]). It is important to note that our algorithm guarantees this bound without further classical optimization. That is, one may select any $r^{(\alpha)} + 1$ columns to form a dependent set at each stage $\alpha$, and this upper bound will hold. Now, we demonstrate that we can achieve a lower estimate of CNOT cost by minimizing the size of the dependent set of columns we select in each stage, entailing a higher classical complexity cost.

**Lemma 3** *A qubit can be diagonalized at stage $\alpha$ with at most $\lfloor \frac{r^{(\alpha)}}{2} \rfloor$ CNOT gate conjugations.*

In exchange for a lower gate cost, one may accept a large classical complexity by searching the entire null space for the vector with the lowest symplectic weight by Lemma 1. Below, we will use the properties of the null space of $(\mathcal{X}|\mathcal{Z})$ at each stage to establish a stricter lower bound on the number of CNOT gates.

The rows of $(\mathcal{Z}^{(\alpha)}|\mathcal{X}^{(\alpha)})$ span a $r^{(\alpha)}$-dimensional subspace of the null space, due to the fact that the Pauli operators represented by each row of $(\mathcal{X}^{(\alpha)}|\mathcal{Z}^{(\alpha)})$ commute with one another. Moreover, the Pauli operators in $(\mathcal{Z}^{(\alpha)}|\mathcal{X}^{(\alpha)})$ may be viewed as a $[[n^{(\alpha)}, k, d]]$ stabilizer code. The code maps $k = n^{(\alpha)} - r^{(\alpha)}$ logical qubits to $n^{(\alpha)}$ physical qubits with the capability of correcting at most $(d-1)/2$ errors. Moreover, we call $S$ the stabilizer generated by the Pauli operators represented by the rows of $(\mathcal{Z}^{(\alpha)}|\mathcal{X}^{(\alpha)})$. For a more general review, see, e.g., Refs. [82, 147].

Let $C(S)$ be the centralizer of $S$, the Pauli operators that commute with each element of $S$. For stabilizer codes, it is known that the normalizer is identical to the centralizer $N(S) = C(S)$ [82]. In Chapter 2.3.1: Approach, we argued that a vector $u$ commutes with every element of $(\mathcal{Z}^{(\alpha)}|\mathcal{X}^{(\alpha)})$, i.e., is an element of $N(S)$, if and only if it is in the null space of $(\mathcal{X}^{(\alpha)}|\mathcal{Z}^{(\alpha)})$. Therefore, the task of finding a null space vector $u$ of weight $\omega$ is equivalent to searching $N(S)$ for a Pauli operator of the desired weight. On the other hand, the quantum Singleton bound [119, 160, 44] directly implies that there exists a Pauli

operator in $N(S)$ with weight $\omega = d \leq \lfloor r^{(\alpha)}/2 \rfloor + 1$. Finally, invoking Lemma 1 concludes the proof.

**Theorem 2** *The number of CNOT gate conjugations required by the algorithm (Chapter 2.3.2: The Algorithm) is at most* $n\lfloor \frac{r}{2} \rfloor - \lfloor \frac{r}{2} \rfloor^2$.

To achieve this bound, at each stage $\alpha$, we select the vector with weight $d \leq \lfloor r^{(\alpha)}/2 \rfloor + 1$ promised by Lemma 3. Then, we follow an argument similar to that of Theorem 1 to find the total cost. That is, while $n^{(\alpha)} \geq r$, we use at most $\lfloor r/2 \rfloor$ CNOT gate conjugations. Since there are at most $n - r + 1$ of such stages, they amount to at most $(n - r + 1)\lfloor r/2 \rfloor$ CNOT conjugations. After the stage $s$ where $n^{(\mathrm{s})} = r$, we use at most $\lfloor (r - i)/2 \rfloor$ for each subsequent stage $s + i$. These stages amount to at most $\sum_{\mathrm{i}=1}^{\mathrm{r}-1} \lfloor (r - i)/2 \rfloor = \lfloor r/2 \rfloor \lfloor (r - 1)/2 \rfloor$ CNOT conjugations. Putting both contributions together, we obtain at most $(n - r + 1)\lfloor r/2 \rfloor + \lfloor r/2 \rfloor \lfloor (r - 1)/2 \rfloor$ CNOT conjugations, which gives us the bound claimed.

In the above argument, we have shown an equivalence between finding the distance of a quantum stabilizer code and reducing the CNOT count at one stage of our qubitwise diagonalization to $\sim r^{(\alpha)}$. Finding the distance of a code is known to be NP-hard [183], and so we may expect to practically find the operator(s) of the normalizer $N(S)$ with the lowest weight only for a relatively small number of qubits ($n \lesssim 30$ on ordinary computers). Equivalently, this problem may be restated as minimizing

$$\min_{\{\mathrm{b}_1 + \cdots + \mathrm{b}_{2\mathrm{n}-\mathrm{r}} \leq \mathrm{z}\}} \omega \left( \sum_{\mathrm{i}=1}^{2\mathrm{n}-\mathrm{r}} b_{\mathrm{i}} N^{\mathrm{i}} \right), \tag{51}$$

where $N^{\mathrm{i}}$ are vectors encoding the independent generators of $N(S)$, each $b_{\mathrm{i}} = 0$ or 1, and the sum between $b_{\mathrm{i}} N^{\mathrm{i}}$ vectors is Boolean (i.e., XOR) and the sum over $b_{\mathrm{i}}$ is decimal. Here, we must take $z = 2n - r$ to search the entirety of $N(S)$ for the lowest-weight solution. Nevertheless, a search through linear combinations of fixed sizes $\leq z$ is still polynomial in

$n$ and still produces a vector of weight at least as low as that obtained from choosing among $N^i$.

On the other hand, it is crucial to note that there is a 'greediness' to optimizing the (symplectic) weight of our null vector at each stage of our algorithm, as opposed to optimizing the choice for a circuit depth overall. In the sense, completely optimizing at this stage might not always produce the overall lowest circuit depth after diagonalizing over *all* qubits of our operators. In the following section, we will discuss further comparisons between circuit depths obtained with null vectors chosen via Gaussian elimination sans optimization (see Lemma 2 and its discussion below) and those chosen via complete optimization at each stage.

### Chapter 2.5: Examples

In this section, we evaluate the performance of our algorithm for a variety of example applications. In particular, we use a proposed method of randomized benchmarking [182] to assess the circuit cost resulting from our algorithm under various circumstances in Chapter 2.5.1: Random Sets of Commuting Pauli Operators. Secondly, in Chapter 2.5.2: Molecular Hamiltonians, we assess the algorithm's performance in diagonalizing molecular Hamiltonians. Finally, we provide an example molecular Hamiltonian for which our algorithm accommodates limited qubit connectivity relatively well in Chapter 2.5.3: Linear Qubit Connectivity.

#### Chapter 2.5.1: Random Sets of Commuting Pauli Operators

In this subsection, we apply our diagonalization algorithm to sets of commuting Pauli operators generated randomly. We use the algorithm constructed in Ref. [182] to generate a sample of 100 distinct sets, each containing $n$ Pauli operators acting on $n$ qubits. In our implementation, we use both the classically efficient algorithm outlined below Lemma 2 ("no optimization") to select a null space vector of weight $\leq r$ and an exhaustive search

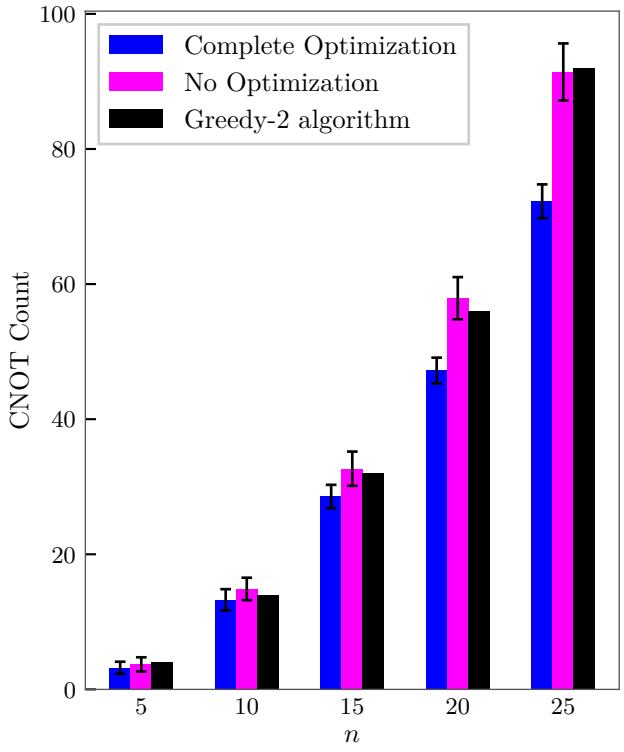


Figure 5: The number of CNOT conjugations involved in diagonalizing $n$ commuting Pauli operators acting on $n$ qubits via our qubitwise diagonalization strategy, averaged over 100 sets generated randomly. Each uncertainty bar is the square root of the sample variance of the 100 sets. We compare gate counts found with and without minimizing the circuit depth, iteratively at each stage of our algorithm (see discussion following Theorem 2). In addition, the magenta (right) bars are in each case the smallest gate counts obtained in Ref. [182], via the "greedy-2" algorithm.

through the null space to select the vector of lowest weight ("complete optimization"). For each value of $n$, we report the average number of CNOT conjugations needed over the 100 sets. The error bars in our results are given by the square root of the sample variance. We also superimpose our results to the lowest results obtained in Ref. [182] in Fig. 5.

In particular, we can see that there is a marked reduction in the quantum circuit cost when searching for a low-weight null vector to prescribe each stage of our algorithm, at least for totally randomized sets of Pauli operators. In other words, here we see a trade off, between classical complexity of producing a low-weight null vector and resulting the quantum circuit complexity. Particularly, for $r \ll n$, this classical complexity may become highly prohibitive since the null space is of dimension $2n - r$, in which case the no optimization case conveniently produces a vector of (low) weight at most $r$ anyhow. For the rest of this section, to assess the costs on a quantum computer of our algorithm while keeping classical complexity low, we limit our algorithm to no optimization (i.e., selecting null vectors via the procedure outlined under Lemma 2).

Now, we illustrate how our number of CNOT gates also depends on $r$, the number of independent generators of a set of commuting Paulis. We first fix $n$, the number of qubits, and again consider randomly generated sets of $r$ independent commuting Pauli operators. To obtain a set with only $r \leq n$ operators, we randomly select $n - r$ operators to delete from the set. Then, we construct diagonalization quantum circuits and report the resulting number of CNOT gates. Figure 6 shows the results for $n = 10$. As expected per our discussion in Chapter 2.4.3: CNOT Gate Count, we find that, for fixed $n$, gate count follows a quadratic trend in $r$ as $f(r) = -ar^2 + br$ [up to a constant shift] for $a, b > 0$.

**Chapter 2.5.2: Molecular Hamiltonians**

Having assessed the algorithm's performance in diagonalizing commuting Hamiltonians generated randomly, we will now consider its performance for a collection of molecular Hamiltonians as more practical examples. In particular, we consider one ionic compound $HeH^+$ as well as the molecules LiH, $BeH_2$, $NH_3$, and $BH_3$.

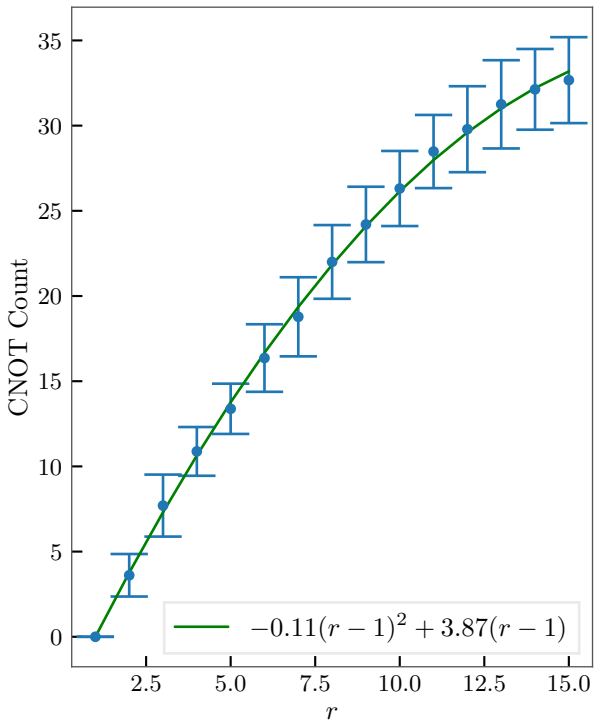


Figure 6: The number of CNOT conjugations obtained in diagonalizing a set of $r$ independent commuting Pauli operators acting on $n = 15$ qubits using the procedure outlined below Lemma 2 (no optimization). The data points are averages over 100 randomly generated sets. The uncertainty bars displayed are the square roots of the variances.

The Hamiltonians as linear combinations of Pauli operators are obtained from Pennylane [22] Quantum Chemistry datasets. For each of these species, we use the STO-3G basis, and the optimal bond length given in the dataset. Given a Hamiltonian, before diagonalization we must divide the Pauli operators into sets of mutually commuting operators. As in Refs. [145, 182, 176], this problem can be reduced to a graph-coloring problem, and we use the independent set strategy in NetworkX [91] to color the graph. Table 1 shows the results of diagonalization of each of these Hamiltonians. In each case, we observe that both the average number of CNOT gate conjugations and the circuit depth tend to be near once or twice the number of independent operators generating each set ($r \leq n$). However, it is worth noting that different choices of strategies to form commuting sets of Pauli operators (while using the same diagonalization algorithm) may allow for

Table 1: Results of qubitwise diagonalization of molecular Hamiltonians. Throughout the diagonalization, the null space vector at each stage is chosen using the (classically efficient) algorithm described below Lemma 2. In each row, $n$ and $N$ are the number of qubits and the total number of Pauli operators in each Hamiltonian, respectively. $\kappa$ is the number of sets of commuting Pauli operators, while $r$ is the average number of independent generators per commuting set. The columns CNOT and Depth list the average numbers of CNOT gate conjugations and the average quantum circuit depths obtained, respectively, with averages taken over the different sets of commuting Pauli operators in the Hamiltonian. Finally CNOT SD and Depth SD are the standard deviations of the corresponding columns.

| Molecule | $n$ | $N$ | $\kappa$ | $r$ | CNOT | CNOT SD | Depth | Depth SD |
|---|---|---|---|---|---|---|---|---|
| $HeH^+$ | 4 | 26 | 3 | 4.00 | 2.00 | 1.63 | 3.33 | 3.40 |
| LiH | 12 | 630 | 25 | 9.00 | 7.44 | 3.42 | 11.12 | 4.34 |
| $BeH_2$ | 14 | 665 | 19 | 11.16 | 9.00 | 3.28 | 11.68 | 4.22 |
| $NH_3$ | 16 | 2296 | 80 | 13.10 | 21.44 | 8.34 | 22.49 | 7.44 |
| $BH_3$ | 16 | 2496 | 97 | 12.01 | 18.21 | 6.36 | 21.26 | 6.64 |

higher or lower average gate counts or depths per set.

Empirically we find that, for these more physically typical Hamiltonian models rather than randomized sets, in fact a lower circuit complexity is obtained from no optimization rather than complete optimization. From these cases, we may reasonably suspect that, in general, relatively local and symmetrical Hamiltonians modeling physical systems are more amenable to this simple classical procedure for producing circuit instructions than arbitrarily non-local and asymmetrical Hamiltonians of randomized benchmarking.

**Chapter 2.5.3: Linear Qubit Connectivity**

Further, we demonstrate the strategy presented in Chapter 2.3.3: Accommodating Qubit Connectivity assuming a hardware with linear connectivity. As a proof of principle, we use the $H_4$ chain Hamiltonian derived in Ref. [143]. This Hamiltonian was obtained by setting the inter-atomic distance $\Delta = 1.0$ and using the STO-3G basis. The Hamiltonian is then mapped to eight-qubit Pauli operators using the Bravyi-Kitaev transformation [33]. To compare, we use the same division of the Hamiltonian into ten collections of commuting Pauli operators.

First, we consider the set of 20 Pauli operators shown in Fig. 15 of Ref. [143]. There, the

authors derived a circuit with 13 H gates, 18 CNOT gates, 21 CZ gates, and 66 SWAP gates assuming a hardware with linear connectivity. Via our algorithm of Chapter 2.3: Qubitwise Diagonalization Algorithm, we can produce a simpler circuit, with only seven H gates, five CNOT gates, and 11 SWAP gates. Figures 7a and 7b show the diagonalization circuit assuming fully connected hardware and linearly connected hardware, respectively.

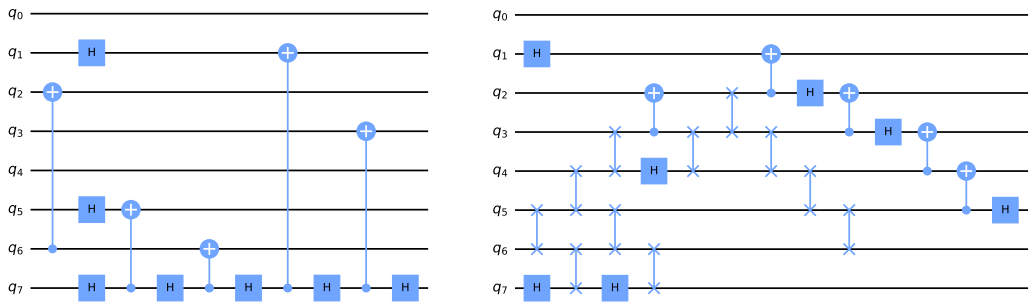


(a) (b)

Figure 7: Diagonalization circuits of a large commuting sub-Hamiltonian of a $H_4$ chain, derived in Fig. 15 of Ref. [143]. We assume a device (a) with full qubit connectivity and (b) with linear qubit connectivity. In the latter case, we apply the methods of Chapter 2.3.3: Accommodating Qubit Connectivity, involving extra SWAP gates in order to implement more local two-qubit operations. We use the no optimization strategy to find a null space vector throughout the diagonalization.

The nine remaining sets of commuting Pauli operators are much simpler than the one discussed above. In the previous literature, the authors were able to derive simple circuits, notably with no SWAP gates and at most two two-qubit gates. Our algorithm produces similar results diagonalizing the Pauli operators in each set with no SWAP gates and at most two two-qubit gates per set.

### Chapter 2.6: Conclusions

This paper introduces an algorithm to simultaneously diagonalize Pauli operators, whose combinations are frequently used to compute observables as well as unitary operations such as in quantum simulation algorithms. Due to the iterative nature of the algorithm, in

which we seek to diagonalize all operators over one qubit at a time, we find this algorithm is additionally convenient in adaptations to quantum hardware on which qubit connectivity is very limited. Moreover, we are able to see from analytic arguments that the scaling for depths of the resulting circuits prescribed by our algorithm is exceptionally low, scaling linearly in the total number of qubits and logarithmically in the number of independent generators of the operators. In kind, we can analytically count the total number of two-qubit gates to be competitive with other recent constructive diagonalization algorithms.

In this paper, we have further demonstrated that the circuits we produce maintain short circuit depth and low two-qubit gate count in example Hamiltonians such as random Hermitian operators and those describing molecular systems. It remains to be demonstrated whether the circuit depth obtained here can be substantially improved or is in fact optimal. Likewise, we have seen that there are choices in our algorithm that can be exploited to further accommodate limited connectivity, though making the optimal such choice may be formulated as a generalized TSP. Therefore, further work can be done to optimize these choices based upon the particular hardware in consideration. Nevertheless, we expect that the framework for diagonalization suggested by our algorithm will enable future work to accommodate such hardware.

Additionally, let us point out that algorithms that form the clusters of commuting operators to be diagonalized must be designed in parallel with these diagonalization algorithms to produce the simplest circuits possible overall. As such, developments in forming commuting clusters of operators would similarly assist in the effort to efficiently diagonalize such clusters overall as well.

## Chapter 3: Quantum Circuits of Diagonal Unitaries

**Abstract**

We discuss the implementation of lattice gauge theories on digital quantum computers, focusing primarily on the number of quantum gates required to simulate their time evolution. We find that to compile quantum circuits, using available state-of-the-art methods with our own augmentations, the cost of a single time step of an elementary plaquette is beyond what is reasonably practical in the current era of quantum hardware. However, we observe that such costs are highly sensitive to the truncation scheme used to derive different Hamiltonian formulations of non-Abelian gauge theories, emphasizing the need for low-dimensional truncations of such models in the same universality class as the desired theories.

### Chapter 3.1: Introduction

Among the many future applications of quantum computing to solving physics problems, the simulation of non-Abelian gauge theories is one of the most desired. Gauge theories describe all fundamental forces of the Universe, but many of their features are inherently non-perturbative and resistant to analytical analysis. Even stochastic numerical methods, despite recent advancements, leave almost untouched the many-body baryon problem and real-time observables, both of which are of great phenomenological importance.
Gauge theories, like any field theory, have an infinite-dimensional Hilbert space, while digital quantum computers have finite and—for the foreseeable future—small quantum registers. Therefore, some kind of truncation of the Hilbert space is necessary. One common truncation is the substitution of the continuum, infinite space by a finite lattice. The use of a spatial lattice has the added benefit of providing an ultraviolet cutoff necessary for the non-perturbative definition of the theory. Since this step has been extensively studied in the context of lattice gauge theories and their numerical simulation

with (classical) computers, much is known about it. For instance, the concept of universality controls the continuum limit that is necessary as the last step of these calculations. It is found that a variety of lattice Hamiltonians lead to the same continuum limit and that some symmetries are essential in recovering the proper continuum limit (for instance, gauge symmetry), while others arise naturally in the continuum limit (for instance, rotational invariance). In purely fermionic theories, the use of a finite spatial lattice is enough to render the Hilbert space finite-dimensional. In contrast, bosonic theories, defined over even a single spatial point (equivalent to the quantum mechanics of a particle in one dimension), already have an infinite-dimensional Hilbert space. As such, it is necessary to have a truncation of not only physical space but also *field* space.
Several methods to accomplish this goal have been suggested in different models [138, 42, 193, 194, 192, 187, 195, 19, 12, 118, 163, 58, 125, 49, 7]. For some of these proposals, besides the spatial continuum limit, an independent field space continuum limit is required. In this case, the dimension of the Hilbert space grows as the last limit is taken, and the issue we consider in the present paper (the cost in terms of quantum gates) becomes more severe. In other proposals, an argument is made that, even with the field space truncated, the resulting theories are in the same universality class of the targeted continuum theory. In that case, the limit where dimension of the Hilbert space grows does not need to be explored, offering a great advantage in terms of simplicity. The combined discretization of physical and field space is sometimes called *qubitization*. For gauge theories in four spacetime dimensions, no general qubitization method has been established, although qubitizations have been found for simpler models [13, 171, 28, 10, 170]. Nevertheless, there are some old discretized models that could play this role and have the proper symmetries and fairly small Hilbert spaces. We use some of these models to estimate the gate-complexity of simulating gauge theories.
In Chapter 3.2: The compilation method we describe the compilation method that we use to find a quantum circuit implementing the Hamiltonian evolution. This method does *not*

exploit specific features of gauge theories and is applicable to any Hamiltonian. The method is composed of many parts; all but the final one have been known in the literature. To our knowledge they have never been put together as we do here.

In Chapter 3.3: Examples we apply this method to a couple of models to test our compilation method. These models, an ensemble of random diagonal Hamiltonians and the $\mathbb{Z}_2$ gauge theory coupled to staggered fermions, have been studied before and quantum circuits for them are known. We find that our method produces shorter circuits than those previously published.

In Chapter 3.4: Qubitization of Non-Abelian Gauge Theories we study two possible qubitizations of $SU(2)$ gauge theory, with a four- and a five-dimensional Hilbert space per link, respectively. These models have the exact $SU(2)$ gauge invariance; thus, by standard universality arguments, one can suspect that they have the same continuum limit as $SU(2)$ gauge theory. One could reasonably conjecture that a finite-dimensional model in the universality class of $SU(2)$ gauge theories cannot be substantially simpler than these models and have a time evolution that can be approximated by a significantly smaller number of gates. We find that, for the four-dimensional model, one time evolution step involves 180 CNOT gates per plaquette, and the five-dimensional model involves 17,168 CNOT gates. The large circuit depth shows the importance of the space field truncation and stresses the need for truncations that are in the same universal class as the continuum model.

Finally, in Chapter 3.5: Discussion we summarize the results and speculate about some directions to pursue significantly reduced gate costs of simulating gauge theories.

**Chapter 3.2: The compilation method**

We describe here a method to take a given finite-dimensional Hamiltonian and encode its time evolution into a series of quantum gates; in other words, we describe the quantum compiler method we used. In order to facilitate use with most quantum programming languages, we compose our circuits only with common gates; in particular, we make heavy

use of CNOT gates and one-qubit rotation gates, defined by

$$\mathrm{CNOT} = |0\rangle\langle 0| \otimes I + |1\rangle\langle 1| \otimes X, \tag{52}$$

$$R_{\mathrm{i}}(\phi) \doteq e^{-\mathrm{i}\phi\sigma_{\mathrm{i}}/2} = \cos\left(\frac{\phi}{2}\right) I - \mathrm{i}\sin\left(\frac{\phi}{2}\right)\sigma_{\mathrm{i}}, \tag{53}$$

for $0 \leq \phi \leq 4\pi$, all expressed in the computational basis $\{|0\rangle, |1\rangle\}$ with qubits. Here, we denote the Pauli gates $\{X, Y, Z\} \doteq \{\sigma_1, \sigma_2, \sigma_3\}$ and the one-qubit identity gate by $I$. Notably, these rotations include the typical phase gate $S = R_{\mathrm{z}}(\pi/2)$ (and its inverse $S^{\dagger}$) and easily generate the Hadamard gate $H = XR_{\mathrm{y}}(\pi/2)$ (up to an irrelevant global phase); more broadly, we can perform arbitrary one-qubit unitary operations, sometimes denoted in an Euler angle basis $U3(\theta, \phi, \lambda) \equiv R_{\mathrm{z}}(\phi)R_{\mathrm{y}}(\theta)R_{\mathrm{z}}(\lambda)$ up to a global phase. We denote the control ($a$) and target ($b$) qubits for each CNOT gate using subscripts $\mathrm{CNOT}_{\mathrm{a,b}}$, corresponding to the former and latter factors in Eq. (52), respectively. For simplicity of the analysis in this work, we assume a hardware with all-to-all connectivity between the qubits, and we do not include an error mitigation strategy in our resulting circuits. The noisiest quantum gates on current hardware are the CNOT gates, so we aim to minimize their use. In fact, the number of CNOT gates will be used as a measure of how good the algorithm is.

It is convenient to break down our compilation method into five overall steps.

**1) Trotterization:** The first step is to break up the time evolution operator over a time $T$ into $\mathcal{N}$ terms $H = \sum_{\mathrm{i}=1} Nh_{\mathrm{i}}$ with matrix norms $\|h_{\mathrm{i}}\| \sim 1$ over several time steps of duration $\delta t = T/N_{\mathrm{t}}$:

$$U(T) = e^{-\mathrm{iHT}} \approx \left(\prod_{\mathrm{i}=1} Ne^{-\mathrm{ih_i}\delta\mathrm{t}}\right)^{\mathrm{N_t}}, \tag{54}$$

incurring an overall error of $O(\delta t)$, due to the nonzero commutators among $h_{\mathrm{i}}$. Also, we point out that, in the case of gauge theories, most actions are a sum over plaquettes (or slightly larger Wilson loops), which commute if they do not share a link. So, one can then split the Hamiltonian into two commuting sets of terms, $E(\mathrm{ven})$ and $O(\mathrm{dd})$, and evolve

each set independently:

$$e^{-iH\delta t} = e^{-i\sum_{\square} H_{\square}\delta t} \approx e^{-i\sum_{E} H_{E}\delta t} e^{-i\sum_{O} H_{O}\delta t}, \tag{55}$$

incurring in kind an error of $O(\|[H_E, H_O]\|\delta t^2)$ for a time step $\delta t$. Since the plaquettes within each set commute, their corresponding quantum gates can be applied in parallel. Consequently, in the $SU(2)$ gauge theory examples we will consider later, it will suffice for us to determine circuits to simulate a single plaquette going forward.

**2) Decomposition into Pauli strings:** Suppose we encode the degrees of freedom of one plaquette into $n$ qubits. The Hilbert space on which $H$ acts is then $2^n$-dimensional. Hermitian $H$ can be written as a real linear combination of Pauli strings on $n$ qubits:

$$H = \sum_{j=0}^{4^n-1} c_j P_j, \tag{56}$$

where $P_j \in \{I, X, Y, Z\}^{\otimes n}$. Further, the inner product on Pauli strings,

$$\frac{1}{2^n}\mathrm{tr}[P_i P_j] = \delta_{ij}, \tag{57}$$

allows one to easily calculate the coefficients above:

$$c_j = \frac{1}{2^n}\mathrm{tr}[P_j H]. \tag{58}$$

**3) Separation of Pauli strings into commuting sets:** Since commuting Pauli matrices can be simultaneously diagonalized, it is useful to split all Pauli strings into commuting sets or "clusters," so that the quantum gates used in diagonalizing each set need to be applied only once. The full time evolution can be Trotterized as the evolution given by each cluster, whose respective Trotterizations each incur no error due to commutativity.

It is possible to efficiently decide whether two Pauli strings commute, by counting the number of positions at which the Pauli matrices of the two strings do not commute. The two Pauli strings commute if and only if this number is even. Moreover, in general, partitioning Pauli strings into clusters of commuting operators can be performed sequentially. Namely, one can process the strings in the order they are given, placing each string in the first available cluster. If no cluster is available, we create a new one and insert the string. As a note of caution for general use, this clustering is not guaranteed to result in the minimal number of clusters,[13] and its outcome in principle can depends crucially on the order in which the strings are processed. Therefore, we will reformulate the clustering in terms of the graph coloring problem, as previously described in Refs. [105, 184, 182, 79]. In this formulation, we construct a graph $\mathcal{G}$ whose vertices are the Pauli strings, where an edge exists between any two Pauli strings $P_i$ and $P_j$ ($j \neq i$) if they do *not* commute. We recall that a vertex coloring of $\mathcal{G}$ assigns colors to the vertices such that any two adjacent vertices have different colors [29]. Therefore, all Pauli strings with the same color will commute. In this formalism, finding the optimal clustering is coloring $\mathcal{G}$ with the least required number of colors, known as the chromatic number of $\mathcal{G}$. Finding the chromatic number of a graph is known to be NP-complete [110], and so there is no known efficient algorithm to do so. Nevertheless, several approximation algorithms provide a coloring close to optimal [34, 50]. In the examples we discuss in Chapter 3.3: Examples, we were able to find convenient commuting clusters with relative ease.

**4) Diagonalization of each cluster:** This step describes how to construct the quantum circuit of an operator that simultaneously diagonalizes the commuting Pauli strings. The approach that we use entails representing the strings in the *tableau* formalism described in Refs. [2, 182, 78].

In particular, we will follow the presentation in Ref. [182] where the tableau is composed

[13] As we will see later in Chapter 3.3: Examples, one can reduce the CNOT-cost per Pauli string for a quantum circuit simulating a Hamiltonian with these Pauli strings if one packs each cluster to be as large as possible.

of the $\mathcal{X}$, $\mathcal{Z}$, and $\mathcal{S}$ blocks, which we will define below. Suppose we have $\mathcal{N}$ Pauli strings, each of length $n$. Then, the $\mathcal{X}$ and $\mathcal{Z}$ blocks are $\mathcal{N} \times n$ matrices, while the $\mathcal{S}$ block is a $\mathcal{N}$-dimensional column vector. For the $i$th Pauli string $P_\mathrm{i}$ in a given ordering with coefficient $c_\mathrm{i} \neq 0$, the entries to the corresponding row of each block are given by

$$\begin{aligned}
\mathcal{X}_{\mathrm{ij}} &= \begin{cases} 0 \text{ if the } j\text{th digit of } P_\mathrm{i} \text{ is } Z \text{ or } I \\ 1 \text{ otherwise} \end{cases} \\
\mathcal{Z}_{\mathrm{ij}} &= \begin{cases} 0 \text{ if the } j\text{th digit of } P_\mathrm{i} \text{ is } X \text{ or } I \\ 1 \text{ otherwise} \end{cases} \\
\mathcal{S}_\mathrm{i} &= \begin{cases} 0 \text{ if } c_\mathrm{i} > 0 \\ 1 \text{ otherwise} \end{cases}
\end{aligned} \tag{59}$$

In other words, $\mathcal{X}_{\mathrm{ij}}$ and $\mathcal{Z}_{\mathrm{ij}}$ encode whether the $j$th digit of the Pauli string $P_\mathrm{i}$ contains a factor of $X$ and $Z$, respectively, while $\mathcal{S}_\mathrm{i}$ simply encodes the sign of the Pauli string's coefficient. Note that a Pauli string $P_\mathrm{i}$ is diagonal if and only if it contains only factors $I$ and $Z$, or, equivalently, all the entries in row $i$ of $\mathcal{X}$ are 0. [182, 143] [54, 182] Consequently, the task of simultaneously diagonalizing commuting Pauli strings may be viewed as applying conjugations with unitary gates that reduce all entries of $\mathcal{X}$ to 0. Since we seek to transform a Pauli string to another, these unitary transformations are Clifford gates, generated by Hadamard, phase, and CNOT gates. The conjugation of these gates acts on the tableau according to the following rules [2]:

- **Hadamard gate conjugation on qubit j** or $H\,(j)$:

$$\begin{aligned}
\mathcal{S}_\mathrm{i} &\leftarrow \mathcal{S}_\mathrm{i} \oplus \mathcal{X}_{\mathrm{ij}}\mathcal{Z}_{\mathrm{ij}} \\
(\mathcal{X}_{\mathrm{ij}}, \mathcal{Z}_{\mathrm{ij}}) &\leftarrow (\mathcal{Z}_{\mathrm{ij}}, \mathcal{X}_{\mathrm{ij}})
\end{aligned} \tag{60}$$

for all $i = 1, \ldots, \mathcal{N}$. That is, we flip the sign of a Pauli string if the Pauli matrix at position $j$ is $Y$. Then, swap the $j$th columns of $\mathcal{X}$ and $\mathcal{Z}$; practically speaking, we replace any factors $X$ or $Z$ in the $j$th digit of each string with $Z$ or $X$ respectively.

- **Phase gate conjugation on qubit j** or $S(j)$:

$$\begin{aligned} \mathcal{S}_{\mathrm{i}} &\leftarrow \mathcal{S}_{\mathrm{i}} \oplus \mathcal{X}_{\mathrm{ij}} \mathcal{Z}_{\mathrm{ij}} \\ \mathcal{Z}_{\mathrm{ij}} &\leftarrow \mathcal{Z}_{\mathrm{ij}} \oplus \mathcal{X}_{\mathrm{ij}} \end{aligned} \tag{61}$$

for all $i = 1, \ldots, \mathcal{N}$. That is, for the Pauli string $P_{\mathrm{i}}$ encoded in row $i$ we flip the sign of its coefficient if its $j$th digit is $Y$, and we replace any factors $X$ or $Y$ in the $j$th digit of each string with $Y$ or $X$ respectively.

- **CNOT conjugation with control qubit a and target b** or CNOT $(a, b)$:

$$\begin{aligned} \mathcal{S}_{\mathrm{i}} &\leftarrow \mathcal{S}_{\mathrm{i}} \oplus \mathcal{X}_{\mathrm{ia}} \mathcal{Z}_{\mathrm{ib}} \left(\mathcal{X}_{\mathrm{ib}} \oplus \mathcal{Z}_{\mathrm{ia}} \oplus 1\right) \\ \mathcal{Z}_{\mathrm{ia}} &\leftarrow \mathcal{Z}_{\mathrm{ia}} \oplus \mathcal{Z}_{\mathrm{ib}} \\ \mathcal{X}_{\mathrm{ib}} &\leftarrow \mathcal{X}_{\mathrm{ib}} \oplus \mathcal{X}_{\mathrm{ia}} \end{aligned} \tag{62}$$

for all $i = 1, \ldots, \mathcal{N}$, and the interpretation is similar to those in Eqs. (60) and (61).

Note that the update on $\mathcal{S}$ should be applied first in each case because the sign update depends on the current values of $\mathcal{X}$ and $\mathcal{Z}$. Here, the symbol $\oplus$ denotes the addition modulo 2.

As an example, consider a Hamiltonian with mutually commuting Pauli strings $H = IXX + ZYZ + XXI$ [14]. The $\mathcal{X}$, $\mathcal{Z}$, and $\mathcal{S}$ blocks are

$$\mathcal{X} = \begin{pmatrix} 0 & 1 & 1 \\ 0 & 1 & 0 \\ 1 & 1 & 0 \end{pmatrix}, \qquad \mathcal{Z} = \begin{pmatrix} 0 & 0 & 0 \\ 1 & 1 & 1 \\ 0 & 0 & 0 \end{pmatrix}, \qquad \mathcal{S} = \begin{pmatrix} 0 \\ 0 \\ 0 \end{pmatrix}, \tag{63}$$

[14] From now on, we omit the tensor product sign.

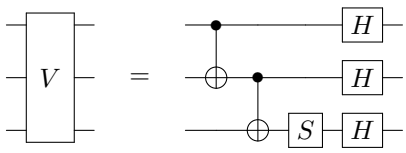


Figure 8: Operator $V$ diagonalizing the Hamiltonian $H = IXX + ZYZ + XXI$

labeling the qubits, left to right, from 1 to 3. We can use $\text{CNOT}_{1,2}$ and $\text{CNOT}_{2,3}$ to nullify the first two columns of the $\mathcal{Z}$ stack. Then, we observe that the third columns of the $\mathcal{X}$ and $\mathcal{Z}$ stacks are identical. Hence, a phase gate conjugation on the third qubit will nullify the $\mathcal{Z}$ stack. Finally, we apply Hadamard gates on all the three qubits to swap the columns of $\mathcal{X}$ and $\mathcal{Z}$. Thus, all of the resulting entries of the $\mathcal{X}$ stack are all 0. Meanwhile, the $\mathcal{Z}$ and $\mathcal{S}$ stacks become

$$\mathcal{Z} = \begin{pmatrix} 0 & 1 & 0 \\ 0 & 1 & 1 \\ 1 & 0 & 0 \end{pmatrix}, \qquad \mathcal{S} = \begin{pmatrix} 0 \\ 1 \\ 0 \end{pmatrix}, \tag{64}$$

respectively. The resulting diagonal Pauli strings are together $V H V^\dagger = IZI - IZZ + ZII$, where we denote the diagonalizing circuit by $V$. Figure 8 depicts the circuit diagonalizing $H$.

In general, it is possible to simultaneously diagonalize an arbitrary cluster of commuting Pauli strings with at most $O(n^2)$ two-qubit gates [182, 143]. Moreover, there exist several algorithms to accomplish this diagonalization, although not necessarily with the minimal number of two qubit gates [54, 182].

**5) Exponentiation of $I/Z$ Pauli strings via a Binary Tree:** Finally, we describe our procedure to compile a quantum circuit simulating a Hamiltonian composed of $\mathcal{N}$ *diagonal* Pauli strings (i.e., in $\{I, Z\}^{\otimes n}$). In particular, we propose a bookkeeping process to search for shared CNOT gates between strings within the cluster, in contrast with existing methods, which compile a circuit individually reducing each Pauli string with

CNOT conjugations (described below) and then look for cancellations *post hoc*.

To start, for a single such Pauli string, we may use Eq. (62)—more specifically, the identity

$$Z \otimes Z = \mathrm{CNOT}_{12}\ (I \otimes Z)\ \mathrm{CNOT}_{12}. \tag{65}$$

By successive applications of this identity we can map any diagonal Pauli string to a string containing a single factor of $Z$. Exponentiating such Pauli strings can then be accomplished with a single one-qubit rotation gate, $R_{\mathrm{z}}(2c_{\mathrm{j}}\delta t)$ on a given qubit:

$$e^{-\mathrm{ic_jI\cdots IZI\cdots I}\delta\mathrm{t}} = I \cdots I R_{\mathrm{z}}(2c_{\mathrm{j}}\delta t) I \cdots I \tag{66}$$

This procedure is equivalent to the gate decomposition of Refs. [129, 143]. For example, a circuit implementing $\exp\left(-\mathrm{i}c_{\mathrm{j}}ZZZ\delta t\right)$ in such a fashion is shown in Fig. a.

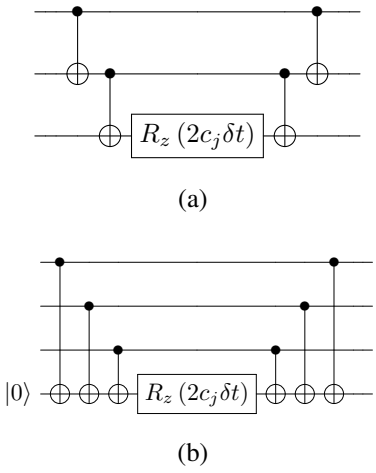


Figure 9: Quantum circuit implementing the factor $\exp\left(-\mathrm{i}c_{\mathrm{j}}ZZZ\delta t\right)$. (a) No ancillary qubit is used. Notably, there are other combinations of CNOT conjugations that one may perform to arrive at other equivalent circuits implementing this operator. (b) One ancillary qubit, prepared as $|0\rangle$, is the target of each CNOT and the site of the rotation, as prescribed in this more common method (c.f. Ref. [147]).

This prescription deviates slightly from the usual technique (e.g., Ref. [148]), which utilizes a single ancillary qubit on which the rotation is performed instead. Via that

alternative procedure, there are more CNOT conjugations required and fewer opportunities for the gates involved to cancel. We display the same example, $ZZZ$, using this procedure in Fig. b.

Equipped now with this generic strategy of reducing individual Pauli strings to one-qubit rotations, we describe in the remainder of this section our own compilation method to efficiently simulate the diagonal Pauli strings together. Our procedure seeks to induce sharing of CNOT gates within the cluster, in the same spirit of reducing circuit depth as in step 4, where we share CNOT costs over a cluster via simultaneous diagonalization. In particular, as we apply the first CNOT gate in each conjugation reducing a Pauli string to a rotation, we keep track of those conjugations in a list or "stack" and classically perform the CNOT conjugations on the remaining strings in the cluster, as per Eq. (62). Moreover, we refrain from applying the second CNOT gate in the conjugation until after the rotation gates of all other Pauli strings have been executed on the circuit. In essence, this approach can be understood as inserting the identity (i.e., a pair of identical, consecutive CNOT gates to cancel) between every pair of remaining Pauli strings in the cluster. We provide instructions to efficiently carry out this procedure below, in terms of a tree traversal algorithm. (See e.g., Ref. [81] for a review of tree data structures and traversal.)

We proceed by representing the linear combination of $N \geq 1$ Pauli strings as a binary tree with $n$ levels where $n$ is the total number of qubits (equivalently the length of the Pauli strings). One calls the zeroth level of the tree the "root" and the nodes of the $n$th and final level the "leaves;" notably the order of these $n$ tree levels may be a permutation of the corresponding qubit digits of the Pauli strings, equivalent to a temporary reordering of the qubit labels on our circuit.[15] Each tree branch (i.e., path from the root to a leaf) corresponds to a Pauli string, and the values of its $n$ nodes are 0 or 1, corresponding to the

[15]For example, one may arrange the levels to label the qubits in descending order of number of Pauli strings sharing a factor $Z$ on that digit. We found this modified ordering of tree levels yielded modest savings $O(n)$ in CNOT cost in some cases, when compared with the straightforward ordering where qubit $j$ is labeled by tree level $j$, and resulted in greater cost in other cases. At this time, the cause of this higher cost is not clear. Determining how the CNOT cost depends on the relabeling of tree levels is the subject of further research.

factors $I$ or $Z$ respectively of the string. Figure 10 shows the tree representation for the Hamiltonian $H = IIZ + IZI + IZZ + ZZZ$. For example, the values of the nodes in the bottom branch are 0, 0, and 1, corresponding to the Pauli string $IIZ$. For an arbitrary linear coefficient of Pauli strings, one includes the coefficient of Pauli string in the corresponding leaf node. (This task can be done for example by creating a leaf object that inherits all the properties of a node object but has an additional coefficient attribute.)

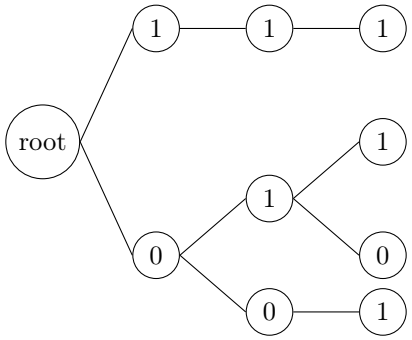


Figure 10: Tree representation of $IIZ + IZI + IZZ + ZZZ$. The value inside each node along a branch indicates the gate $I$ or $Z$ on each qubit for the corresponding Pauli string term. For a general linear combination, the coefficient of a Pauli string is stored with its corresponding leaf.

Mapping a commuting cluster of Pauli strings to this tree structure, we now present how to derive a quantum circuit from a traversal of this tree. Our routine traverses the tree via a preorder Depth-First-Search (DFS) (see e.g., Ref. [81]).[16] Reading along each branch from the root to its leaf, when a pair of nodes both with value 1 is encountered—say, at levels $i$ and $j > i$ — a $\text{CNOT}_{ji}$ gate will be applied on the circuit. We then classically perform a $\text{CNOT}_{ji}$ conjugation to all Pauli strings on the tree, i.e., update the values along their branches according to Eq. (62); the child node ($j$) value is flipped when the parent node ($i$) value is 1. Lastly, the latter CNOT gate in the conjugation is stored in a stack, if there is no copy already in the stack; otherwise, we discard both the CNOT gate and its copy in the stack (an operation we will justify later). By this procedure, after reaching the leaf there

[16] We comment in passing that other orders are possible, equivalent to implementing Pauli strings in a different ordering.

will be precisely one node ($i$) with value 1 along the branch, corresponding to a rotation on qubit $i$, $R_z(2\,c\,\delta t)$, where $c$ is the coefficient of the string stored with the leaf/branch. The procedure continues until the last branch is processed. Then, the CNOT gates from the stack are applied to the end of the circuit, from the latest to the earliest gate added into the stack. Figure 11 depicts the quantum circuit obtained for the example
$H = IIZ + IZI + IZZ + ZZZ$.

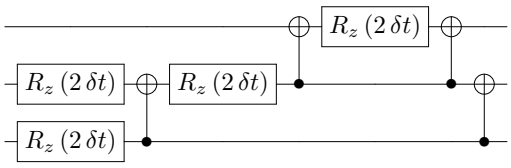


Figure 11: Circuit simulating one Trotterized time step with the Hamiltonian $H = IIZ + IZI + IZZ + ZZZ$. Here $\delta t$ is the Trotterization time step. The qubits are ordered from top to bottom (i.e., as increasing levels in the tree structure of Fig. 10).

Now, we explain why we may discard a CNOT gate and its copy in the stack. First, we note that all CNOT gates with the same target qubit appear consecutively in the stack and commute with each other. Additionally, the control qubit $j$ for each $\mathrm{CNOT_{ji}}$ always corresponds to the child node in a pair $i, j$. Therefore, the stack will have at most $\binom{n}{2}$ CNOT gates. There may be opportunities for further CNOT gate simplification particularly within this stack due to cancellations described in Refs. [137, 129]; however, by an argument listed below, we observe that such cancellations will not eliminate the bulk of the remaining CNOT cost in our final circuit.

To conclude, we comment on the cancellations among CNOT gates induced by this algorithm. Within a cluster of commuting Pauli strings acting on $n$ qubits, we may have in general $\mathcal{N} \leq 2^n$ such strings and in fact we typically have $\mathcal{N} \gg n$. So, without any CNOT gate cancellation, a simulation of each Pauli string independently could in principle require $O(n\mathcal{N})$ CNOT gates on the circuit before all one-qubit rotations have been performed and equally as many after (i.e., in the stack). However, on the stack there can only be $O(n^2)$ such gates as we have argued above, so cancellation among CNOT gates in this stack alone

can yield a factor of $\sim 2$ savings in CNOT cost; the bulk of possible CNOT gates in the stack will cancel for large enough $\mathcal{N} \gg n$. Moreover, we find that at least for our models in consideration, the CNOT cost turns out to be only $\mathcal{O}(\mathcal{N})$, due to other savings among the CNOT gates performed before one-qubit rotations. In Appendix Chapter 3.7.1: CNOT-cost lower bound of simulating Pauli strings we establish $\sim \mathcal{N}$ to be a generic lower bound on the number of CNOT gates entailed for direct simulations of $\mathcal{N}$ (diagonal) Pauli strings. We also stress that the use of a tree is a data structure choice. For example, it is possible to store the Pauli strings in a list instead and perform the same CNOT conjugations according to our procedure. However, processing this list can result in more classical operations surpassing the cost of the binary tree.

The above discussion summarizes the method to decompose the time evolution into ordinary quantum gates. It is important to note that steps 4 and 5, the most involved in the whole method, can be bypassed at the expense of arriving at an algorithm with a larger number of CNOT gates. In fact, we can use $H$ and $S$ gates to diagonalize each of the Pauli strings separately; however, the increase in CNOT cost is substantial in the cases we considered.

### Chapter 3.3: Examples

We now apply the general method outlined in the previous section to a couple of specific models. These examples – random diagonal Hamiltonians and $\mathbb{Z}_2$ gauge theory – are discussed here in order to establish the method as competitive with other methods one might consider. The $\mathbb{Z}_2$ gauge theory is very simple and, actually, has been simulated in real quantum computers (with tiny lattices).

#### Chapter 3.3.1: Random Diagonal Hamiltonians

To assess the relative performance of our method discussed particularly in step 5 above, we consider CNOT costs to simulate already diagonalized $n$-qubit Hamiltonians, which may

be written as a linear combination of $\mathcal{N} \leq 2^n$ operators $\{I, Z\}^{\otimes n}$.

Consider first the $\mathcal{N} = 2^n$ case. It is known that the time evolution operator $U = \exp(-iH\delta t)$ due to such a Hamiltonian can be implemented exactly with $O(n\,2^n)$ CNOT gates because each Pauli string can be implemented with at most $(n-1)$ CNOT gates. A previous study [40] showed that this unitary operator can be realized with $2^{n+1} - 3$ CNOT gates, roughly twice the minimal cost. In Appendix Chapter 3.7.2: CNOT gate count for a diagonal Hamiltonian with $\mathcal{N} = 2^n$ Pauli Strings, we show that our method produces a circuit with $2^n - 2$ CNOT gates for arbitrary $n \geq 2$ qubits, achieving the optimal cost derived in Ref. [40]. This result lends credence that the method we outlined is competitive with any other method currently available.

In the $\mathcal{N} < 2^n$ case, there are many choices of Hamiltonians and the final circuit depends on the specific Pauli strings contained in the Hamiltonian. Thus, we applied our compilation method to a random sample of $M = 10$ Hamiltonians with $\mathcal{N}$ diagonal Pauli strings and consider how the number of CNOT gates depends on $\mathcal{N}$. There exist $\binom{2^n-1}{\mathcal{N}}$ distinct sets of $\mathcal{N}$ Pauli strings, and so there are certain cases where the number of possible Hamiltonians is less than $M$; in these cases, we would have explored all the $< M$ possible Hamiltonians of $\mathcal{N}$ Pauli strings. Otherwise, the $M$ Pauli strings we have explored comprise only a small subset of the Hamiltonians with $\mathcal{N}$ Pauli strings. Of course, we expect that increasing the value of $M$ will produce yet more precise estimates of average CNOT cost. For each value of $\mathcal{N}$, we calculate a mean and standard error on the mean.

A recent study [176] formulated the problem of minimizing the CNOT gates as solving the Traveling Salesman Problem (TSP) (see e.g., Ref. [110]). In this case, the vertices of the graph correspond to commuting Pauli strings and the weight on each edge is given by a CNOT-cost function they define. Given that the TSP is in general NP-Complete [110], they use the Christofides-Serdyukov (CS) algorithm, which returns a solution with a CNOT cost that is at most a factor of 1.5× the minimal cost [48, 181]. Moreover, they demonstrate that their ordering of Pauli strings on a quantum circuit based on the CS algorithm outperforms

standard solutions such as those based on lexicographical ordering [177, 97], "Deplete Group," and "Magnitude" ordering [178]. We therefore apply the method in Ref. [176] on the diagonal Pauli strings we generated. Figure 12 shows the CNOT cost with the number of Pauli strings for $n = 8$ qubits. We also include a lower bound derived in Appendix Chapter 3.7.1: CNOT-cost lower bound of simulating Pauli strings. The resulting CNOT gate counts are comparable for small $\mathcal{N}$. However, as $\mathcal{N}$ increases, our procedure yields a smaller number of CNOT gates. In addition, the count from this current method approaches this lower bound while the other does not.

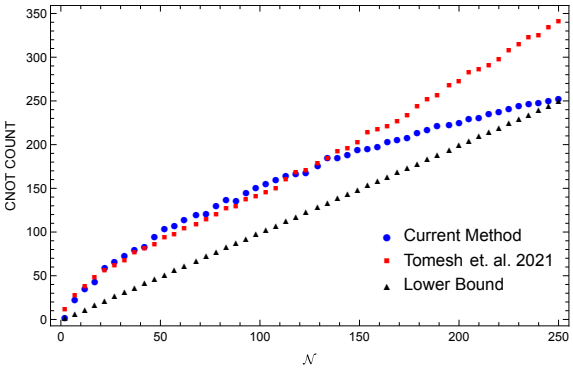


Figure 12: The average CNOT gate count required to simulate a diagonal Hamiltonian as function of the number of Pauli strings for $n = 8$ qubits. The blue data points are obtained using the compilation method described in step 5. The red data points are obtained using the method in [176]. A lower bound for each case is the number of Pauli strings acting nontrivially on more than one qubit, as derived in Appendix Chapter 3.7.1: CNOT-cost lower bound of simulating Pauli strings. Uncertainty bars derived from statistical sample sizes of 10 Pauli strings per choice of $\mathcal{N}$ are smaller than the data points depicted above.

### Chapter 3.3.2: $\mathbb{Z}_2$ Gauge Theory

As a first example of a gauge theory, we consider the smallest nontrivial group, $\mathbb{Z}_2$, for our gauge symmetry. Despite involving only a small discrete, abelian group, its simplicity as well as its familiarity in previous literature (e.g., Refs. [117, 87, 126]) on quantum simulations of lattice gauge theories make it a natural candidate for introducing our methods. Furthermore, the case of a $\mathbb{Z}_2$ gauge coupled to staggered fermions yields a

slightly less trivial example, where comparison of our relatively low circuit depth with that of circuits suggested in past studies [126] will show an early benefit to our methods of circuit compilation.

In particular, we consider here staggered fermions in 1 + 1 dimensions, as given in Ref. [126] and similar to a related model in Ref. [117]. There, an ancillary qubit was used to simulate each term of the Hamiltonian

$$H = \sum_{\mathrm{i}=1}^{\mathrm{L}} -\frac{m}{2}(-1)^{\mathrm{i}}\sigma_3(i) + \sum_{\mathrm{i}=1}^{\mathrm{L}-1}\sigma_1(i,i+1) + \frac{1}{4}\sum_{\mathrm{i}=1}^{\mathrm{L}-1}(-1)^{\mathrm{i}}\sigma_3(i,i+1)[\sigma_1(i)\sigma_1(i+1) + \sigma_2(i)\sigma_2(i+1)], \tag{67}$$

where $L$ is the number of fermion sites, $m$ is the fermion mass, $\sigma_{\mathrm{k}}(i)$ denotes Pauli matrices $\sigma_{\mathrm{k}}$ applied to the subspace for the $i$th fermion site, and $\sigma_{\mathrm{k}}(i, i+1)$ denotes $\sigma_{\mathrm{k}}$ applied to the subspace for the gauge link connecting sites $i$ and $i+1$.

Choosing $L = 4$ with open boundary conditions, an encoding of the global Hilbert space with only seven qubits is sufficient. However, with an extra eighth, ancillary qubit included in the methods of Ref. [126], there are fewer opportunities for rearrangement and cancellation of CNOT gates on the quantum circuit. Consequently, the total CNOT cost for simulation of one time step was found to be 36. Using the methods of section Chapter 3.2: The compilation method, one can perform the same simulation without this ancilla and therefore reduce a CNOT cost to only 18. The Hamiltonian in Eq. (67) is a linear combination of 13 Pauli strings. Using the sequential algorithm described in step 3 in Chapter 3.2: The compilation method, we obtain three clusters of commuting Pauli strings, containing seven, four, and two Pauli strings. Each cluster was diagonalized as discussed in Chapter 3.2: The compilation method before implementing our routine to construct the quantum circuit for each of the corresponding diagonalized clusters of Pauli

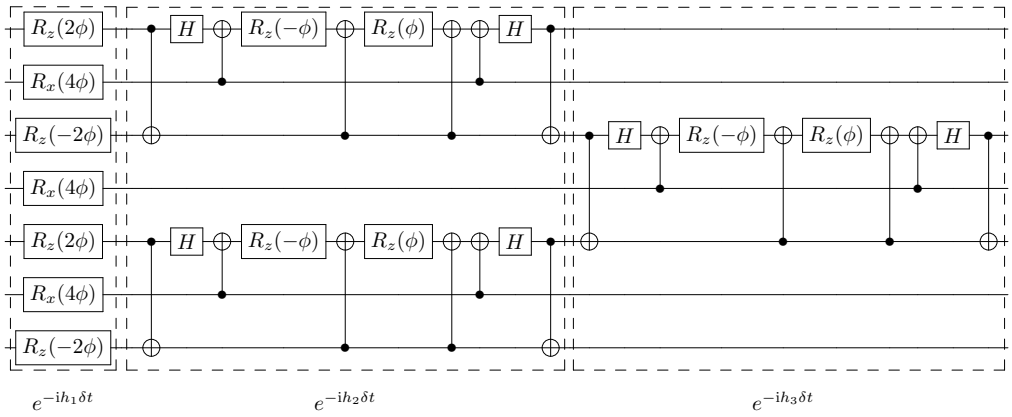


Figure 13: Quantum circuit approximately simulating one time step for a $\mathbb{Z}_2$ gauge theory with staggered fermions in 1 + 1 dimensions for $L = 4$ lattice sites without a periodic boundary condition. We use the first qubit to encode the first fermion site, the second qubit for the first gauge link, the third qubit for the second site, and so on. The boxes denote the clusters of commuting Pauli strings, which were partitioned as follows: the Hamiltonian $h_1$ consists of the one-body terms of Eq. (67), while $h_2$ consists of the multi-site terms acting on the gauge links $(1, 2)$ and $(3, 4)$, and $h_3$ likewise consists of the multi-site terms acting on link $(2, 3)$. We define the phase $\phi \equiv \Delta t/2$.

strings. Setting the fermion mass $m = 1$, the whole quantum circuit is shown in Fig. 13.

This benefit for a relatively simple model shows promise that our methods for circuit compilation will help keep CNOT cost relatively low compared to standard methods as we proceed to consider larger gauge groups.

**Chapter 3.4: Qubitization of Non-Abelian Gauge Theories**

We will now consider a broader class of models where the gauge dynamical degrees of freedom can be thought as lying on the links of a spatial cubic lattice. The Hilbert space is the product of the $\ell$ local Hilbert spaces of each link (on $q$ qubits): $\mathcal{H} = (\mathbb{C}^{2^q})^{\otimes \ell}$ with a Hamiltonian of the form

$$H = g^2 K - \frac{1}{g^2} \sum_{\mathrm{x},\mu,\nu} \mathrm{tr}\left(U_{\mathrm{x},\mu} U_{\mathrm{x}+\mu,\nu} U^{\dagger}_{\mathrm{x}+\nu,\mu} U^{\dagger}_{\mathrm{x},\nu}\right), \tag{68}$$

where $U_{\mathrm{x},\mu}$ is an operator acting on the Hilbert space of the link connecting sites $x$ and

$x + \mu$[17]. The "kinetic" term $K$ will be specified later as it depends on the model considered. In a standard formulation of quantum $SU(N)$ gauge theories, each entry of the $N \times N$ unitary matrix $U_{x,\mu}$ is itself an operator acting on an infinite-dimensional Hilbert space. Here, instead, we take each entry to act on a finite-dimensional operator. Thus, for $SU(2)$ gauge theory, on which we will focus the remainder of this section, we take $U = 1 \otimes \Gamma_4 + i\sigma_k \otimes \Gamma_k$, where the matrices $\Gamma_\alpha$ ($\alpha = 1, 2, 3, 4$) will depend on the specific model. Notice that for each $x$ and $\mu$, $U_{x,\mu}$ carries two pairs of matrix indices: one taking values $1, 2$ and another taking values up to the dimension of $\Gamma_\alpha$.

Furthermore, a local $SU(2)$ gauge transformation corresponds to an assignment of a different element of $SU(2)$ at each site. Under gauge transformations the link operators $U$ transform as

$$U_{ab} \mapsto L_{aa'} U_{a'b'} (R^\dagger)_{b'b}, \tag{69}$$

with $a, b = 1, 2$ and two elements of $SU(2)$, $L = \exp(i\alpha_k \sigma_k/2)$ and $R = \exp(i\beta_k \sigma_k/2)$. These transformations clearly leave the plaquette term in Eq. 68 unchanged. They are implemented within the Hilbert space as

$$U_{ab} \mapsto L_{aa'}\, U_{a'b'}\, (R^\dagger)_{b'b} = \mathcal{R}\, \mathcal{L}\, U\, \mathcal{L}^\dagger\, \mathcal{R}^\dagger, \tag{70}$$

with $\mathcal{L} = \exp\left(i\alpha_k J_k^L\right)$, $\mathcal{R} = \exp\left(i\alpha_k J_k^R\right)$ for certain matrices $J_k^L, J_k^R$ ($k = 1, 2, 3$) with the same dimension as $\Gamma_\alpha$. In Ref. [151] it was shown that the 10 matrices $\Gamma_\alpha, J_k^L, J_k^R$ satisfy 70 if they are chosen to be the generators of a representation of SO(5). As such, a choice of irreducible representation (irrep) of SO(5) gives a model with a finite-dimensional Hilbert space and exact $SU(2)$ gauge symmetry and, therefore, a candidate for a qubitization of $SU(2)$ gauge theory. Generically, the smaller irreps yield lower-dimensional Hilbert spaces for the theory, and fewer quantum gates are expected to represent its time evolution. The two smallest irreps are discussed here.

[17]Here, we use the notation used in lattice gauge theory where the nearest point to $x$ in the direction $\mu$ is denoted by $x + \mu$.

**Chapter 3.4.1:** $N = 4$ **(spinor) irrep**

The smallest irrep of SO(5) is the four-dimensional spinor representation given by

$$\begin{aligned} \Gamma_4 &= \frac{1}{2}\begin{pmatrix} 0 & 1 \\ 1 & 0 \end{pmatrix}, \quad \Gamma_{\mathrm{k}} = \frac{1}{2}\begin{pmatrix} 0 & -\mathrm{i}\sigma_{\mathrm{k}} \\ \mathrm{i}\sigma_{\mathrm{k}} & 0 \end{pmatrix}, \\ J_{\mathrm{k}}^{\mathrm{L}} &= \frac{1}{2}\begin{pmatrix} \sigma_{\mathrm{k}} & 0 \\ 0 & 0 \end{pmatrix}, \quad J_{\mathrm{k}}^{\mathrm{R}} = \frac{1}{2}\begin{pmatrix} 0 & 0 \\ 0 & \sigma_{\mathrm{k}} \end{pmatrix}. \end{aligned} \tag{71}$$

However, this list of operators so far only suggests the form of a plaquette term, while $J_{\mathrm{k}}^{\mathrm{L}} J_{\mathrm{k}}^{\mathrm{L}} + J_{\mathrm{k}}^{\mathrm{R}} J_{\mathrm{k}}^{\mathrm{R}}$ is proportional to the identity. A theory with only a single plaquette term cannot have a continuum limit, because the eigenvectors of the Hamiltonian are independent of the only parameter in the theory, $g^2$. Therefore, the correlation length of the ground state cannot be made arbitrarily large (in units of lattice spacing). As such, it is necessary to include another term to make eigenvectors and, consequently, correlation lengths tunable. In the four-dimensional representation, there is one term

$$K = \sum_{\mathrm{l}} \Gamma_5(l), \tag{72}$$

where

$$\Gamma_5 = \frac{1}{2}\begin{pmatrix} I & 0 \\ 0 & -I \end{pmatrix}. \tag{73}$$

Together, the plaquette term and $K$ form a plausible qubitization of the $SU(2)$ gauge theory. This model was first considered in Ref. [151] where it was speculated to be in the same universality class as $SU(2)$ gauge theory in 3+1 spacetime dimensions. In order to encode this formulation on a quantum computer, only two qubits per link are required. Now, we discuss the results of applying our method to this model. The $K$ term consists of four Pauli strings, which are all diagonal one-qubit operators; they can all be implemented without any CNOT gate. Next, we turn to the plaquette term in Eq. (68). After tracing out

the shared two-dimensional space, we can write it as $\sum_{i,j,k,l=1}^{4} c_{ijkl}\,\Gamma_{ijkl}$ where $c_{ijkl} \equiv \mathrm{tr}[\sigma_i\sigma_j\sigma_k\sigma_l]$ (taking $\sigma_4 \equiv I$) and $\Gamma_{ijkl} \equiv \Gamma_i \otimes \Gamma_j \otimes \Gamma_k \otimes \Gamma_l$. By a counting argument or explicit computation, one finds that only 64 of the coefficients $c_{ijkl}$ are non-zero. In addition, each $\Gamma_k$ in this representation corresponds to a single Pauli string. Therefore, the expansion of the plaquette term results in 64 Pauli strings.

Using the sequential algorithm described in step 3, these latter 64 operators can be grouped into four clusters, each containing 16 Pauli strings. We used $2 \times 28 = 56$ CNOT gates altogether to diagonalize these clusters. With each cluster diagonalized, we can apply the method developed in step 5 to compile the time evolution circuit. The total CNOT gate count to compile the time evolution of all the diagonal clusters is 124. Thus, we use $56 + 124 = 180$ CNOT gates per plaquette to simulate a time evolution step of this model.

**Chapter 3.4.2:** $N = 5$ **(fundamental) irrep**

In a five-dimensional truncation, we consider the fundamental representation of SO(5), given by

$$\Gamma_1 = \begin{pmatrix} 0 & 1 & 0 & 0 & 0 \\ 1 & 0 & 0 & 0 & 0 \\ 0 & 0 & 0 & 0 & 0 \\ 0 & 0 & 0 & 0 & 0 \\ 0 & 0 & 0 & 0 & 0 \end{pmatrix}, \qquad \Gamma_2 = \begin{pmatrix} 0 & 0 & 1 & 0 & 0 \\ 0 & 0 & 0 & 0 & 0 \\ 1 & 0 & 0 & 0 & 0 \\ 0 & 0 & 0 & 0 & 0 \\ 0 & 0 & 0 & 0 & 0 \end{pmatrix},$$

$$\Gamma_3 = \begin{pmatrix} 0 & 0 & 0 & 1 & 0 \\ 0 & 0 & 0 & 0 & 0 \\ 0 & 0 & 0 & 0 & 0 \\ 1 & 0 & 0 & 0 & 0 \\ 0 & 0 & 0 & 0 & 0 \end{pmatrix}, \qquad \Gamma_4 = \begin{pmatrix} 0 & 0 & 0 & 0 & 1 \\ 0 & 0 & 0 & 0 & 0 \\ 0 & 0 & 0 & 0 & 0 \\ 0 & 0 & 0 & 0 & 0 \\ 1 & 0 & 0 & 0 & 0 \end{pmatrix},$$

$$J_1^{\mathrm{L}} = \frac{1}{2}\begin{pmatrix} 0 & 0 & 0 & 0 & 0 \\ 0 & 0 & 0 & 0 & -i \\ 0 & 0 & 0 & -i & 0 \\ 0 & 0 & i & 0 & 0 \\ 0 & i & 0 & 0 & 0 \end{pmatrix}, \quad J_2^{\mathrm{L}} = \frac{1}{2}\begin{pmatrix} 0 & 0 & 0 & 0 & 0 \\ 0 & 0 & 0 & i & 0 \\ 0 & 0 & 0 & 0 & -i \\ 0 & -i & 0 & 0 & 0 \\ 0 & 0 & i & 0 & 0 \end{pmatrix}, \quad J_3^{\mathrm{L}} = \frac{1}{2}\begin{pmatrix} 0 & 0 & 0 & 0 & 0 \\ 0 & 0 & -i & 0 & 0 \\ 0 & i & 0 & 0 & 0 \\ 0 & 0 & 0 & 0 & -i \\ 0 & 0 & 0 & i & 0 \end{pmatrix},$$
$$J_1^{\mathrm{R}} = \frac{1}{2}\begin{pmatrix} 0 & 0 & 0 & 0 & 0 \\ 0 & 0 & 0 & 0 & i \\ 0 & 0 & 0 & -i & 0 \\ 0 & 0 & i & 0 & 0 \\ 0 & -i & 0 & 0 & 0 \end{pmatrix}, \quad J_2^{\mathrm{R}} = \frac{1}{2}\begin{pmatrix} 0 & 0 & 0 & 0 & 0 \\ 0 & 0 & 0 & i & 0 \\ 0 & 0 & 0 & 0 & i \\ 0 & -i & 0 & 0 & 0 \\ 0 & 0 & -i & 0 & 0 \end{pmatrix}, \quad J_3^{\mathrm{R}} = \frac{1}{2}\begin{pmatrix} 0 & 0 & 0 & 0 & 0 \\ 0 & 0 & -i & 0 & 0 \\ 0 & i & 0 & 0 & 0 \\ 0 & 0 & 0 & 0 & i \\ 0 & 0 & 0 & -i & 0 \end{pmatrix}. \tag{74}$$

Here, a non-trivial "kinetic term" of the form

$$K = \sum_l K(l) = \sum_l J_{\mathrm{k}}^{\mathrm{L}} J_{\mathrm{k}}^{\mathrm{L}}(l) \tag{75}$$

($l$ indexes the links) is possible; note here $J_{\mathrm{k}}^{\mathrm{L}} J_{\mathrm{k}}^{\mathrm{L}} = J_{\mathrm{k}}^{\mathrm{R}} J_{\mathrm{k}}^{\mathrm{R}}$. This model is sometimes called the Horn model [100].[18]

Three qubits are required to encode the five-dimensional Hilbert space in each link. Since $2^3 = 8 = 5 + 3$, three directions are "wasted" in this encoding. The matrix elements of the Hamiltonian involving these extra three dimensions are unphysical and can be chosen arbitrarily, with no change in the Physics. Unfortunately, we have not been able to exploit this freedom to simplify the quantum circuits. Notably, one may attempt to encode the global Hilbert space at once in a smaller basis of $\lceil 4 \log_2(5) \rceil = 10$ qubits, where a given qubit may actually include information from the local Hilbert spaces of multiple links.

[18] There has been work to generalize the Horn model by including the coupling to gradually larger representations of $SU(N)$ for $N \geq 2$; however, while this effort may help extrapolate away the error of this truncation of the links [42, 192], it necessarily relinquishes the relatively low Hilbert space dimension of the Horn model.

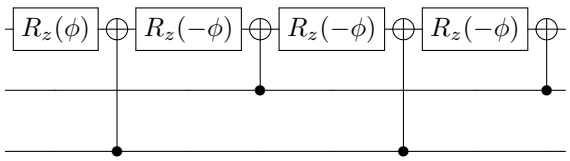


Figure 14: Quantum circuit simulating a time step for the kinetic term K as encoded in Eq. (76). Here, we have set $\phi \equiv 3\delta t/8$.

However, though one might expect to reduce circuit depth by reducing the number of qubits in the encoding, we instead find that such an encoding results in an even greater circuit depth, as it requires more terms in the Hamiltonian in order to derive an operator that is applied only on the desired gauge link.

The operator $K$ can be decomposed into Pauli strings as (a sum over links of)

$$\begin{aligned} K(l) &= \frac{3}{4}\,\mathrm{diag}(0,1,1,1,1,0,0,0) \\ &= \frac{3}{16}(2III + ZII - ZIZ - ZZI - ZZZ), \end{aligned} \tag{76}$$

where we have appended each $K(l)$ with zero eigenvalues to encode over three qubits. We note in passing that other paddings of these operators are possible, but we did not find significant changes to gate counts. The operator $\exp(\mathrm{i}\phi III)$ corresponds to a global phase, having no effect on measurements, and is ignored. Because these Pauli strings are already diagonal, we can immediately apply the routine discussed in the step 5 to obtain the quantum circuit in 14. Note that this circuit has to be applied to every link individually. Therefore, the cost of applying $K$ for an elementary plaquette is 16 CNOT gates.

As discussed in Chapter 3.4.1: $N = 4$ (spinor) irrep, there are 64 terms in the $\sum_{\mathrm{i,j,k,l=1}}^{4} c_{\mathrm{ijkl}}\,\Gamma_{\mathrm{ijkl}}$ expansion of the plaquette term. In this representation, however, each $\Gamma_{\mathrm{i}}$ can be decomposed into four Pauli strings. Consequently, each $\Gamma_{\mathrm{ijkl}}$ decomposes into $4 \times 4 \times 4 \times 4 = 256$ Pauli strings, and each plaquette therefore is a combination of $64 \times 256 = 16,384$ Pauli strings. By the sequential algorithm discussed in step 3 of the method, we find that these Pauli strings can be grouped into 64 clusters, each containing

256 commuting Pauli strings. We diagonalize each cluster as per step 4 and compile the circuit of each resulting diagonal cluster as per step 5.

As expected, most of the complexity of this procedure lies in compiling the circuit of the diagonal cluster. In fact, the total number of CNOT gates required for diagonalizing all the clusters is $2 \times 320 = 640$. On the other hand, the total number of CNOT gates needed to compile all 64 diagonal clusters is 16,512. Therefore, we use 17,152 CNOT gates to compile one plaquette term of the Hamiltonian. Since 16 CNOT gates were used to compile the kinetic part of the Hamiltonian, we obtain a circuit with 17168 CNOT gates, or $\approx 1.05$ CNOT gates per Pauli string.

It is worth mentioning a recent proposal to exploit the symmetries of wave functions satisfying the Gauss's law condition of $SU(2)$ lattice gauge theory to more sparsely (i.e., in fewer dimensions) encode the nontrivial representations of $SU(2) \times SU(2)$ on qubits [118, 16]. In particular, the space of wave functions for lattices whose vertices each see exactly three links meeting can be constrained at the classical level (i.e., before encoding on qubits) in a relatively simple fashion to solve the $SU(2)$ Gauss's law condition of the theory automatically and thereby reduce the $2 \oplus \bar{2}$ representation subspace to one physical dimension. This design results in a model requiring exactly one qubit per gauge link, however severely restricting the geometry of gauge links and vertices. In order to avoid this restriction and more broadly allow for arbitrary $d$ spatial dimensions, we consider a square lattice geometry and focus our attention to the aforementioned encoding of each gauge link on qubits separately without yet imposing Gauss's law, ensuring a more modular nature to this procedure upon which we can build larger lattice model simulations. Nonetheless, the methods we present may also be applied to a Hamiltonian with a different geometry or encoding, and we will return to a discussion of non-cubic lattice geometries later in Chapter 3.5: Discussion.

**Chapter 3.5: Discussion**

In this paper, we have offered a contribution to the very thorny and important problem of

understanding, in detail, the resource requirements for quantum simulations—including but not limited to $SU(2)$ gauge theories. In particular, we assembled state-of-the-art quantum circuit compilation methods and showed specifically how $SU(2)$ gauge theory simulations would be prohibitive on digital quantum computers in the current era. Moreover, we can see from these methods that larger-dimensional gauge links for these theories will also necessitate quantum error correction codes to address the severe noise introduced by such large resource estimates. We hope that other efforts will build upon this work as a foundation, either to develop more efficient resource usage or perhaps to show these circuits to be as efficient as we can obtain.

We believe that the compilation method we used is at least competitive with the other methods currently available, as it performs well in several cases where other methods have been tried or rigorous bounds are known. Nevertheless, the compilation method is very generic, as it applies to any finite-dimensional Hamiltonian and makes no use of specific features of gauge theories.

In particular, the fact that the *physical* Hilbert space is a small subspace of the theory (as many states are just gauge copies of each other) was not exploited here. Conversely, it is not obvious how to utilize gauge invariance in this formulation, since it is generally acknowledged that rewriting a gauge theory in terms of gauge-invariant quantities leads to non-localities, which could make the circuit depths even larger. Still, this reduction is a possible avenue for improvement, and perhaps a gauge-fixed version of the formalism can also be used for this purpose.

There is another sense in which the large Hilbert spaces we encountered could be shrunk. For instance, the five-dimensional local Hilbert space of the Horn model was encoded onto three qubits, leaving $2^3 - 5 = 3$ dimensions unused. This redundancy is present in any qubitization with a local Hilbert space whose dimension is not a power of 2. It is possible that some alternative encoding of these links will permit a quantum circuit to properly evolve the five-dimensional subspace that actually describes each link of the model and yet

has a different action on the remaining three dimensions from what we have prescribed. At this time, we do not have a systematic way of exploiting this freedom to shorten circuits. Finally, a key point: the large circuit depths we found stresses the importance of having a field space truncation with small dimensions. In particular, this point reinforces the need for qubitization in the same universality class as the continuum model. This way, the final continuum limit will require an increase in the number of spatial lattice sites (linearly increasing the number of qubits required yet not the circuit depth) but not that the field truncation be lifted—a step that would enormously increase the circuit depth as we saw in the examples shown here.

**Chapter 3.6: Acknowledgements**

This material is based upon work supported in part by the U.S. Department of Energy, Office of Nuclear Physics under Award Number(s) DE-SC0021143, and DE-FG02-93ER40762, and DE-FG02-95ER40907. The modules *Qiskit* [159] and *Numpy* [94] have been significantly used throughout this project.

**Chapter 3.7: Appendix**

**Chapter 3.7.1: CNOT-cost lower bound of simulating Pauli strings**

In this appendix, we elaborate on the $O(N)$ lower bound estimate of CNOT cost in simulating a diagonal Hamiltonian (See Chapter 3.3.1: Random Diagonal Hamiltonians), where $N$ is the number of Pauli strings in its expansion. This lower bound applies to methods that utilize CNOT conjugations to reduce a Pauli string into an one-qubit operator, as described at the beginning of step 5 in Chapter 3.2: The compilation method. We argue that at least one CNOT is required between the rotation gates for simulating diagonal $\exp(\mathrm{i}\phi_\mathrm{i} P_\mathrm{i})$ and $\exp\left(\mathrm{i}\phi_\mathrm{j} P_\mathrm{j}\right)$ sequentially, for $j \neq i$ and with $P_\mathrm{i}$ or $P_\mathrm{j}$ consisting of at least two nontrivial factors. Here, the only restriction on the phases $\phi_\mathrm{i}$ and $\phi_\mathrm{j}$ is that they cannot both be equal to odd integer multiples of $\pi$.

Since $P_\mathrm{i}$ and $P_\mathrm{j}$ are diagonal, they may contain only factors $I$ (trivial) and $Z$ (non-trivial).

Let $\omega\left[P_{\mathrm{i}}\right]$ be the number of non-trivial factors in $P_{\mathrm{i}}$, or equivalently the Hamming weight of $P_{\mathrm{i}}$ (i.e., $\omega[I]=0$ and $\omega[Z]=1$). In addition, let $C_{\mathrm{i}}$ be a product of CNOT gates whose conjugation of $P_{\mathrm{i}}$ reduces to a string of Hamming weight 1. We will prove that $C_{\mathrm{i}} \neq C_{\mathrm{j}}$, implying the existence of at least one CNOT gate that may not be canceled when implementing $P_{\mathrm{i}}$ and $P_{\mathrm{j}}$ in sequence.

We can readily observe that $C_{\mathrm{i}} \neq C_{\mathrm{j}}$ if $\omega\left[P_{\mathrm{i}}\right] \neq \omega\left[P_{\mathrm{j}}\right]$, as this assumption implies that $C_{\mathrm{i}}$ and $C_{\mathrm{j}}$ are sequences of different lengths. Therefore, we turn our focus to the case $\omega\left[P_{\mathrm{i}}\right]=\omega\left[P_{\mathrm{j}}\right]=k \geq 2$, for which we will prove $C_{\mathrm{i}} \neq C_{\mathrm{j}}$ by induction on $k$.

First, consider the base case $k=2$: Let $P_{\mathrm{i}} \neq P_{\mathrm{j}}$ and $\omega\left[P_{\mathrm{i}}\right]=\omega\left[P_{\mathrm{j}}\right]=2$. Perform a $\mathrm{CNOT}_{\mathrm{a,b}}$ gate conjugation, with $a$ and $b$ chosen such that $P_{\mathrm{i}} \mapsto P_{\mathrm{i}}^{\prime}$ with $\omega\left[P_{\mathrm{i}}^{\prime}\right]=1$. Suppose the same CNOT conjugation also results in $\omega\left[P_{\mathrm{j}}^{\prime}\right]=1$. Then Eq. (62) implies necessarily $P_{\mathrm{i}}=P_{\mathrm{j}}$, contradicting the assumption $P_{\mathrm{i}} \neq P_{\mathrm{j}}$. (To see this conclusion, repeat the same conjugation again to $P_{\mathrm{i}}^{\prime}$ and $P_{\mathrm{j}}^{\prime}$, reproducing $P_{\mathrm{i}}$ and $P_{\mathrm{j}}$ respectively, which both have Hamming weight 2. Consequently, we see that $P_{\mathrm{i}}^{\prime}$ and $P_{\mathrm{j}}^{\prime}$ must each act nontrivially only on qubit $b$, meaning $P_{\mathrm{i}}^{\prime}=P_{\mathrm{j}}^{\prime}$.) Therefore, there is a distinct CNOT conjugation needed to implement $P_{\mathrm{j}}$, and hence $C_{\mathrm{i}} \neq C_{\mathrm{j}}$.

Having taken care of the base case, we state the induction hypothesis: there exists an integer $k \geq 2$ such that if $P_{\mathrm{i}} \neq P_{\mathrm{j}}$ while $\omega\left[P_{\mathrm{i}}\right]=\omega\left[P_{\mathrm{j}}\right]=k$ then $C_{\mathrm{i}} \neq C_{\mathrm{j}}$. Finally, we prove the inductive step; consider the case where $P_{\mathrm{i}} \neq P_{\mathrm{j}}$ while $\omega\left[P_{\mathrm{i}}\right]=\omega\left[P_{\mathrm{j}}\right]=k+1$. Perform a $\mathrm{CNOT}_{\mathrm{a,b}}$ conjugation resulting in $P_{\mathrm{i}}^{\prime}$ and $P_{\mathrm{j}}^{\prime}$ such that $\omega[P_{\mathrm{i}}^{\prime}]=k$. If $\omega[P_{\mathrm{j}}^{\prime}] \neq k$, then we are done, by the observation made before the beginning of this induction proof. Now, if $\omega[P_{\mathrm{j}}^{\prime}]=\omega[P_{\mathrm{i}}^{\prime}]=k$, we consider the remaining cases: $P_{\mathrm{i}}^{\prime}=P_{\mathrm{j}}^{\prime}$ (already yielding a contradiction to our assumption $P_{\mathrm{i}} \neq P_{\mathrm{j}}$ by a similar reasoning as in the base case) and $P_{\mathrm{i}}^{\prime} \neq P_{\mathrm{j}}^{\prime}$. In this latter case, we may invoke the inductive hypothesis, to see that $C_{\mathrm{i}}^{\prime}$ and $C_{\mathrm{j}}^{\prime}$ corresponding to $P_{\mathrm{i}}^{\prime}$ and $P_{\mathrm{j}}^{\prime}$ are not equal. Therefore, we also have $C_{\mathrm{i}} \neq C_{\mathrm{j}}$, completing our inductive step.

Iterating this argument over all consecutive pairs of the $\mathcal{N}$ diagonal Pauli strings in a given

order for Trotterized time evolution, we find that there must be greater than $\mathcal{N}_2$ CNOT gates used to implement the complete circuit, where $\mathcal{N}_2$ is the number of Pauli strings with Hamming weight greater than one, which means $\mathcal{N} - (n+1) \leq \mathcal{N}_2 \leq \mathcal{N}$. In addition, when considering our method prescribed in Chapter 3.2: The compilation method, there is a cost of uncomputing the CNOT conjugations instantiated with each $C_i$; however, we argue in step 5 of our procedure that this cost is $O(n^2)$. In kind, the diagonalization of Pauli strings has a CNOT cost of $O(n^2)$ as well. For $\mathcal{N} \gg n$, we thus expect a scaling in CNOT cost that is at least $\sim \mathcal{N}$.

It is worth noting that relative CNOT cost of simulating consecutive Pauli strings with one ancilla was found to define a metric space over these strings [176], which would imply a generic lower bound cost of at least $\sim \mathcal{N}$ as well. However, we do not find this formulation for assessing relative CNOT costs to be applicable to our method.

### Chapter 3.7.2: CNOT gate count for a diagonal Hamiltonian with $\mathcal{N} = 2^n$ Pauli Strings

In this section, we prove for general $n \geq 2$ that, given a diagonal Hamiltonian with all $2^n - 1$ Pauli strings besides the identity, our algorithm realizes the exact time evolution with precisely $2^n - 2$ CNOT gates. To simplify the wording of our proof, we also include the identity Pauli string, so that we have $2^n$ Pauli strings, contributing only an extra global phase and without changing the CNOT gate count.

First, recall our tree traversal procedure for compiling the circuit of a diagonal Hamiltonian in step 5 of Chapter 3.2: The compilation method. We perform a CNOT gate conjugation once we encounter a node of value 1 that has a parent with value 1, flipping the value of the child node in the process. For the tree representing a Hamiltonian composed of $2^n$ Pauli strings, every node has an equal number of children with values 0 and 1 at each deeper level. Consequently, any CNOT gate conjugation preserves the number of children nodes of value 1 that have a parent with value 1, even if we perform the CNOT conjugation on multiple branches simultaneously. Since a CNOT conjugation is

applied when we encounter such a child node, the number of CNOT conjugations is precisely the number of such children. With these observations in hand, we are ready to find the CNOT cost of a circuit prescribed by our procedure.

Neglecting the root of the tree, we label the levels by $l = 1, \ldots, n$. The number of level $l$ nodes that have a parent node with value 1 is $2^{l-1} - 1$ in a complete binary tree (a binary tree in which every node besides the leaves has 2 children). Then, the total number of such nodes is $\sum_{l=1}^{n} 2^{l-1} - 1 = 2^n - (n+1)$, which corresponds to the total number of CNOT conjugations. As discussed in step 5, this quantity is precisely the number of CNOT gates that are implemented on the circuit before inserting any of the CNOT gates from the stack into the circuit. Thus, determining the overall CNOT cost has been reduced to calculating the remaining number of CNOT gates in the stack. Having every possible diagonal Pauli string in our Hamiltonian, we must perform every possible $\mathrm{CNOT}_{ji}$ with $j > i$ as prescribed. For each $i, j$, the number of $\mathrm{CNOT}_{ji}$ gates in the stack is odd if and only if $j - i = 1$ because every node with value 1 at a level $i$ has precisely $2^{(j-i)-1}$ children at level $j > i$ with value 1. Having the same target qubit, these CNOT gates are all consecutive in the stack, and we may cancel all the CNOT gates with $j - i \neq 1$, leaving only one of each CNOT gate with $j - i = 1$, of which there are $n - 1$. Hence, the total CNOT cost is therefore $2^n - (n+1) + (n-1) = 2^n - 2$.

# Chapter 4: Fuzzy Gauge Theory


## Abstract

Continuous gauge theories, because of their bosonic degrees of freedom, have an infinite-dimensional local Hilbert space. Encoding these degrees of freedom on qubit-based hardware demands some sort of "qubitization" scheme, where one approximates the behavior of a theory while using only finitely many degrees of freedom. We propose a novel qubitization strategy for gauge theories, called "fuzzy gauge theory," building on the success of the fuzzy $\sigma$-model in earlier work. We provide arguments that the fuzzy gauge theory lies in the same universality class as regular gauge theory, in which case its use would obviate the need of any further limit besides the usual spatial continuum limit. Furthermore, we demonstrate that these models are relatively resource-efficient for quantum simulations.


## Chapter 4.1: Introduction

There are many obstacles to the use of quantum computers in quantum field theory calculations. Besides the need for more reliable hardware than currently available, there are a number of conceptual questions to be answered before these calculations become feasible. This paper addresses one of these obstacles: how to reduce the infinite-dimensional Hilbert space of a bosonic field theory, in particular a gauge theory, to a finite-dimensional Hilbert space that "fits" onto a quantum computer with finite registers.[19]

Before proceeding, let us emphasize the importance of this direction and briefly contrast this approach to alternative numerical methods. The dimension of the Hilbert space in a finite-dimensional field theory grows exponentially with the volume ($\sim DV$ for local Hilbert space dimension $D$); therefore, the direct diagonalization of the time evolution

[19] The application of tensor network methods also favors theories with a finite-dimensional Hilbert space. See, for instance Ref. [17].

operator by classical computers also has a computational cost that grows exponentially with the volume $\mathsf{V}$. Monte Carlo methods are more efficient, with a cost scaling roughly like $\sim \mathsf{V}$, but they are limited to problems that can be framed as an evolution in *imaginary* time. This restriction leaves real-time evolution and finite-chemical potential problems, among others, mostly out of reach of Monte Carlo methods. The culprit of this limitation is the famous sign problem that has resisted valiant attempts to bypass it (see Refs. [3, 157, 60, 146, 112, 76, 6] for reviews in the context of QCD simulations.) The quantum simulation of the evolution can instead be performed directly in real time, manipulating a number of qubits proportional to $\mathsf{V}$ (and not exponential in $\mathsf{V}$). Therein lies a possible (exponential) quantum advantage over classical methods.

The first step of qubitization is the substitution of the continuous, $d$-dimensional physical space by a lattice with a finite lattice spacing $\mathsf{a} > 0$ and finite extent $\mathsf{L} = \mathsf{aN}$ in each direction. Space discretization is a well understood topic, since it is a routine part of the lattice field theory approach. Whether this discretization of spatial domain alone suffices depends on the spin statistics of one's theory. For purely fermionic theories, the resulting Hilbert space is already finite-dimensional, and so in principle it can be readily encoded and simulated on a quantum computer. However, for bosonic fields the occupation numbers at a lattice site may be arbitrarily large; even the Hilbert space of a bosonic theory defined on a single spatial site (or link) is infinite-dimensional. Therefore, for bosons some truncation of the *field* space is also required to render the *local* Hilbert space finite. This reduction of the Hilbert space to a finite-dimensional one is sometimes called "qubitization." Many methods to accomplish this truncation have been proposed, which we briefly review below.

Perhaps the most obvious approach for qubitization is the substitution of the field space manifold by a finite subset. For instance, the substitution of the sphere $S^2$ in the $(1+1)$-dimensional $O(3)$ $\sigma$-model by the vertices of a platonic solid. The internal symmetries are reduced to a finite group and Monte Carlo studies have shown (after

substantial discussion in the literature) that these models are *not* in the same universality class as the $O(3)$ $\sigma$-model [96, 43] although fairly large, but finite, correlation lengths are achievable. In the $(3+1)$-dimensional $SU(3)$ gauge theory a similar phenomenon occurs. In Ref. [12], a gauge theory based on the $S(1080)$ group, the largest (and therefore finest) "crystal-like" discrete subgroup of $SU(3)$ was simulated. The result shows that this lattice theory does not have a continuum limit although fairly large correlation lengths can be achieved, corresponding to a lattice spacing of the order of $\mathsf{a} \approx 0.08$ fm, small enough to be of phenomenological use. The reason these truncations fail to have a continuum limit can be intuited by considering the imaginary time path integral. Due to the discretization of the field values, there is a gap between the smallest and the next-to-smallest value of the action. When the coupling becomes small all field configurations except one are exponentially suppressed, resulting in the "freezing" of the system. Nevertheless, there are many on-going efforts to work around this issue in the case of $SU(2)$ gauge theory, including different samplings from the gauge group manifold [95, 103] as well as studies of finite subgroups [4, 80, 90, 88, 136], $q$-deformed groups [190], and different encodings of physical degrees of freedom [16, 14, 161, 163, 118, 1, 59].

Another common approach to qubitization is to truncate the one-site (or one-link) Hilbert space to some finite irrep of the Laplacian on the target space of the theory [18, 93, 42, 192, 131]. For instance, in the $O(3)$ $\sigma$-model, where the fields take value on a sphere $S^2$, this strategy truncates the Hilbert space of spherical harmonics up to some value $\ell \leq \ell max$ of the angular momentum. In an $SU(2)$ gauge theory, on each link one would truncate the basis of Wigner functions $\mathcal{D}^{\mathrm{j}}_{\mathrm{mm}'}$ up to $j \leq jmax$. Such a truncation preserves the gauge symmetry of the theory, but it has serious drawbacks. First, because such a basis diagonalizes a kinetic energy operator and the truncation restricts to low irreps, one expects such a truncation to effectively capture the physics of the original theory only in a strong-coupling limit. In asymptotically free theories, this limit coincides with a large lattice spacing and therefore is not expected to be well-suited for studying

continuum physics. Secondly, as demonstrated in the case of the $\sigma$-model, such a truncation can entirely fail to have a continuum limit outright [9]. Lastly, as a practical consideration: while such discretizations of field space can be arbitrarily improved by increasing $jmax$, doing so comes at the price of the number of qubits per register (i.e., site or link) and the number of gates in the simulation circuit. In fact, there is evidence that the number of gates required to simulate the time evolution grows considerably with the number of qubits per link/site [145]. This observation suggests that there is a high cost in approaching the continuum limit that most likely negates the potential quantum advantage in such a framework.

We note that there have been alternatives to the truncation strategy described above to obtain a finite gauge theory, wherein one searches for finite matrices satisfying the exact quantum symmetry algebra [123] and constructs a gauge-invariant Hamiltonian out of those matrices. For example, the first such proposal was due to Horn in 1981 [100], who explored an $SU(2)$ gauge theory with a five-dimensional one-link Hilbert space. The extension to higher gauge groups was considered, but then dismissed due to the presence of a spurious $U(1)$ gauge symmetry. Orland and Rohrlich [151] later proposed "gauge magnets" as a family of finite $SU(2)$ gauge theories, with its smallest representation being of dimension 4 per link. In 1996, the "quantum link" framework was introduced by Chandrasekaran et al. [45], which could be formulated for arbitrary $SU(N)$ [38]. For $SU(2)$ the smallest representation was again four-dimensional, but this representation had the spurious $U(1)$ problem, as Horn's did; to remedy this complication, they proposed carrying out calculations with a six-dimensional representation for each link.

Regardless of the discretization strategy, one ultimately wants not only a finite-dimensional model with gauge symmetry, but also a model that reproduces the spectrum of the desired continuum gauge theory in a critical limit. To that end, we propose a framework for "fuzzifying" gauge theory. It constitutes a generalization of the strategy

we employed in the fuzzy $\sigma$-model [13, 10, 9]. Although the fuzzy approach[20] is closer in spirit to the finite gauge theory strategy, it is guided by analogies with the original theory in the field space representation, entailing a different Hilbert space from the models outlined above. Although nonperturbative simulations of the theory are not yet accessible, we will identify throughout the paper various properties that the fuzzy model satisfies and we believe must be satisfied by any qubitization of non-Abelian gauge theories. For reference, these properties, together with our degrees of confidence in them vis-à-vis the fuzzy model, are summarized finally in the Conclusions (Chapter 4.6: Conclusions).

The bulk of this article is organized as follows. In Chapter 4.2: Lattice gauge theory in the hamiltonian formalism, we briefly review the Hamiltonian formulation of untruncated gauge theories on a lattice. In Chapter 4.3: Fuzzy lattice gauge theory, we describe the properties of "fuzzy" qubitizations of lattice gauge theories in general, and we consider an explicit realization in the $SU(2)$ case. Then, in Chapter 4.4: The continuum limit of fuzzy theories, we explore the features of fuzzy models that allow for a continuum limit, first in the simpler case of the fuzzy $\sigma$-model, then in the case of the fuzzy $SU(2)$ gauge theory. Finally, in Chapter 4.5: Quantum Circuitry, we demonstrate the simulability of the fuzzy $SU(2)$ proposal.

**Chapter 4.2: Lattice gauge theory in the hamiltonian formalism**

The fuzzy gauge theory that we propose will be formulated in the Hamiltonian language, convenient for quantum computer implementations. As such, we begin by reviewing some features of untruncated lattice gauge theory in this language. This formalism has been well-understood since Kogut & Susskind first described it [123], and so we only briefly recapitulate it here to establish notation and highlight a few points that will be pertinent later. Although we will take the case of an $SU(N)$ gauge theory, the formulation readily generalizes to other compact groups.

[20] We stress the difference between our approach, where the *target* space of the theory is substituted by its fuzzy version, from the extensively studied fuzzy field theories where *spacetime* becomes a non-commuting space. See Ref. [64] for a review.

We start with a $d$-dimensional spatial lattice (and continuum time). The target space on each link is the gauge group in consideration – here an $SU(N)$ manifold (see, e.g., Refs. [165, 56] for $N = 2$) – constituting the bosonic degrees of freedom of the theory. The wave function for a single link is a complex function of an $SU(N)$ matrix $U$, and furthermore the wave function for the total system will be a function of all links, $\psi(U_1, U_2, \ldots)$, describing both "physical" and "unphysical" states each to be distinguished later. The wave function on a single link may be expanded in an infinite Taylor series

$$\psi(U) = \psi_0 + \psi_{\mathrm{ij}} U_{\mathrm{ij}} + \widetilde{\psi}_{\mathrm{ij}} U^*_{\mathrm{ij}} + O(U^2), \tag{77}$$

with implied summation over repeated color indices $i, j = 1, \ldots, N$. Notably, these states belong to an infinite-dimensional Hilbert space, even if the spatial lattice has a finite number of links.

A gauge transformation at a site $x$ is defined by multiplying all links connected to $x$ by an element of $SU(N)$, from either the left or the right (depending on the orientation of the links). Thus, a one-link wave function $\psi$ transforms as

$$\begin{aligned} \psi(U) &\mapsto \mathbb{L}\psi(U) = \psi(L^{-1}U), \\ \psi(U) &\mapsto \mathbb{R}\psi(U) = \psi(UR), \end{aligned} \tag{78}$$

depending on whether the link points away from ($L$) or into ($R$) the site $x$. These operators can be written in terms of infinitesimal generators, $\mathbb{T}^{\mathrm{L,R}}_{\mathrm{a}}$ ($a = 1, \ldots, N^2 - 1$), as

$$\mathbb{L} = e^{-\mathrm{i}\,\omega^{\mathrm{L}}_{\mathrm{a}} \mathbb{T}^{\mathrm{L}}_{\mathrm{a}}}, \quad \mathbb{R} = e^{-\mathrm{i}\,\omega^{\mathrm{R}}_{\mathrm{a}} \mathbb{T}^{\mathrm{R}}_{\mathrm{a}}}, \tag{79}$$

where real coefficients $\omega^{\mathrm{L,R}}_{\mathrm{a}}$ parametrize the group elements $L = \exp\bigl(-\mathrm{i}\,\omega^{\mathrm{L}}_{\mathrm{a}}\,\lambda_{\mathrm{a}}/2\bigr), R = \exp\bigl(-\mathrm{i}\,\omega^{\mathrm{R}}_{\mathrm{a}}\,\lambda_{\mathrm{a}}/2\bigr)$ with $\frac{1}{2}\lambda_{\mathrm{a}}$ being the generators of the fundamental representation of $SU(N)$. On a single link, the generators are Hermitian,

first-order differential operators [141, 132] satisfying

$$[\mathbb{T}^{\mathrm{L}}_{\mathrm{a}}, \mathbb{T}^{\mathrm{L}}_{\mathrm{b}}] = \mathrm{i} f_{\mathrm{abc}} \mathbb{T}^{\mathrm{L}}_{\mathrm{c}}, \tag{80}$$

$$[\mathbb{T}^{\mathrm{R}}_{\mathrm{a}}, \mathbb{T}^{\mathrm{R}}_{\mathrm{b}}] = \mathrm{i} f_{\mathrm{abc}} \mathbb{T}^{\mathrm{R}}_{\mathrm{c}}, \tag{81}$$

$$[\mathbb{T}^{\mathrm{L}}_{\mathrm{a}}, \mathbb{T}^{\mathrm{R}}_{\mathrm{b}}] = 0, \tag{82}$$

where $f_{\mathrm{abc}}$ is the totally antisymmetric structure tensor of $SU(N)$.

We define field operators $\mathbb{U}_{\mathrm{ij}}$ at every link by

$$\mathbb{U}_{\mathrm{ij}} \psi(U) = U_{\mathrm{ij}} \psi(U), \tag{83}$$

which implies the commutation relations

$$[\mathbb{U}_{\mathrm{ij}}, \mathbb{U}_{\mathrm{kl}}] = [\mathbb{U}_{\mathrm{ij}}, \mathbb{U}^{*}_{\mathrm{kl}}] = 0. \tag{84}$$

Now, the links $U$ are $SU(N)$ matrices whose components obey the relations

$$U^{*}_{\mathrm{ji}} U_{\mathrm{jk}} = \; U_{\mathrm{ij}} U^{*}_{\mathrm{kj}} = \delta_{\mathrm{ik}}, \tag{85}$$

$$\det U = 1. \tag{86}$$

The same relations are therefore satisfied by the field operators $\mathbb{U}_{\mathrm{ij}}, \mathbb{U}^{*}_{\mathrm{ij}}$, and the ordering of the operators is immaterial since $\mathbb{U}_{\mathrm{ij}}, \mathbb{U}^{*}_{\mathrm{ij}}$ commute amongst themselves.

From the previous definition of gauge transformations, one finds that the link operators transform as

$$\mathbb{R}^{\dagger}\, \mathbb{L}^{\dagger}\, \mathbb{U}_{\mathrm{ij}}\, \mathbb{L}\, \mathbb{R} = L_{\mathrm{ii'}} \mathbb{U}_{\mathrm{i'j'}} (R^{-1})_{\mathrm{j'j}}, \tag{87}$$

the infinitesimal versions of which satisfy

$$[\mathbb{T}^{\mathrm{L}}_{\mathrm{a}}, \mathbb{U}_{\mathrm{ij}}] = -(\tfrac{1}{2}\lambda_{\mathrm{a}})_{\mathrm{ii'}}\mathbb{U}_{\mathrm{i'j}}, \tag{88}$$

$$[\mathbb{T}^{\mathrm{R}}_{\mathrm{a}}, \mathbb{U}_{\mathrm{ij}}] = +\mathbb{U}_{\mathrm{ij'}}(\tfrac{1}{2}\lambda_{\mathrm{a}})_{\mathrm{j'j}}. \tag{89}$$

Finally, the physical Hilbert space of the theory is defined as the gauge-invariant subspace of the total Hilbert space, that is, the wave functions satisfying

$$e^{-\mathrm{i}\omega_{\mathrm{a}}\mathbb{G}_{\mathrm{a}}(\mathrm{x})}\psi_{\mathrm{phys}}(\{U_\ell\}) = \psi_{\mathrm{phys}}(\{U_\ell\}), \tag{90}$$

$$\mathbb{G}_{\mathrm{a}}(x) = \sum_{\mu}\left[\mathbb{T}^{\mathrm{L}}_{\mathrm{a}}(x,\mu) + \mathbb{T}^{\mathrm{R}}_{\mathrm{a}}(x-\hat{\mu},\mu)\right] \tag{91}$$

for all $x$ and $a$; here, $\mu$ runs over all spatial directions. The infinitesimal condition $\mathbb{G}_{\mathrm{a}}(x)\psi_{\mathrm{phys}}(\{U_1\}) = 0$ is the quantum version of Gauss's law.
Using Eqs. (80-81) and (88-89), we may confirm the gauge invariance of the Kogut-Susskind Hamiltonian,

$$\begin{aligned}\mathsf{a}\mathbb{H} = \frac{g^2}{2}\sum_{\ell}\left[\mathbb{T}^{\mathrm{L}}(\ell)^2 + \mathbb{T}^{\mathrm{R}}(\ell)^2\right] \\ - \frac{1}{2g^2}\sum_{\mathrm{P}}\square(P) + \mathrm{h.c.},\end{aligned} \tag{92}$$

where $\ell = (x,\mu)$ label the links of the lattice, and $P = (x,\mu,\nu)$ label the plaquettes,

$$\square(P) = \mathbb{U}_{\mathrm{ij}}(\ell_1)\,\mathbb{U}_{\mathrm{jk}}(\ell_2)\,\mathbb{U}_{\mathrm{lk}}(\ell_3)^*\,\mathbb{U}_{\mathrm{il}}(\ell_4)^*. \tag{93}$$

Here, $\mathbb{U}(\ell_{\mathrm{i}})$ are the positively-oriented links comprising a plaquette $P$. We work in units of the lattice spacing, so that $g^2$ is dimensionless for any chosen spacetime. For $d < 3$, the dimensionful bare coupling is $\mathsf{a}^{\mathrm{d}-3}g^2$, but the continuum limit is achieved by $g^2 \to 0$. Of course, many other gauge-invariant terms may be added to Eq. (92), but such modified

Hamiltonians are believed to lead to the same continuum limit as $g^2 \to 0$.[21] Taking this limit is a non-trivial process, which has been studied extensively. To summarize that analysis, it is found that as $g^2 \to 0$, correlation lengths $\xi$ become exponentially larger than the lattice spacing ($\xi/\mathsf{a} \sim \exp(1/g^2)$) and the continuum limit is thus achieved. Additional terms in the Hamiltonian, *as long as they don't break any symmetry*, only change the rate at which this same limit is approached, on account of the universality of critical phenomena [188]. These additional terms are sometimes used to achieve higher accuracy with coarser lattices (i.e., the so-called Symanzik improvement program [175, 153]).
The ingredients we have presented, namely: a Hilbert space, a realization of gauge transformations on this space, and consequently the structure of typical gauge-invariant observables such as the Hamiltonian, are enough to define a quantum gauge theory. Note that the commutativity of field operators, as expressed in 84, did not play an essential role in the (gauge) symmetry properties of the theory.

**Chapter 4.3: Fuzzy lattice gauge theory**

Our goal is to define a theory with a finite-dimensional Hilbert space having the same continuum limit as that of the $SU(N)$ gauge theory defined in the previous section. To this end, we borrow a strategy from the philosophy of non-commutative geometry: at each link of the lattice, we replace the Hilbert space of functions on $SU(N)$ by a *finite-dimensional space of matrices*, in which each matrix element $U_{ij}$ is replaced by a $D \times D$ matrix $\mathcal{U}_{ij}$ for each $i, j = 1, \ldots, N$, with $D$ yet to be determined. If the $\mathcal{U}_{ij}$, together with their conjugate-transposes $(\mathcal{U}_{ij})^\dagger$ and products thereof, span the space of matrices, then states on this "fuzzy $SU(N)$" will be expressible as a series, analogous to 77,

$$\Psi = \Psi_0 1 + \Psi_{ij}\mathcal{U}_{ij} + \widetilde{\Psi}_{ij}(\mathcal{U}_{ij})^\dagger + O(\mathcal{U}^2), \tag{94}$$

where the complex numbers $\widetilde{\Psi}_{ij}$ are again not necessarily related to $\Psi_{ij}$. Because

[21] To recover Lorentz invariance in the continuum limit, one should multiply the operators in $\mathbb{H}$ by an appropriately-determined renormalization constant $\eta(g^2)$ [167], as described also in Ref. [10].

sufficiently high powers of these finite matrices will not be linearly independent from lower powers, the series must terminate at a finite order. The Hilbert space on each link has the inner product $\langle\Psi|\Phi\rangle := \mathrm{tr}[\Psi^\dagger\Phi]$ and dimension $D^2$.

At a minimum, the finite theory should have the same internal symmetries as the untruncated theory, according to the standard universality arguments of Wilsonian renormalization group. In particular, we must find $D \times D$ matrices $\mathcal{L}$ and $\mathcal{R}$ that realize gauge transformations via conjugation:

$$\Psi \;\mapsto\; \mathcal{R}\,\mathcal{L}\,\Psi\,\mathcal{L}^\dagger\,\mathcal{R}^\dagger. \tag{95}$$

The generators of these transformations are given by

$$\mathcal{T}_a^{\mathrm{L}} = [T_a^{\mathrm{L}}, \bullet], \quad \mathcal{T}_a^{\mathrm{R}} = [T_a^{\mathrm{R}}, \bullet]. \tag{96}$$

where $T_a^{\mathrm{L,R}}$ are $D$-dimensional representations of the $\frac{1}{2}\lambda_a$, satisfying the algebra Eqs. (80-82). From this one can readily check that $\mathcal{T}_a^{\mathrm{L,R}}$ also satisfy this same algebra. To constitute a gauge symmetry, the operators $\mathcal{T}_a^{\mathrm{L,R}}$ and $\mathcal{U}_{ij}$ together must also satisfy analogues of Eqs. (88-89). This property will be guaranteed as long as $T_a^{\mathrm{L,R}}$ themselves with $\mathcal{U}_{ij}$ obey those equations, owing to the Leibniz rule obeyed by commutators $\mathcal{T}_a^{\mathrm{L,R}}$. Thus, for any matrices $\mathcal{U}_{ij}$, $T_a^{\mathrm{L,R}}$ satisfying a $D$-dimensional representation of the gauge symmetry algebra, the operators $\mathcal{U}_{ij}, \mathcal{T}_a^{\mathrm{L,R}}$ will satisfy an (adjoint) representation of that

same algebra,

$$[\mathcal{T}_a^L, \mathcal{T}_b^L] = i f_{abc} \mathcal{T}_c^L \tag{97}$$

$$[\mathcal{T}_a^R, \mathcal{T}_b^R] = i f_{abc} \mathcal{T}_c^R \tag{98}$$

$$[\mathcal{T}_a^L, \mathcal{T}_b^R] = 0 \tag{99}$$

$$[\mathcal{T}_a^L, \mathcal{U}_{ij}] = -(\tfrac{1}{2}\lambda_a)_{ii'} \mathcal{U}_{i'j} \tag{100}$$

$$[\mathcal{T}_a^R, \mathcal{U}_{ij}] = +\mathcal{U}_{ij'} (\tfrac{1}{2}\lambda_a)_{j'j}, \tag{101}$$

when acting on the fuzzy Hilbert space. It follows, for example, that the link matrices transform like

$$\begin{aligned} e^{-i\,\omega_a^R \mathcal{T}_a^R} e^{-i\,\omega_a^L \mathcal{T}_a^L} \mathcal{U}_{ij} &= \mathcal{R}\,\mathcal{L}\,\mathcal{U}_{ij}\,\mathcal{L}^\dagger\,\mathcal{R}^\dagger \\ &= L_{ii'} \mathcal{U}_{i'j'} (R^{-1})_{j'j}, \end{aligned} \tag{102}$$

with $\mathcal{L} = \exp\left(-i\,\omega_a^L T_a^L\right)$ and $\mathcal{R}$ defined analogously. From these matrices, one may construct gauge-invariant operators in the same way as in the untruncated gauge theory (i.e. by contracting color and adjoint indices appropriately).

For lattice gauge theories or chiral models with target space $SU(N)$, the 'classical' elements $U_{ij} \in \mathbb{C}$ satisfy special unitarity Eqs. (85-86) defining the $SU(N)$ manifold. In a fuzzy theory, one seeks matrices $\mathcal{U}_{ij}$ which satisfy analogues of these equations, though it is clear that the noncommutativity of matrices implies that there may not be a unique way to define the fuzzy manifold counterpart to Eqs. (85-86). For example, a natural choice would be to find matrices satisfying the set of $N^2$ equations

$$\begin{aligned} &\tfrac{1}{2}\left\{(\mathcal{U}_{ji})^\dagger, \mathcal{U}_{jk}\right\} = \delta_{ik} 1 \\ \text{or} \quad &\tfrac{1}{2}\left\{\mathcal{U}_{ij}, (\mathcal{U}_{kj})^\dagger\right\} = \delta_{ik} 1, \end{aligned} \tag{103}$$

where $\{\bullet, \bullet\}$ is the anticommutator, and we have regarded $(\mathcal{U}_{ij})^\dagger$ as the noncommutative counterpart to $U^*_{ij}$. By using the anticommutator, we have totally symmetrized the products that occur in the classical manifold definition. We also stress that the unitarity constraints themselves are gauge invariant, as one observes by applying the transformation Eq. (102). One can furthermore seek operator-valued manifold relations corresponding to the classical determinant condition (up to a chosen symmetrization of the products of $\mathcal{U}$s),

$$\frac{1}{N!}\varepsilon_{i_1\cdots i_N}\varepsilon_{j_1\cdots j_N}\mathcal{U}_{i_1 j_1}\cdots\mathcal{U}_{i_N j_N} = 1, \tag{104}$$

where $\varepsilon$ is the Levi-Civita pseudotensor of rank $N$. (In Appendix I: A Generalization To $U(N)$ Gauge Groups, we describe a family of fuzzy models satisfying a different kind of fuzzy unitarity.)

For the case of $N = 2$, we can parametrize

$$\mathcal{U}_{ij} = \delta_{ij}\Gamma_0 - i(\sigma_a)_{ij}\Gamma_a, \tag{105}$$

with Hermitian matrices $\Gamma_0$ and $\Gamma_a$, $a = 1, 2, 3$, analogous to the real coefficients of $U_{ij} = \delta_{ij}x_0 - i(\sigma_a)_{ij}x_a$. A series of representations of $\mathcal{U}_{ij}, T_a^{L,R}$ (or, alternatively, $\Gamma_0, \Gamma_a, T_a^{L,R}$) were worked out in Ref. [151]. There it was shown that the 10 operators $T_a^L$, $T_a^R$, $\Gamma_0$, and $\Gamma_a$ can be recognized as the 10 generators of SO(5) and thus every irrep of SO(5) defines a representation of Eqs. (80-82) and (88-89). Just as well, $\mathcal{T}_a^{L,R}, \mathcal{U}_{ij}$ are also then specified by these irreps, by definition, as per Eqs. (96) and (105). For instance, the four-dimensional (i.e., spinorial) representation of SO(5), leads to

$$\begin{aligned}
\Gamma_0 &= \frac{1}{2}\begin{pmatrix} 0 & 1 \\ 1 & 0 \end{pmatrix}, \quad \Gamma_a = \frac{1}{2}\begin{pmatrix} 0 & i\sigma_a \\ -i\sigma_a & 0 \end{pmatrix}, \\
T_a^R &= \frac{1}{2}\begin{pmatrix} \sigma_a & 0 \\ 0 & 0 \end{pmatrix}, \qquad T_a^L = \frac{1}{2}\begin{pmatrix} 0 & 0 \\ 0 & \sigma_a \end{pmatrix}.
\end{aligned} \tag{106}$$

In this representation, fuzzy analogues of the special unitarity constraints, Eqs. (103-104), are satisfied. The wave function (of a single link) can then be expanded for example as

$$\begin{aligned}\Psi =& \Psi_0 1 + \Psi_5 \Gamma_5 + \Psi_\alpha \Gamma_\alpha \\ &+ \mathrm{i}\, \Psi_{5\alpha} [\Gamma_5, \Gamma_\alpha] + \mathrm{i}\, \Psi_{\alpha\beta} [\Gamma_\alpha, \Gamma_\beta],\end{aligned} \tag{107}$$

where $\Gamma_5 = 8\, \Gamma_1 \Gamma_2 \Gamma_3 \Gamma_0$, and therefore has the form of Eq. (94). This example forms a 16-dimensional Hilbert space (per link), in contrast with the original, four-dimensional (i.e., vector-valued) representation of the model in Ref. [151]. Higher powers of $\Gamma_\alpha$ are not linearly independent from the lower ones, so the series terminates as promised.

We emphasize that, contrary to usual gauge theories, the field operators $\mathscr{U}_{\mathrm{ij}}$ and $(\mathscr{U}_{\mathrm{ij}})^\dagger$ here do not commute among themselves, and our Hilbert space is itself comprised by finite-dimensional matrices. As remarked above, this property has no bearing on the gauge symmetry of the theory. Heuristically, it is as if $\Psi$ could be viewed as a "function" of non-commuting variables $\mathscr{U}_{\mathrm{ij}}$ in a way analogous to how $\psi(U)$ is a function of the commuting variable $U_{\mathrm{ij}}$.

The construction thus far guarantees the usual gauge symmetry but does not exclude the possibility of the theory having a larger symmetry. In particular, past (finite) Hamiltonian formulations of gauge theories, such as Refs. [100, 38], contain an extra $U(1)$ symmetry. In ordinary $SU(N)$ lattice gauge theory, the links $U$ cannot be transformed under $U(1)$ without carrying them out of the target space $SU(N)$. However, in a finite gauge theory, the finite-dimensional link operators are not $SU(N)$-valued, so it is possible that there exist matrices that generate left and right $U(1)$ transformations. This property would make the theory possess an unintended $U(1)$ gauge symmetry. Such a situation leads one to either *break* the extra $U(1)$ explicitly in the Hamiltonian, or otherwise devise a method to project to the trivial irrep of $U(1)$ on each link. Nevertheless, one can prove that in our case there do not exist matrices that generate a $U(1)$ gauge symmetry, in the sense that

there are no matrices $T_0^{\mathrm{R,L}}$ satisfying

$$e^{-\mathrm{i}\omega \mathrm{T}_0^{\mathrm{R,L}}}\, \mathscr{U}_{\mathrm{ij}}\, e^{\mathrm{i}\omega \mathrm{T}_0^{\mathrm{R,L}}} = e^{\mp \mathrm{i}\omega} \mathscr{U}_{\mathrm{ij}},$$

while commuting with the $SU(2)$ generators.

Just like in the regular gauge theory, the gauge-invariant physical states form a subspace of the total Hilbert space defined by

$$e^{-\mathrm{i}\omega_{\mathrm{a}} \mathcal{G}_{\mathrm{a}}(\mathrm{x})} \Psi_{\mathrm{phys}} = \Psi_{\mathrm{phys}}, \tag{108}$$

where

$$\begin{aligned} \mathcal{G}_{\mathrm{a}}(x) &= \sum_{\mu=1}^{\mathrm{d}} \left( \mathcal{T}_{\mathrm{a}}^{\mathrm{L}}(x,\mu) + \mathcal{T}_{\mathrm{a}}^{\mathrm{R}}(x-\hat{\mu},\mu) \right), \\ &= [G_{\mathrm{a}}(x), \bullet] \end{aligned} \tag{109}$$

with $G_{\mathrm{a}}(x)$ defined as in the ordinary theory, Eqs. (90-91), with $\mathbb{T}_{\mathrm{a}}^{\mathrm{L,R}} \to T_{\mathrm{a}}^{\mathrm{L,R}}$. We remark that in a fuzzy gauge theory, the state with identity matrices on all links is always a trivially gauge-invariant state. A family of gauge-invariant states can be constructed from this trivial singlet by applying invariant products of $\mathscr{U}$s. In fact, any invariant state of the *untruncated* theory can be directly mapped into a fuzzy state, and therefore previous enumerations of the gauge-invariant states of the full theory may be of use [165, 41]. However, only a finite subset of such states will be linearly-independent, due to the closure of the matrix algebra. Furthermore, the fuzzy gauge theory may have *more* gauge-invariant products of field operators than those enumerated by the family above (up to closure redundancy), due to the non-commutativity of the $\mathscr{U}_{\mathrm{ij}}$s.

The construction of possible Hamiltonian operators for a fuzzy gauge theory proceeds by

analogy with the Kogut-Susskind Hamiltonian. The immediate choice is to take

$$\mathsf{a}\mathcal{H} = \frac{\eta g^2}{2} \sum_{\ell} \mathcal{K}(\ell) \pm \frac{\eta}{2g^2} \sum_{\mathrm{P}} \square(P) + \mathrm{h.c.}, \tag{110}$$

where $\square$ is the plaquette term

$$\square(P) = \mathscr{U}_{\mathrm{ij}}(\ell_1)\mathscr{U}_{\mathrm{jk}}(\ell_2)\mathscr{U}_{\mathrm{lk}}(\ell_3)^\dagger \mathscr{U}_{\mathrm{il}}(\ell_4)^\dagger, \tag{111}$$

and $\mathcal{K}$ the kinetic term

$$\begin{aligned} \mathcal{K}_1 &= (\mathcal{T}^{\mathrm{L}})^2 + (\mathcal{T}^{\mathrm{R}})^2 \\ &= [T^{\mathrm{L}}_{\mathrm{a}}, [T^{\mathrm{L}}_{\mathrm{a}}, \bullet]] + [T^{\mathrm{R}}_{\mathrm{a}}, [T^{\mathrm{R}}_{\mathrm{a}}, \bullet]] \end{aligned} \tag{112}$$

on each link. Above, $\ell_{\mathrm{i}}$ indexes the links of an elementary plaquette $P$ on a lattice, and each link operator $\mathscr{U}_{\mathrm{ij}}$ acts via left multiplication, for reasons we explain in the next section. The coupling $g^2$ is taken to be dimensionless. If the model has a critical point as $g^2 \to 0$, then we expect $g^2$ to be closely related to the bare coupling of the original theory. The multiplicative factor $\eta(g^2)$ is included to allow for the recovery of Lorentz covariance in the event that the above Hamiltonian has a relativistic dispersion relation. Other gauge-invariant terms can be added to the Hamiltonian. For instance,

$$\mathcal{K}_2 = -\mathscr{U}_{\mathrm{ij}} \bullet (\mathscr{U}_{\mathrm{ij}})^\dagger - (\mathscr{U}_{\mathrm{ij}})^\dagger \bullet \mathscr{U}_{\mathrm{ij}}, \tag{113}$$

$$\mathcal{K}_3 = \Gamma_5 \tag{114}$$

can be used as kinetic terms instead of (or in addition to) $\mathcal{K}_1$.[22] Similarly, one can add terms involving the product of $\mathscr{U}_{\mathrm{ij}}$ over Wilson loops larger than a single plaquette.

[22] We remark that fuzzy unitarity, such as in Eq. (103), combined with the demand of time-reversal invariance, implies that the seemingly viable kinetic term $\mathcal{K}_4 = \mathscr{U}_{\mathrm{ij}}(\mathscr{U}_{\mathrm{ij}})^\dagger + (\mathscr{U}_{\mathrm{ij}})^\dagger \mathscr{U}_{\mathrm{ij}} \propto 1$ does not alter the dynamics of the theory.

Nevertheless, the only thing that is required of the terms included is that, *in the continuum limit*, they reproduce an $SU(N)$ gauge theory, and experience with regular lattice gauge theories strongly suggests that the addition of larger Wilson loops to the Hamiltonian does not change the universality class of the theory. Still, the question of whether the fuzzy theory (with one or more of the kinetic terms above) reduces to regular gauge theory in the continuum limit is a delicate question, to be discussed in the next section.

Now that we have defined a Hamiltonian model as well as our Hilbert space, we may also observe that our fuzzy $SU(2)$ gauge theory carries a certain *global* center $\mathbb{Z}_2$ symmetry [139] [23]. Let us define a center transformation by $\mathcal{Z}_S = \prod_{\ell \perp S} \mathcal{Z}(\ell)$, where

$$\mathcal{Z}(\ell) = e^{-i2\pi \mathcal{T}_a^L(\ell)} = \gamma_5(\ell) \bullet \gamma_5(\ell), \tag{115}$$

acting via conjugation by $\gamma_5$ only on the links intersecting with an affine (i.e., $(d-1)$-dimensional) hyperplane of the spatial lattice. Two important identities of this operator are $\mathcal{Z}_S \mathcal{U}_{ij}(\ell) \mathcal{Z}_S^\dagger = s_\ell \mathcal{U}_{ij}(\ell)$, with $s_\ell = -1$ if $\ell \perp S$ and $s_\ell = +1$ otherwise, and $\mathcal{Z}_S$ commutes with all $\mathcal{T}_a^{L/R}$. From the second identity, we conclude that the global center symmetry transformation commutes with the local fuzzy gauge transformations generated by the operators of Eq. (109). From the first identity, we can see that an elementary square plaquette is invariant under such transformations, while a Wilson loop intersecting with this hyperplane on a lattice with periodic boundary conditions will flip sign. Meanwhile, the possible kinetic terms $\mathcal{K}_1$, $\mathcal{K}_2$, and $\mathcal{K}_3$ are all invariant under the center transformation. In summary, the Hamiltonian of our fuzzy $SU(2)$ gauge theory possesses a global center symmetry just as in the untruncated theory.

**Chapter 4.4: The continuum limit of fuzzy theories**

Whether the fuzzy gauge theory defined above is equivalent to ordinary gauge theory in the continuum limit is a dynamical question that, just like most dynamical questions in

[23] We thank Aleksey Cherman for asking insightful questions on this point.

non-Abelian gauge theories, is difficult to settle. In order to gain some insights into this question, let us first consider the fuzzy qubitization of the better-understood $(1+1)$-dimensional $O(3)$ non-linear $\sigma$-model, and identify the salient features indicating the correct universality class. We then discuss the corresponding features in the fuzzy gauge theory.

**Chapter 4.4.1: The continuum limit of fuzzy theories**

The lattice $O(3)$ $\sigma$-model can be defined as follows. Consider a one-dimensional spatial lattice with $\mathsf{N} = \mathsf{L}/\mathsf{a}$ sites. The local Hilbert space defined at each site $x$ is the set of square-integrable complex functions of a three-dimensional unit vector $\mathbf{n}$: $\psi(\mathbf{n})$. These states can be expanded in an infinite series of the components $\mathbf{n}_\mathrm{i}$ $(i = 1, 2, 3)$:

$$\psi(\mathbf{n}) = \psi_0 + \psi_\mathrm{i}\mathbf{n}_\mathrm{i} + O(\mathbf{n}_\mathrm{i}\mathbf{n}_\mathrm{j}). \tag{116}$$

The global Hilbert space of the theory is the tensor product of all one-site Hilbert spaces. We define "position operators" $\mathbb{n}(x)$ at every site $x$ as multiplication by $\mathbf{n}$: $\mathbb{n}(x)\psi(\{\mathbf{n}(x)\}) = \mathbf{n}(x)\psi(\{\mathbf{n}(x)\})$. A (global) $O(3)$ rotation $R$ is implemented on the wave function by the operator $\mathbb{R}$ defined by $\mathbb{R}\psi(\{\mathbf{n}(x)\}) = \psi(\{R^{-1}\mathbf{n}(x)\})$, which can be written in terms of generating operators as $\mathbb{R} = \exp(-\mathrm{i}\omega_\mathrm{k}\mathbb{T}_\mathrm{k})$. In the "position space" representation, $\mathbb{T}_\mathrm{k}$ are differential operators on the sphere. The operators $\mathbb{n}$ and $\mathbb{T}$ at one site satisfy the algebra:

$$[\mathbb{n}_\mathrm{i}, \mathbb{n}_\mathrm{j}] = 0, \tag{117}$$

$$[\mathbb{T}_\mathrm{i}, \mathbb{T}_\mathrm{j}] = \mathrm{i}\epsilon_\mathrm{ijk}\mathbb{T}_\mathrm{k}, \tag{118}$$

$$[\mathbb{T}_\mathrm{i}, \mathbb{n}_\mathrm{j}] = \mathrm{i}\epsilon_\mathrm{ijk}\mathbb{n}_\mathrm{k}, \tag{119}$$

while operators at distinct sites commute. Additionally, since $\mathbf{n}$ are unit vectors, the

operators obey the constraints

$$\big(\mathbb{n}(x) \cdot \mathbb{n}(x) - 1\big)\psi = 0, \tag{120}$$

for all states $\psi$ and every site $x$. A Hamiltonian invariant under $O(3)$ is

$$\mathsf{a}\mathbb{H} = \eta g^2 \sum_{\mathrm{x}} \mathbb{T}(x)^2 - \frac{\eta}{g^2} \sum_{\mathrm{x}} \mathbb{n}(x) \cdot \mathbb{n}(x+1). \tag{121}$$

The continuum limit is obtained as $g^2 \to 0$, where the correlation lengths diverge (in units of the lattice spacing). In order to recover Lorentz invariance, the parameter $\eta$, which alters the energy levels but not the wave function or correlation length $\xi$, has to be tuned so that the energy gap equals $1/\xi$. The continuum theory is solvable [191] and describes a triplet of particles with mass $M = 1/\xi$ interacting elastically with the phase shift of a $\delta$-distribution potential. There are two limiting energy scale regimes to consider: $E \ll M \ll 1/\mathsf{a}$ (infrared) and $M \ll E \ll 1/a$ (ultraviolet).[24] In the ultraviolet regime the theory is asymptotically free, like non-Abelian gauge theories.

As mentioned in Chapter 4.1: Introduction, one can try to qubitize this theory by substituting the target space (the unit sphere $S^2$) by a finite set of points equally spaced over the sphere (i.e., the vertices of Platonic solids). This approach lacks a continuum limit [43, 154, 96], although large finite correlation lengths can be found. An analogous approach is taken in Refs. [11, 7] for $SU(3)$ gauge theories and leads to similar results. Another approach would be to restrict the local Hilbert space at every site to functions that can be expanded in terms of spherical harmonics up to some value $\ell \leq \ell max$: $\psi(\mathbf{n}) = \sum_{\ell=0}^{\ell \mathrm{max}} \psi_{\ell \mathrm{m}} Y_{\ell \mathrm{m}}(\mathbf{n})$. In Ref. [39] evidence was found that the $\sigma$-model is recovered in the limit $\ell max \to \infty$, followed by the $g^2 \to 0$ limit. Taking the continuum limit requires taking larger $\ell max$ truncations, since it is known from Ref. [9] that at fixed $\ell max$ the theory does not have a critical point.

[24] The $E \gtrsim 1/\mathsf{a}$ regime is not universal and consequently is of no interest.

The final $\sigma$-model regularization that we consider is the fuzzy qubitization, whose gauge theory generalization we have outlined in previous sections. This model was proposed in Refs. [13, 172] and further studied in Refs. [10, 9, 28, 131]. It exhibits a high degree of universality which suggests that the continuum $\sigma$-model can be recovered in an appropriate limit, even at finite regularization.

Here, we substitute the local Hilbert space of the $\sigma$-model with a Hilbert space of dimension $(2j+1)^2$, where $j$ indexes irreps of $SU(2)$: $j = 0, \frac{1}{2}, 1, ....$ The elements of every local Hilbert space are $(2j+1) \times (2j+1)$ matrices. The (one-site) wave functions can be expanded as

$$\Psi = \psi_0 1 + \psi_k T_k + O(T^2), \tag{122}$$

where $T_k$ are the generators of the $j$ irrep of $SU(2)$. In contrast with the expansion in 116, this series terminates. $O(3)$ rotations act as:

$$\Psi \mapsto \mathcal{R}^\dagger \Psi \mathcal{R} = e^{-i\omega_k \mathcal{T}_k} \Psi, \tag{123}$$

where $\mathcal{T}_k = [T_k, \bullet]$. Since the $T_k$ satisfy $[T_i, T_j] = i\epsilon_{ijk} T_k$, so do $\mathcal{T}_k$. The analog to the position operators are

$$\mathfrak{n}_k = \frac{1}{\sqrt{j(j+1)}} T_k, \tag{124}$$

which act via left-multiplication. Because $\mathfrak{n}^2 = T^2/j(j+1) = 1$, all states in the Hilbert space satisfy 120. Now, whereas $[\mathbb{n}_i, \mathbb{n}_j] = 0$, the $\mathfrak{n}_i$ do not commute:

$$[\mathfrak{n}_i, \mathfrak{n}_j] = \frac{1}{\sqrt{j(j+1)}} i\epsilon_{ijk} \mathfrak{n}_k. \tag{125}$$

The Hamiltonian is

$$\mathsf{a}\mathcal{H} = \eta g^2 \sum_x \mathcal{T}(x)^2 \pm \frac{\eta}{g^2} \sum_x \mathfrak{n}(x) \cdot \mathfrak{n}(x+1) \tag{126}$$

where the neighbor operator is chosen to act on states from the left. The construction we have given is just the well-known construction of the fuzzy sphere [99, 134]. In the limit $j \to \infty$, the operator algebra of the fuzzy $\sigma$-model reduces to that of the untruncated lattice $\sigma$-model, i.e., Eqs. (117-119).

A more relevant consideration is whether, at *fixed* $j$, the fuzzy model has a continuum limit that matches the continuum $\sigma$-model. We focus on $j = 1/2$ in the following discussion. To study this problem let us use the basis of matrices $\mathrm{E}_{\mathrm{ab}} = \mathrm{e}_{\mathrm{a}} \otimes \mathrm{e}_{\mathrm{b}}$, with

$$\mathrm{e}_1 = \begin{pmatrix} 1 \\ 0 \end{pmatrix}, \qquad \mathrm{e}_2 = \begin{pmatrix} 0 \\ 1 \end{pmatrix}, \tag{127}$$

and expand the (one-site) wave function in this basis: $\Psi = \psi_{\mathrm{ab}}\mathrm{E}_{\mathrm{ab}}$. The result of acting on a state with $\mathfrak{n}_{\mathrm{k}}$ is

$$\mathfrak{n}_{\mathrm{k}}\Psi = \frac{2}{\sqrt{3}}(T_{\mathrm{k}})_{\mathrm{aa'}}\psi_{\mathrm{a'b}}\mathrm{E}_{\mathrm{ab}}, \tag{128}$$

while the $\mathcal{T}_{\mathrm{k}}$ operator involves multiplication from the left and from the right

$$\mathcal{T}_{\mathrm{k}}\Psi = [T_{\mathrm{k}}, \Psi] = \big((T_{\mathrm{k}})_{\mathrm{aa'}}\psi_{\mathrm{a'b}} - \psi_{\mathrm{ab'}}(T_{\mathrm{k}})_{\mathrm{b'b}}\big)\mathrm{E}_{\mathrm{ab}}. \tag{129}$$

Meanwhile, since the neighbor operator $\mathcal{V} = \sum_{\mathrm{x}} \mathfrak{n}(x) \cdot \mathfrak{n}(x+1)$ involves only left multiplication, its eigenstates factorize as

$$\begin{aligned} \Psi &= (\psi_{\mathrm{n}})_{\mathrm{a_1 \cdots aN}}\chi_{\mathrm{b_1 \cdots bN}}\mathrm{E}_{\mathrm{a_1 b_1}} \otimes \cdots \otimes \mathrm{E}_{\mathrm{aNbN}} \\ &\equiv |n\rangle \otimes |\chi\rangle \,. \end{aligned} \tag{130}$$

where $|n\rangle$ is an energy eigenstate of the spin-1/2 Heisenberg chain, while $\chi_{\mathrm{b_1 \cdots bN}}$ can be any $2N$-dimensional state. (Notably, this feature is not guaranteed if the neighbor operator acts by a mixture of left- and right-multiplication.) Thus, there is a $\geq 2N$-degenerate family of eigenstates of $\mathcal{V}$ for each $n$.

The factorization property of $\mathcal{V}$ can also be understood as follows: each site $x$ sees an "$a$" ("$b$") spin acted on via left- (right-)multiplication operations. Therefore, in this basis, the one-dimensional $j = 1/2$ fuzzy chain is seen to be equivalent to the Heisenberg comb of Ref. [172], which consists of two spins-1/2 at every site. Specifically, the neighbor operators in $\mathcal{V}$ couple neighboring $a$ spins, while the kinetic operator $\mathcal{T}(x) \cdot \mathcal{T}(x)$ couples the $a$ and $b$ spins at each site, but no coupling is set between neighboring $b$ spins; this picture yields a comb structure. Moreover, we shall see that this basis is convenient for demonstrating and characterizing the continuum limit of this fuzzy model, due to its ability to build on existing knowledge of the Heisenberg chain.

The spectrum of the spin-1/2 Heisenberg chain is well-known, so let us recall its relevant characteristics here for studying the low-lying spectrum of $\mathcal{H}$ as $g^2 \to 0$. In the ferromagnetic case (the "$-$" sign in 126), the ground state has spins pointing in the same direction. One-particle states (magnons) have a quadratic dispersion relation $E(p) \sim p^2$ ($p = 0, 2\pi/\mathsf{L}, \ldots$). In the antiferromagnetic case (the "+" sign in 126), the ground state is much more complicated; the ground state is not formed simply by alternate spins, but it can still be found by the Bethe ansatz [27]. (For a more contemporary introduction, see, e.g., Refs. [107, 109, 73].) Assuming $\mathsf{N}$ is even, the ground state then has zero total spin ($s = 0$) and it has components in all states of the computational basis with vanishing total $S_z = 0$. The excitations, in the case of half-integer spin, are gapless [92] with a linear dispersion relation $E(p) \sim p$ (spinons). Even-$\mathsf{N}$ lattices can have only integer-spin states, and so the first excited states are spinon pairs with $s = 1$.

As we will now argue, the features above strongly suggest that the model has a critical point as $g^2 \to 0$. First, since the kinetic term acts on both the left and the right of each site, it breaks the degenerate eigenspace of $\mathcal{V}$ associated with each $|n\rangle$, for any $g^2 > 0$. In particular, in the ground $\mathcal{V}$-eigenspace ($n = 0$) a gap exists between a singlet ground state and a triplet of first excited states. Consequently, for any *finite* lattice size, the gap must vanish as $g^2 \to 0$, since the spectrum of $\mathsf{a}\mathcal{H}$ in Eq. (126) reduces to that of $\mathcal{V}/g^2$ in that

limit. Moreover, the degenerate spaces have dimension $\geq 2N$, implying the number of states merging together as $g^2 \to 0$ is exponential in the volume, as desired of any field theory. In strictly infinite volume, on the other hand, we cannot prove gaplessness as $g^2 \to 0$. That the infinite-volume theory indeed becomes gapless in the limit was demonstrated numerically in Ref. [9] using the density matrix renormalization group (DRMG) algorithm.[25]

Alone, the existence of a critical point argued above does not guarantee that one obtains the asymptotically free $\sigma$-model in the continuum limit. To that end, we can gain more insight by studying the small $g^2$ limit in perturbation theory. Since the ground state of $\mathcal{V}$ is highly degenerate, we adopt the effective Hamiltonian approach to degenerate perturbation theory [166].

The first-order term $\mathsf{a}\mathcal{H}^{(1)}eff$ is simply the kinetic operator restricted to the ground subspace, $\{|\Psi_\alpha\rangle = |0\rangle \otimes |\chi_\alpha\rangle\}$ with $\alpha = 1, \ldots, 2N$,

$$\begin{aligned} \mathcal{K}_{\alpha\beta} &= \eta g^2 \langle \Psi_\alpha | \sum_{\mathrm{x}} \mathcal{T}(x)^2 \left| \Psi_\beta \right\rangle \\ &= \eta g^2 A_1 \delta_{\alpha\beta} \\ &\quad - \eta g^2 A_2 \sum_{\mathrm{x,k}} \underbrace{\langle 0 | T_{\mathrm{k}}(x) | 0 \rangle}_{=0} \langle \chi_\alpha | T_{\mathrm{k}}(x) \left| \chi_\beta \right\rangle \end{aligned} \tag{131}$$

where we use the fact that $\mathcal{T}^2 = [T_{\mathrm{k}}, [T_{\mathrm{k}}, \bullet]] = T^2 \bullet + \bullet T^2 - 2T_{\mathrm{k}} \bullet T_{\mathrm{k}}$ and $T^2 \propto 1$, and $A_{1,2}$ are constants. We can see that the second term above must vanish because the Heisenberg-chain ground state is rotationally invariant. Since $(\mathcal{H}eff^{(1)})_{\alpha\beta} = \mathcal{K}_{\alpha\beta} \propto \delta_{\alpha\beta}$, there is no first-order contribution to the gap $\Delta E = E_1 - E_0$ in the degenerate subspace of $|0\rangle$. Therefore, we expect the gap to scale as $\mathsf{a}\Delta E \sim (1/g^2)(Ag^4 + Bg^8 + \cdots) \sim g^6$, with $A = 0$.[26] We confirm this behavior numerically by exact diagonalization of 126 in small

[25] The neighbor term in the $\ell max$ truncation is gapped in any finite volume and therefore does not have an exponentially-degenerate ground state. Together these facts may explain the failure of that model to have a critical point [9].

[26] Since $\eta(g^2)$ converges to a positive constant as $g^2 \to 0$ [9], we denote this limit simply as $\eta$, with any

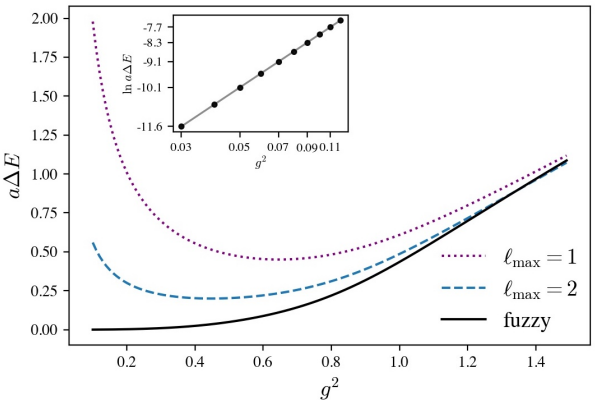


Figure 15: Comparison of the energy gaps in the fuzzy $\sigma$-model with those of the $\ell max$ truncation strategy for $\ell max = 1, 2$. The chain length is $\mathsf{N} = 4$ in each case. The inset displays the small-$g^2$ behavior of the fuzzy gap on a log-log scale; the slope of the line is 3.

volumes; see Fig. 15.

Although this perturbative expansion is valid in small enough boxes, $\mathsf{L} = \mathsf{aN} \ll 1/M$, it breaks down in larger volumes, $\mathsf{L} = \mathsf{aN} \gg 1/M$, due to an infrared divergence of the $B$ coefficient in $\mathsf{a}\Delta E$. We have observed this behavior numerically by directly computing $B$ via exact diagonalization up to $\mathsf{N} = 18$ (see Fig. 16), but we can also understand it analytically. The second-order contribution to the effective Hamiltonian in the ground subspace of $\mathcal{V}$ is determined by the matrix[27]

$$\begin{aligned}
\mathsf{a}(\mathcal{H}^{(2)}eff)_{\alpha\beta} &= \langle\Psi_\alpha|\,\mathcal{K}P_1\left[v_0P_1 - P_1\mathcal{V}P_1\right]^{-1}P_1\mathcal{K}\,|\Psi_\beta\rangle \\
&= 2\sum_{\mathrm{m}\geq 1}\sum_{\mathrm{x,y}}\frac{\eta g^6}{v_\mathrm{m} - v_0}\,\langle 0|\,T_\mathrm{i}(x)\,|m\rangle\,\langle m|\,T_\mathrm{j}(y)\,|0\rangle \\
&\qquad \times\langle\chi_\alpha|\,T_\mathrm{i}(x)T_\mathrm{j}(y)\,|\chi_\beta\rangle
\end{aligned} \tag{132}$$

where $P_1$ is a projector to the excited subspaces $\{|m\rangle \otimes |\chi\rangle : m \geq 1\}$ of $\mathcal{V}$, and $v_0, v_\mathrm{m}$ are the respective eigenvalues of $|0\rangle, |m\rangle$. The $m$-sum includes the low-lying two-spinon states with $v_\mathrm{m} - v_0 \sim p$ ($p \approx 2\pi/\mathsf{L}, \ldots$ at large $\mathsf{L}$). Note that the matrix elements

correction resulting in a high-order function in $g^2$ that we may safely neglect, if we are only concerned with the lowest-order correction in $g^2$.

[27]The perturbed eigen*states* are found by choosing the unperturbed kets to be eigenstates of $\mathcal{H}eff^{(2)}$, instead of the leading matrix $\mathcal{K}$, in contrast to standard degenerate perturbation theory.

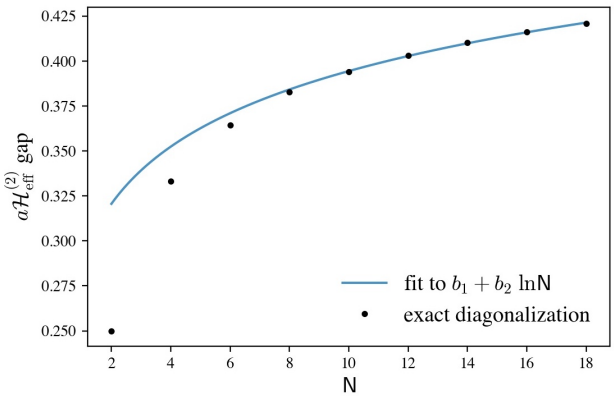


Figure 16: Behavior of the perturbative coefficient of $g^6$ in $\mathsf{a}\Delta E$ for the fuzzy $\sigma$-model, as determined by the gap in $\mathcal{H}eff^{(2)}$, 132, for chains up to size $\mathsf{N} = 18$. The blue curve is a fit to $b_1 + b_2 \log \mathsf{N}$, indicating a logarithmic divergence in infinite volume.

$\langle 0| T_{\mathrm{i}}(x) |m\rangle$ do not vanish for states $|m\rangle$ with total spin 1. Therefore, for large $\mathsf{L}$, unless those matrix elements vanish at small $p$, the sum over $m$ will diverge logarithmically:

$$\mathsf{a}\Delta E \sim \int_{2\pi/\mathsf{L}}^{\pi/\mathsf{a}} \frac{\mathrm{d}p}{p} \sim \ln(\mathsf{L}/\mathsf{a}), \tag{133}$$

indicating the breakdown of perturbation theory in large volumes.

The features described above, namely, the existence of a critical point with an exponentially degenerate Hilbert space, and the breakdown of perturbation theory at large distances, are hallmarks of asymptotically free continuum field theories.

**Chapter 4.4.2: Gauge Theory**

Much of the reasoning above carries over to the fuzzy gauge theory, with a Hamiltonian given in 110. Again, the potential (plaquette) operator acts only from the left on fuzzy states, and the eigenstates factorize as before: $|\Psi_{\mathrm{n}}\rangle = |n\rangle \otimes |\chi\rangle$ with potential energy $v_{\mathrm{n}}$. Here the $|n\rangle$ are eigenstates of a plaquette operator acting on a four-dimensional one-link Hilbert space (rather than $4 \times 4$ matrix-states). In fact, this "reduced" plaquette operator is just the simplest example of a "gauge magnet" as proposed by Orland & Rohrlich in Ref. [151]. In a spin-wave analysis, the pure-plaquette case of the gauge magnet was argued to be gapless with a nonrelativistic dispersion relation. However, since the

eigenstates are independent of the overall coupling of the plaquette term, so is the correlation length (in lattice units). Therefore, the coupling cannot be tuned such that $\xi/\mathsf{a} \to \infty$ (continuum limit) while $\xi \to$ constant, as is necessary to reproduce the physics of an asymptotically free gauge theory. An equivalent argument is to point out that the usual mechanism of "dimensional transmutation" can only occur if there is a coupling constant to be tuned to alter the eigenstates.[28]

Due to the factorization property outlined above, each eigenvalue $v_{\mathrm{n}}$ of the *fuzzy* plaquette operator is at least $4N$-fold degenerate (for now, including unphysical states), where $\mathsf{N}$ is the number of links. As we detail below, the degeneracy of the ground state is lifted by a suitable choice of kinetic term. In 17 we confirm this behavior by exact diagonalization in a small volume, where also the gaps are compared with the two simplest angular momentum $jmax$ truncations (described in Chapter 4.1: Introduction). As $g^2 \to 0$, the low-lying states merge into the degenerate ground subspace of the fuzzy plaquette operator, and the number of such states grows exponentially with the volume, which strongly suggests the existence of a critical point suitable for continuum physics.

The choice of kinetic terms $\mathcal{K}_1$, $\mathcal{K}_2$, or some combination thereof, is unclear. Both operators are positive-semidefinite, as in the standard Kogut-Susskind Hamiltonian. While $\mathcal{K}_1$ resembles the kinetic term of the Kogut-Susskind Hamiltonian, since it is the quadratic Casimir on the fuzzy Hilbert space, it does not completely lift the degeneracy of the ground state in the one-plaquette system; a two-fold degeneracy in the ground state subspace, not present in continuum gauge theories, remains. Meanwhile, $\mathcal{K}_2$ *does* completely lift this degeneracy, but it is not as directly associated with the Casimir operator of the original gauge theory. Only a deeper insight into the dynamics of fuzzy

[28]The gauge magnet of Ref. [151] was proposed as a candidate for a finite-dimensional model in the same universality class as Yang-Mills gauge theory. This model allows for the inclusion of a kinetic term which acts on each four-dimensional one-link Hilbert space via multiplication with $\gamma_5$. We have exactly diagonalized this model in the one-plaquette (with open boundaries) and four-plaquette (with periodic boundaries) systems. The behavior for small $g^2$ is qualitatively similar to the $jmax$ qubitizations. Still, a gapless point at a nonzero $g^2$ exists in the four-plaquette system (though not in the one-plaquette system). It is not clear if the number of degenerate states is exponential in the volume, unlike the fuzzy model. In any case, this model warrants further study by nonperturbative means. See also Ref. [150].

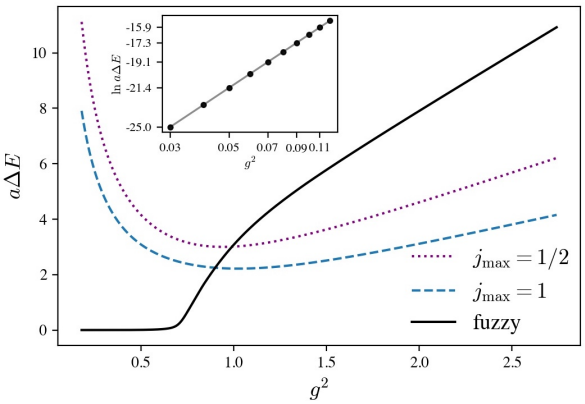


Figure 17: Energy gaps in the *physical* subspace of qubitized $SU(2)$ gauge theories for a single-plaquette system. We compare the fuzzy model (with kinetic term $\mathcal{K}_2$) to the angular momentum $jmax$ truncation models discussed in the introduction. In each case, as $g^2 \to 0$, the behavior is dominated by the plaquette operator $\square$. For the $jmax$ models the finite gap of $\square$ yields a diverging energy gap, while for the fuzzy model the degeneracy of $\square$ ensures gaplessness. The inset plots the fuzzy gap versus $g^2$ on a log-log scale for small $g^2$; a fit to a straight line is in gray, with a slope of 7.

gauge theories can settle which—if any—kinetic terms lead to the proper continuum limit. Furthermore, without a complete understanding of the dynamics of the Orland-Rohrlich gauge magnet, we cannot provide an analytic argument for the breakdown of perturbation theory with increasing volume, nor can the fuzzy gauge theory be exactly diagonalized beyond the one-plaquette system on current hardware. Still, we have observed in the one-plaquette system, that the leading order term in the effective Hamiltonian of the degenerate ground state subspace must scale like $\mathsf{a}\Delta E \sim g^{14}$, as depicted in 17, which corresponds to fourth-order perturbation theory in $g^4$. This high-order first non-vanishing correction suggests impracticality and perhaps even lack of efficacy of perturbation theory in studying this theory (i.e., if non-perturbative in nature). Likewise, if the spin-wave analysis of the Orland-Rohrlich model holds, where the gauge magnet is predicted to be gapless, then it is possible for the perturbative coefficients of the fuzzy gauge theory to have infrared divergences in a manner similar to the $\sigma$-model analysis of Chapter 4.4.1: The continuum limit of fuzzy theories.

Before we conclude our discussion, let us justify a subtle problem of local gauge theories

not present in the theories with only global symmetries: ensuring the exponential growth of the *physical* Hilbert subspace with volume. We implicitly claimed earlier that the growth in the ground state degeneracy survives the restriction to the physical subspace; we argue for this point as follows. First note that in the product basis, the all-left-multiplying plaquette operator of our fuzzy $SU(2)$ model is simply a tensor product of the gauge magnet plaquette operator and an identity operator of the same dimension, as remarked earlier. Let $|n\rangle$ be a gauge-invariant eigenstate of the Orland-Rohrlich total plaquette operator with energy $v_{\mathrm{n}}$. Then, the degenerate $v_{\mathrm{n}}$-eigenspace of the *fuzzy* plaquette operator includes states that, in the $\mathrm{E}_{\mathrm{ab}}$ product basis, take the form

$$|\Psi_{\mathrm{n}}\rangle = |n\rangle \otimes |\chi\rangle \,, \tag{134}$$

where $|\chi\rangle$ is a $4N$-dimensional state. The action of the gauge generator $\mathcal{G}_{\mathrm{a}}(x)$ in the fuzzy theory acts on this basis as

$$\mathcal{G}_{\mathrm{a}}(x)\,|\Psi_{\mathrm{n}}\rangle = -\,|n\rangle \otimes G_{\mathrm{a}}(x)\,|\chi\rangle \,, \tag{135}$$

since $|n\rangle$ is gauge-invariant, $G_{\mathrm{a}}(x)\,|n\rangle = 0$, c.f. Eq. (108). Therefore, the *physical* fuzzy states with plaquette energy $v_{\mathrm{n}}$ include all states satisfying $G_{\mathrm{a}}(x)\,|\chi\rangle = 0$, and the set of such states is the entire physical subspace of the Orland-Rohrlich gauge magnet, with dimension $DOR$. We note that there also exist physical states in the fuzzy model that cannot be written as the tensor product of two invariant gauge-magnet states. Thus the dimension $D_{\mathrm{f}}$ of the physical fuzzy Hilbert space satisfies $D_{\mathrm{f}} \geq (DOR)^2$, and the dimension $D_{\mathrm{f0}}$ of the physical fuzzy degenerate ground subspace satisfies $D_{\mathrm{f0}} \geq DOR$. It then follows that if the Orland-Rohrlich model has a physical Hilbert space that is exponential in the volume, then the (physical) degenerate ground state subspace of the fuzzy plaquette operator will be exponentially large as well, ensuring that the number of physical states which merge in the $g^2 \to 0$ limit is exponential. We have verified

numerically, by computing the nullity of $\sum_{x,a} G_a(x)^2$, that the Orland-Rohrlich model has two physical states in the one-plaquette system and 50 physical states in the four-plaquette system. More generally, based upon the diagrammatic arguments of Ref. [150] (i.e., observing that there is at least one extra degree of freedom per site in a diagram representing a global physical state on the lattice), we expect the physical Hilbert space in the fuzzy $SU(2)$ gauge theory to grow at least exponentially in the volume, for all spatial dimensions $d$.

**Chapter 4.5: Quantum Circuitry**

In this section, we explain how we construct a quantum circuit performing the Hamiltonian time evolution, working explicitly with the case of $SU(2)$. To this end, we compute the Hamiltonian in the computational basis given by single-entry matrices, $E_{\alpha\beta}$ ($\alpha, \beta = 0, \ldots, 3$). If we flatten the indices as $\alpha\beta \mapsto A$ with $A = 1, \ldots, 16$, then the operator $O$ represented in this computational basis has elements

$$[O]_{A,B} := \mathrm{tr}\left[E_A^\dagger \, O \, E_B\right]. \tag{136}$$

With a local Hilbert space dimension of $16 = 2^4$, we can neatly encode these operators by their action on four qubits $|q_1, q_2, q_3, q_4\rangle$, where $q_i = 0, 1$ encode $A - 1$ in a binary representation. We build the link operators out of gamma matrices, which are given by

$$\Gamma_\alpha \doteq \frac{1}{2}\gamma_\alpha \otimes 1_4 = \frac{1}{2}\begin{pmatrix} +XI \\ -YX \\ -YY \\ -YZ \end{pmatrix} \otimes II \tag{137}$$

(c.f., Eq. (106)) to compose the $\mathscr{U}$ as in Eq. (105), as well as

$$\Gamma_5 \doteq \frac{1}{2}\gamma_5 \otimes 1_4 = -\frac{1}{2} ZIII. \tag{138}$$

The local operators relevant for the kinetic terms, Eqs. (112-113), are given by

$$(\mathcal{T}^{\mathrm{L}})^2 + (\mathcal{T}^{\mathrm{R}})^2 \doteq - IXIX + IYIY - IZIZ \\ - ZXZX + ZYZY - ZZZZ, \tag{139}$$

and

$$-\mathcal{U}_{\mathrm{ij}} \bullet \mathcal{U}_{\mathrm{ij}}^{\dagger} - \mathcal{U}_{\mathrm{ij}}^{\dagger} \bullet \mathcal{U}_{\mathrm{ij}} \\ \doteq - XIXI + YXYX - YYYY + YZYZ. \tag{140}$$

These are relatively easy to include in quantum simulations.

With these local operators encoded on qubits in hand, we may straightforwardly construct quantum circuits to simulate the real-time evolution of the Hamiltonian of Eq. (110) with $\mathcal{K} = \mathcal{K}_2$ of Eq. (113). For details elaborating how we compile such circuits, please refer to Appendix II: Compiling Quantum Circuits for a Fuzzy Gauge Theory. In summary, we find that 236 CNOT gates and 88 rotation gates are involved in simulating both the kinetic and potential terms of a Hamiltonian for an individual plaquette. In addition, we depict some classical simulations of the quantum circuit for a one-plaquette system in Fig. 18. The relatively low gate count in a circuit simulating one plaquette may be surprising when compared with the counts found in Ref. [145]: 180 and ~16,000 CNOT gates demanded by the models of Orland and Rohrlich [151] and Horn [100], respectively. In those cases, the operations on a given link were four- and five-dimensional, respectively, and gate costs were dominated by the number of Pauli operators involved in the plaquette term of each model. We also find that the large resource costs seen for the Horn model are similar for the angular momentum $jmax$ truncation strategy compared earlier. Moreover, one could see for Hamiltonians approximating $\sigma$-models that gradually lifting a truncation in angular momentum cutoffs would necessitate more qubits to encode the models and consequently

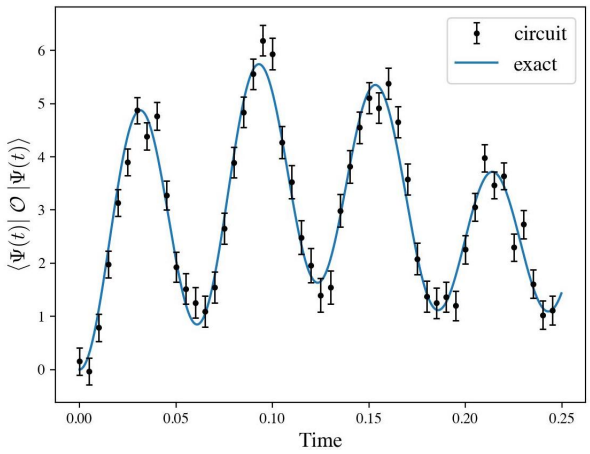


Figure 18: Expectation value of the plaquette operator $\mathcal{O} = \square$ with respect to the evolved state $|\Psi(t)\rangle = \exp(-it\mathcal{H})\,|\Psi(0)\rangle$, choosing a gauge-invariant initial state $\Psi(0) \doteq 1_4{}^{\otimes 4}$ and kinetic term $\mathcal{K}_2$ for example. The solid line is obtained by numerically calculating $\Psi(t)$. The data points shown are obtained by repeatedly applying the quantum circuit of $Q \approx \exp(-i\delta\mathcal{H})$, constructed as described in Appendix II: Compiling Quantum Circuits for a Fuzzy Gauge Theory and using the prescription in Ref. [145]. Uncertainty bars on each data point show the shot noise of 4000 measurements at each time value. Time steps of size $\delta = 0.0025\,\mathsf{a}$ were taken, while the results of only every other time step are shown for clarity in the plot. Additionally, the state at each time $\Psi(t)$ was prepared by applying $t/\delta$ iterations of $Q$ to $\Psi(0)$, independently of the results of $\Psi(t-\delta)$, leaving measurements at different times uncorrelated.

involve much greater gate costs to simulate the many new Pauli operators involved [9], so we expect this trend to apply for the $jmax$ truncation as well.

As a result, one might then be apprehensive that a model encoding an individual link's degrees of freedom on four qubits instead of two or three would entail much greater complexity to simulate. However, note that the fuzzy link operators as represented in Eq. (137) are proportional to those of the Orland-Rohrlich model. Therefore, the cost in quantum gates demanded to simulate our fuzzy plaquette of Eq. (111) is exactly the same as for the plaquette acting on only two-qubits per link. The only additional costs from our proposed fuzzy gauge model come from the kinetic term in Eq. (139), which is now somewhat more involved. While Ref. [151] proposed a kinetic term proportional to $\gamma_5$ on each link, which can be simulated with a single rotation gate, our one-link fuzzy kinetic terms involve a handful of CNOT gates.

**Chapter 4.6: Conclusions**

In the above we have proposed a novel procedure to render a bosonic gauge theory finite-dimensional. We hope that this scheme is a helpful step in the ongoing effort to develop scalable quantum computation methods that can be applied to nuclear physics problems. In fact, it is likely that such a scheme will be *necessary*, given that the removal of a truncation, such as in the $jmax$ truncation strategy, is prohibitively expensive in a quantum circuit. As noted before, the proposed Hamiltonian is relatively straightforward to simulate, allowing one to work in only the number of spacetime dimensions required by the theory and sidestepping the need for a truncation or other regularization to be removed. A central motivation for our work was the search for a theory with a finite-dimensional Hilbert space (per volume) and in the same universality class as non-abelian gauge theories. We proposed a theory that exhibits several features (listed below) that are plausibly necessary toward that end. Unfortunately, a nonperturbative numerical calculation providing clear evidence for the correct continuum limit has not yet been possible. Preliminary attempts to simulate the Hamiltonian of the fuzzy gauge theory via

Monte Carlo suggest, as in many truncated theories, the presence of a severe sign problem. In the simpler case of the $(1+1)$-dimensional qubitized $\sigma$-model, tensor network methods [10, 9] and Monte Carlo methods specific to $1+1$ dimensions [172, 28] were used to provide such evidence. Neither method is available for $(3+1)$-dimensional gauge theories, though tensor network methods may be feasible in $2+1$ dimensions. Alternatively, if a renormalization group argument valid at weak coupling could be devised, it would shed light on this question; we are actively pursuing such a strategy.

An appealing aspect of the fuzzy strategy—for both $\sigma$-models and gauge theories—is the formal similarity with the corresponding original lattice theories; in particular, states of the fuzzy models can be thought of as "functions" of the noncommutative $\mathcal{U}_{ij}$, the symmetry generators satisfy the Leibniz rule on any state, and the $\mathcal{U}_{ij}$ satisfy an analogue of the classical special-unitarity constraints. Moreover, we have identified throughout the paper various concrete properties that we believe any qubitization of non-Abelian gauge theory must satisfy. Namely, the qubitization should possess

(A) the same gauge symmetry as the original theory (i.e., $SU(N)$),

(B) the same global symmetries as the original theory (i.e., center $\mathbb{Z}_N$ symmetry),

(C) a Hilbert space that grows exponentially with the volume,

(D) a critical point at fixed, finite local Hilbert space dimension,

(E) a nonperturbative mass gap consistent with asymptotic freedom,

(F) the desired spacetime symmetry (i.e., Lorentz covariance) in the critical limit, and

(G) a small local Hilbert space at the cutoff scale.

The conventional wisdom is that merely possessing the right symmetries, (A) and (B), would suffice to place a model in the correct universality class. However, a lesson of searches for qubitizations of the $\sigma$-model is that more properties are required [9], as emphasized by the list above.

Let us now collect what evidence we have produced for these conditions in fuzzy gauge theory. By its definition in Chapter 4.3: Fuzzy lattice gauge theory, the fuzzy gauge theory satisfies condition (A), and we demonstrated that it also satisfies (B). In Chapter 4.4: The continuum limit of fuzzy theories, we first reviewed how the fuzzy $\sigma$-model satisfies conditions (A-C) before providing new evidence in favor of conditions (D) and (E); while these properties were not completely proven here, they were previously demonstrated nonperturbatively using DMRG [10, 9]. We then showed evidence that conditions (C-E) are again satisfied by the fuzzy gauge theory, but we cannot produce as much evidence for condition (E) in fuzzy gauge theory as in the fuzzy $\sigma$-model. We cannot yet assert condition (F) with any confidence. Condition (G), though not strictly necessary, is highly desirable for efficient simulation, and we have demonstrated the reasonable circuit depth of the fuzzy qubitization in Chapter 4.5: Quantum Circuitry.

Over the decades much effort has been put into understanding gauge dynamics from the Hamiltonian point of view, starting with Ref. [123] in the 1970s. It is possible that a fuzzy gauge theory, by virtue of its simplicity, while still conjectured to be equivalent to continuum gauge theory, might be used to advance this program. Historically, many-body physics had several breakthroughs based on wave function ansätze, but the same has not yet occurred in field theory (see, for instance, Refs. [86, 85, 108, 132, 128, 162] for work in this direction). Perhaps the fuzzy approach that we have explored here will help in this effort.

## Appendix

### Appendix I: A Generalization To $U(N)$ Gauge Groups

As mentioned in Chapter 4.3: Fuzzy lattice gauge theory, one can come up with explicit matrices to satisfy fuzzy unitarity constraints. Here, we provide an example of these matrices here for a generalization to $U(N)$ and discuss obstacles to efficiently reduce the

theory to avoid a potentially undesired extra $U(1)$ gauge symmetry in this example.

For the case of fuzzy unitary matrices for large gauge groups, we propose a subtly different parametrization of matrices in $U(N) \ni U = x_0 1_{\mathrm{N}} + x_{\mathrm{a}} \lambda_{\mathrm{a}}$, where $a = 1, \ldots, N^2 - 1$ and $\lambda_{\mathrm{a}}$ are generalized Gell-Mann matrices. In this case, we allow $(x_0, x_{\mathrm{a}}) \in \mathbb{C}^{\mathrm{N}^2}$, as the complex span of $1_{\mathrm{N}}$ and $\lambda_{\mathrm{a}}$ includes all unitary matrices. Correspondingly, the operators to which we will promote these parameters are not necessarily Hermitian. In particular, we propose Based upon a complex parametrization of the $U(N)$ manifold, we could propose new operator-valued parameters form a link operator

$$\mathscr{U}_{\mathrm{ij}} = \delta_{\mathrm{ij}} X_0 + (\lambda_{\mathrm{a}})_{\mathrm{ij}} X_{\mathrm{a}}, . \tag{141}$$

Given this parametrization of $\mathscr{U}$, one can show that a slightly different operator constraint for fuzzy unitarity,[29]

$$\frac{1}{2}\{\mathscr{U}, \mathscr{U}^\dagger\}_{\mathrm{ij}} = \delta_{\mathrm{ij}} 1, \tag{142}$$

is equivalent to $N^2$ constraints

$$N\{X_0, X_0^\dagger\} + 2\{X_{\mathrm{a}}, X_{\mathrm{a}}^\dagger\} = 2N1, \tag{143}$$

$$\{X_{\mathrm{a}}, X_0^\dagger\} + \{X_0, X_{\mathrm{a}}^\dagger\} + h_{\mathrm{abc}}(X_{\mathrm{b}} X_{\mathrm{c}}^\dagger + X_{\mathrm{b}}^\dagger X_{\mathrm{c}}) = 0, \tag{144}$$

where $h_{\mathrm{abc}} = d_{\mathrm{abc}} + \mathrm{i} f_{\mathrm{abc}}$ with totally symmetric and antisymmetric structure constants $d$ and $f$, respectively. One finds that the above equations are satisfied by

$$X_0 = \frac{1}{r_0} \sigma_+ \otimes 1_{\mathrm{N}} \tag{145}$$

$$X_{\mathrm{a}} = \frac{1}{r_{\mathrm{a}}} \sigma_+ \otimes \lambda_{\mathrm{a}}, \tag{146}$$

[29] Notably, this constraint is *not* gauge-invariant for $N \geq 2$. That is, non-Abelian gauge transformations of matrices satisfying these anti-commutation relations do not result in more fuzzy unitary matrices. Nevertheless, gauge-invariant states and Hamiltonian operators can be constructed from these matrices.

where $\sigma_+ = (\sigma_x + i\sigma_y)/2$, $r_0^2 = N^2/2$, and $r_a = (2/N)r_0$. Fascinatingly, one can then see for the matrix elements of $\mathscr{U}$ that

$$\mathscr{U}_{ij} = \sqrt{2}\,\sigma_+ \otimes E_{ji}, \tag{147}$$

using the Fierz identity of SU($N$) for $\lambda_a \otimes \lambda_a$. Here, we have defined the single entry matrix $E_{ij} = e_i e_j^\top$ (with unit vectors $e_i$). In other words, these $\mathscr{U}$ matrices are actually similar to those proposed in Ref. [38], albeit with different normalization and intended here for action on a matrix-valued Hilbert space.[30]

Moreover, we demand that these new link operators $\mathscr{U}$ behave as expected under gauge group transformations. Technically speaking, we find that the Kogut-Susskind relations of $\mathscr{U}_{ij}$ of Eqs. (88-89) are equivalently

$$[T_A^{R/L}, X_0] = \pm\frac{1}{N} X_a, \tag{148}$$

$$[T_a^R, X_b] = +\frac{1}{2}\delta_{ab} X_0 + \frac{1}{2} h_{abc} X_c, \tag{149}$$

$$[T_a^L, X_b] = -\frac{1}{2}\delta_{ab} X_0 - \frac{1}{2} h^*_{abc} X_c. \tag{150}$$

With the natural choice of $T_a^{R/L} = (1 \pm \sigma_z) \otimes \lambda_a/4$ (just as we did in Chapter 4.3: Fuzzy lattice gauge theory), we find that all of the above commutation relations are indeed satisfied.

Finally, let us point out that these $X$ operators are nilpotent with degree 2, meaning $XX' = 0$ and so $\mathscr{U}$ inherits this nilpotence. Nonetheless, importantly, $X^\dagger X'$ and $XX'^\dagger$ are nontrivial, indicating $\mathscr{U}_{ij}\,(\mathscr{U}_{kl})^\dagger$ and $(\mathscr{U}_{ij})^\dagger\,\mathscr{U}_{kl} \neq 0$, and the link operators' products with generators $T_a^{R/L}$ are also nontrivial. Still, this property does mean that most generalizations of the determinant for matrices over non-commutative rings still result in $\det \mathscr{U} = 0$. While one might desire an operator $\det \mathscr{U} = 1$ for a "fuzzy" $SU(N)$ theory, we note that this

[30] We note that our use of the quantum link matrices does not involve an appeal to dimensional reduction, and as such will be formulated directly in the space dimension of interest.

difference does not necessarily preclude a prediction of an $SU(N)$ theory by this model if one can still decouple a possible extra $U(1)$ symmetry lingering in the formulation, as we shall describe below. Additionally, there may be benefits to this nilpotence; certain extra gauge-invariant operators that may complicate the Hamiltonian of this model are trivialized in this way. For example, consider for $N = 2$ the operator on two adjacent links

$$O = \varepsilon_{il}\varepsilon_{kn}\,\mathcal{U}_{ij}(1)\,\mathcal{U}_{jk}(2)\,\mathcal{U}_{lm}(1)\,\mathcal{U}_{mn}(2) \tag{151}$$

with $\varepsilon = i\sigma_y$, which is gauge-invariant as long as the Kogut-Susskind relations are satisfied (otherwise regardless of one's choice of promoting $U \mapsto \mathcal{U}$), and yet $\mathcal{U}_{ij}(\ell)\,\mathcal{U}_{lm}(\ell) = 0$ for either $\ell = 1, 2$. As such, this nilpotence property may help keep the form of our Hamiltonian particularly simple, involving our usual plaquette term and few other options for kinetic terms.

In this distinct proposal for matrices $\mathcal{U}$, there do exist generators of $U(1)$ gauge transformations: $T_0^{R/L} = (1 \pm \sigma_3) \otimes 1_N$. In this case, there are multiple strategies for dealing with the additional symmetry. The first is to explicitly break the $U(1)$ symmetry by adding to the Hamiltonian a non-invariant term. The simplest option would be a generalized determinant $\varepsilon_{ik}\mathcal{U}_{ij}\mathcal{U}_{kl}\varepsilon_{jl}$; however, this operator vanishes in the fundamental rep of $SU(2N)$. Ref. [38] suggests working with larger reps of $SU(2N)$, in which the determinant is non-trivial, but doing so here increases the fuzzy Hilbert space dimension; for $N = 2$, it would be 36-dimensional. Alternatively, one could implement a $U(1)$ projector on each one-link Hilbert space.

**Appendix II: Compiling Quantum Circuits for a Fuzzy Gauge Theory**

In this section, we detail the methods used to compile the quantum circuits for which we present simulation results in Chapter 4.5: Quantum Circuitry. As a broad outline: We first trotterize our time evolution operator into a sequence of operators, each of which we may diagonalize relatively efficiently. To complete the compilation procedure, we use methods

prescribe in an earlier article [145] to determine circuits that perform the appropriate multi-qubit rotations to simulate the diagonalized unitary operators produced by the earlier step.

As is common in procedures for quantum compilation of unitary circuits $\exp(-\mathrm{i}Ht)$ and as per the approach of Ref. [145], we choose to expand the Hamiltonian $H$ of Eq. (110) in the Pauli operator basis,

$$H = \sum_{\mathrm{j}} c_{\mathrm{j}} P_{\mathrm{j}}, \tag{152}$$

where $P_{\mathrm{j}} \in \{I, X, Y, Z\}^{\otimes \mathrm{n}}$ (a tensor product of $n$ Pauli matrices), $n$ is the number of qubits chosen to represent the system on a quantum computer, and $c_{\mathrm{j}} = \mathrm{tr}[P_{\mathrm{j}} H]/2^{\mathrm{n}}$. Moreover, as in Ref. [145], we perform a trotterization by collecting commuting Pauli operators. That is, we write

$$H = \sum_{\mathrm{j}=1}^{\mathrm{k}} h_{\mathrm{j}} \tag{153}$$

where Pauli operators comprising a given $h_{\mathrm{j}}$ commute with one another. As in Refs. [145, 182, 176], collecting these commuting Pauli operators can be reduced to the well-known graph coloring problem.

In the case of a single plaquette system, we use $n = 16$, and decomposing its Hamiltonian in this fashion yields 88 Pauli operators with non-zero coefficients, excluding the identity. Moreover, we use the DSATUR algorithm of Ref. [35] to obtain $k = 5$ commuting clusters of Pauli operators. Now, having reduced our problem to the simulation of commuting clusters $\{h_{\mathrm{j}}\}$, we turn our attention to how to compile a circuit for any one such Hamiltonian $h_{\mathrm{j}}$.

Since Pauli operators comprising a cluster $h_{\mathrm{j}}$ commute with each other, they can be exactly diagonalized simultaneously. Moreover, such a diagonalization can be performed with $O(n^2)$ CNOT gates [182, 53]. In particular, let $V_{\mathrm{j}}$ be an unitary transformation diagonalizing $h_{\mathrm{j}}$. We obtain $V_{\mathrm{j}}$ via the method developed in Ref. [144], which guarantees shallow circuits with depths $O\left(n \log_2 r\right)$ where $r \leq n$ is the number of independent

generators of the commuting cluster. As an upshot, we can then reduce $D_j = V_j h_j V_j^\dagger$, and so overall

$$\begin{aligned} e^{-iH\delta t} &\approx \prod_j e^{-ih_j\delta t} \\ &= \prod_j V_j^\dagger \, e^{-iD_j\delta t} V_j. \end{aligned} \tag{154}$$

Finally, we can employ the "tree algorithm" of Ref. [145] to implement an exact circuit for $e^{-iD_j\delta t}$ using relatively few two-qubit gates. Namely, we demand only 236 CNOT gates here for fuzzy gauge theory, as opposed to $\sim 17000$ CNOT gates entailed by simulating Horn's model of $SU(2)$ gauge theory [100] for example.

## Chapter 5: Conclusion

In summary, my thesis has aimed at formulating lattice gauge theories in finite-dimensional Hilbert spaces and designing quantum algorithms to perform the Hamiltonian time evolution of such resulting theories. First, I have outlined a general procedure for compiling a quantum circuit of the time evolution for an arbitrary Hamiltonian.

This general procedure naturally divides the quantum circuit compilation problems into two problems that can be solved independently. The first problem is that of finding the quantum circuit of a unitary operator that simultaneously diagonalizes a set of commuting Pauli strings. On the other hand, the second problem is that of finding the time evolution quantum circuit for a diagonal Hamiltonian, a much simpler problem compared to that of an arbitrary Hamiltonian.

Addressing the first problem, I have designed an algorithm to find a quantum circuit for the simultaneous diagonalization of commuting Pauli operators. The algorithm is recursive in that it proceeds one qubit after another. After a finite number of iterations (at most the number of qubits), the Pauli matrix at each qubit is either $I$ or $Z$, thus concluding the diagonalization. This recursive nature ensures a remarkably low circuit depth, the best known for this problem at the time of writing. In addition, the algorithm straightforwardly accounts for a potential limit in qubits connectivity on an arbitrary device. In particular, for quantum computers of linear connectivity, I have demonstrated that this algorithm significantly outperformed state-of-the-art literature. Furthermore, our empirical investigations reveal that the circuits generated by our algorithm maintain minimal circuit depth and a low count of two-qubit gates across a variety of Hamiltonians, including those representing random Hermitian operators and molecular systems.

For the second problem, I have developed an asymptotically optimal algorithm to generate an exact quantum circuit for an arbitrary diagonal unitary. That is, the gate count approaches the optimal result as the number of Pauli strings increases. In particular, when the number of Pauli strings is maximal, the algorithm achieves the optimal result. The

formal proof of this result was obtained by establishing a lower bound on the number of gates. For problems much below the worst-case problem, investigations showed a comparable gate count with known algorithms. To finish, the algorithm also limits the classical cost of the compilation by performing a tree traversal to efficiently process the whole Hamiltonian and compile a quantum circuit.

With the two quantum algorithms at hand, I have shifted my attention toward the second requirement – truncating the Hilbert space at each link. For a brief reminder, the Hilbert space at each link may be infinite-dimensional, and so a truncation is required to encode the theory on a quantum computer. Moreover, we require a truncation to be a valid *qubitization*. That is, the truncated theory is in the universality class of the original theory. To this end, I have described the Fuzzy gauge theory formulation, a formulation that shows evidence of a qubitization of gauge theory. In addition, I have applied this method to construct a SU(2) gauge theory with sixteen-dimensional Hilbert space at each link. Applying the general quantum circuit compilation algorithm above resulted in a low gate count. These results suggest that small simulations of Fuzzy gauge theories may be practical in the near future, and that fuzzy gauge theory may be a valid method to study gauge theories on quantum computers.

In conclusion, the quantum circuit algorithms presented in this thesis along with the fuzzy gauge theory formulation mark a significant step towards simulating gauge theory on quantum computers. What remains is to explicitly establish directly that fuzzy gauge theories constitute a qubitization of gauge theories. Importantly, due to their low quantum gate cost, establishing that they are qubitization may be done directly on a quantum computer. In addition, regarding quantum circuit constructions, an important future step is to optimize algorithms for future fault-tolerant quantum computers.

## References


[1] Sarmed A Rahman, Randy Lewis, Emanuele Mendicelli, and Sarah Powell. SU(2) lattice gauge theory on a quantum annealer. *Phys. Rev. D*, 104(3):034501, 2021.

[2] Scott Aaronson and Daniel Gottesman. Improved simulation of stabilizer circuits. *Phys. Rev. A*, 70:052328, Nov 2004.

[3] Gert Aarts. Introductory lectures on lattice qcd at nonzero baryon number. *Journal of Physics: Conference Series*, 706:022004, Apr 2016.

[4] M. Sohaib Alam, Stuart Hadfield, Henry Lamm, and Andy C. Y. Li. Primitive quantum gates for dihedral gauge theories. *Phys. Rev. D*, 105(11):114501, 2022.

[5] Andrei Alexandru, Gök çe Başar, Paulo F. Bedaque, and Neill C. Warrington. Complex paths around the sign problem. *Rev. Mod. Phys.*, 94:015006, Mar 2022.

[6] Andrei Alexandru, Gokce Basar, Paulo F. Bedaque, and Neill C. Warrington. Complex paths around the sign problem. *Rev. Mod. Phys.*, 94(1):015006, 2022.

[7] Andrei Alexandru, Paulo F. Bedaque, Ruairí Brett, and Henry Lamm. Spectrum of digitized QCD: Glueballs in a S(1080) gauge theory. *Phys. Rev. D*, 105(11):114508, 2022.

[8] Andrei Alexandru, Paulo F. Bedaque, Andrea Carosso, Michael J. Cervia, Edison M. Murairi, and Andy Sheng. Fuzzy Gauge Theory for Quantum Computers. *arXiv e-prints*, page arXiv:2308.05253, August 2023.

[9] Andrei Alexandru, Paulo F. Bedaque, Andrea Carosso, Michael J. Cervia, and Andy Sheng. Qubitization strategies for bosonic field theories. *Phys. Rev. D*, 107(3):034503, 2023.

[10] Andrei Alexandru, Paulo F. Bedaque, Andrea Carosso, and Andy Sheng. Universality of a truncated sigma-model. *Phys. Lett. B*, 832:137230, 2022.

[11] Andrei Alexandru, Paulo F. Bedaque, Siddhartha Harmalkar, Henry Lamm, Scott Lawrence, and Neill C. Warrington. Gluon field digitization for quantum computers. *Phys. Rev. D*, 100:114501, Dec 2019.

[12] Andrei Alexandru, Paulo F. Bedaque, Siddhartha Harmalkar, Henry Lamm, Scott Lawrence, and Neill C. Warrington. Gluon field digitization for quantum computers. *Phys. Rev. D*, 100:114501, Dec 2019.

[13] Andrei Alexandru, Paulo F. Bedaque, Henry Lamm, and Scott Lawrence. $\sigma$ Models on Quantum Computers. *Phys. Rev. Lett.*, 123(9):090501, 2019.

[14] Ramesh Anishetty and T. P. Sreeraj. Mass gap in the weak coupling limit of (2+1)-dimensional SU(2) lattice gauge theory. *Phys. Rev. D*, 97(7):074511, 2018.

[15] David Bailin and Alexander Love. *Introduction to Gauge Field Theory*. Routledge, January 2019.

[16] D. Banerjee, F. J. Jiang, T. Z. Olesen, P. Orland, and U. J. Wiese. From the $SU(2)$ quantum link model on the honeycomb lattice to the quantum dimer model on the kagomé lattice: Phase transition and fractionalized flux strings. *Phys. Rev. B*, 97(20):205108, 2018.

[17] Mari Carmen Banuls, Krzysztof Cichy, J. Ignacio Cirac, Karl Jansen, and Stefan Kühn. Tensor networks and their use for lattice gauge theories. In *Proceedings of The 36th Annual International Symposium on Lattice Field Theory — PoS(LATTICE2018)*. Sissa Medialab, may 2019.

[18] Michael N. Barber and John L. Richardson. Critical Behavior in Truncated Quantum O($n$) Spin Systems. *Nucl. Phys. B*, 180:248–252, 1981.

[19] Julian Bender, Erez Zohar, Alessandro Farace, and J. Ignacio Cirac. Digital quantum

simulation of lattice gauge theories in three spatial dimensions. *New J. Phys.*, 20(9):093001, 2018.

[20] Paul Benioff. The computer as a physical system: A microscopic quantum mechanical hamiltonian model of computers as represented by turing machines. *Journal of Statistical Physics*, 22(5):563–591, May 1980.

[21] Paul Benioff. The computer as a physical system: A microscopic quantum mechanical hamiltonian model of computers as represented by turing machines. *Journal of Statistical Physics*, 22(5):563–591, 1980.

[22] Ville Bergholm et al. PennyLane: Automatic differentiation of hybrid quantum-classical computations. *arXiv e-prints*, page arXiv:1811.04968, November 2018.

[23] Ethan Bernstein and Umesh Vazirani. Quantum complexity theory. *SIAM Journal on Computing*, 26(5):1411–1473, October 1997.

[24] Dominic W. Berry, Andrew M. Childs, Richard Cleve, Robin Kothari, and Rolando D. Somma. Exponential improvement in precision for simulating sparse hamiltonians. In *Proceedings of the Forty-Sixth Annual ACM Symposium on Theory of Computing*, STOC '14, page 283–292, New York, NY, USA, 2014. Association for Computing Machinery.

[25] Dominic W. Berry, Andrew M. Childs, Richard Cleve, Robin Kothari, and Rolando D. Somma. Simulating hamiltonian dynamics with a truncated taylor series. *Phys. Rev. Lett.*, 114:090502, Mar 2015.

[26] Dominic W. Berry, Andrew M. Childs, and Robin Kothari. Hamiltonian simulation with nearly optimal dependence on all parameters. In *2015 IEEE 56th Annual Symposium on Foundations of Computer Science*, pages 792–809, 2015.

[27] H. Bethe. Zur theorie der metalle. *Zeitschrift für Physik*, 71(3):205–226, 1931.

[28] Tanmoy Bhattacharya, Alexander J. Buser, Shailesh Chandrasekharan, Rajan Gupta, and Hersh Singh. Qubit regularization of asymptotic freedom. *Phys. Rev. Lett.*, 126(17):172001, 2021.

[29] Béla Bollobás. *Colouring*, pages 88–102. Springer New York, New York, NY, 1979.

[30] Joppe Bos, Leo Ducas, Eike Kiltz, T Lepoint, Vadim Lyubashevsky, John M. Schanck, Peter Schwabe, Gregor Seiler, and Damien Stehle. Crystals - kyber: A cca-secure module-lattice-based kem. In *2018 IEEE European Symposium on Security and Privacy (EuroSP)*, pages 353–367, 2018.

[31] Sergey Bravyi and Alexei Kitaev. Universal quantum computation with ideal clifford gates and noisy ancillas. *Phys. Rev. A*, 71:022316, Feb 2005.

[32] Sergey B. Bravyi and Alexei Yu. Kitaev. Fermionic Quantum Computation. *Annals Phys.*, 298:210–226, 2002.

[33] Sergey B. Bravyi and Alexei Yu. Kitaev. Fermionic quantum computation. *Annals of Physics*, 298(1):210–226, 2002.

[34] Daniel Brélaz. New methods to color the vertices of a graph. *Commun. ACM*, 22(4):251–256, apr 1979.

[35] Daniel Brélaz. New methods to color the vertices of a graph. *Commun. ACM*, 22(4):251–256, apr 1979.

[36] Jacob Bringewatt, Jonathan Kunjummen, and Niklas Mueller. Randomized measurement protocols for lattice gauge theories. *arXiv e-prints*, page arXiv:2303.15519, March 2023.

[37] R. Brower, S. Chandrasekharan, and U.-J. Wiese. Qcd as a quantum link model. *Phys. Rev. D*, 60:094502, Sep 1999.

[38] R. Brower, S. Chandrasekharan, and U. J. Wiese. QCD as a quantum link model. *Phys. Rev. D*, 60:094502, 1999.

[39] Falk Bruckmann, Karl Jansen, and Stefan Kühn. O(3) nonlinear sigma model in mml:math xmlns:mml="http://www.w3.org/1998/math/MathML" display="inline"mml:mrowmml:mn1/mml:mnmml:mo/mml:momml:mn1/mml:mn/mml:mrow/mml:math dimensions with matrix product states. *Physical Review D*, 99(7), apr 2019.

[40] Stephen S. Bullock and Igor L. Markov. Smaller Circuits for Arbitrary n-qubit Diagonal Computations. *arXiv e-prints*, pages quant–ph/0303039, March 2003.

[41] G. Burgio, R. De Pietri, H. A. Morales-Tecotl, L. F. Urrutia, and J. D. Vergara. The Basis of the physical Hilbert space of lattice gauge theories. *Nucl. Phys. B*, 566:547–561, 2000.

[42] Tim Byrnes and Yoshihisa Yamamoto. Simulating lattice gauge theories on a quantum computer. *Phys. Rev. A*, 73:022328, 2006.

[43] Sergio Caracciolo, Andrea Montanari, and Andrea Pelissetto. Asymptotically free models and discrete non-abelian groups. *Physics Letters B*, 513(1-2):223–231, jul 2001.

[44] Nicolas J. Cerf and Richard Cleve. Information theoretic interpretation of quantum error correcting codes. *Phys. Rev. A*, 56:1721, 1997.

[45] S. Chandrasekharan and U. J. Wiese. Quantum link models: A Discrete approach to gauge theories. *Nucl. Phys. B*, 492:455–474, 1997.

[46] Mitchell Chiew and Sergii Strelchuk. Discovering optimal fermion-qubit mappings through algorithmic enumeration. *Quantum*, 7:1145, October 2023.

[47] Andrew M. Childs, Yuan Su, Minh C. Tran, Nathan Wiebe, and Shuchen Zhu. Theory of trotter error with commutator scaling. *Phys. Rev. X*, 11:011020, Feb 2021.

[48] Nicos Christofides. Worst-case analysis of a new heuristic for the travelling salesman problem. Technical Report 388, Carnegie-Mellon Univ Pittsburgh Pa Management Sciences Research Group, 1976.

[49] Anthony Ciavarella, Natalie Klco, and Martin J. Savage. Trailhead for quantum simulation of su(3) yang-mills lattice gauge theory in the local multiplet basis. *Phys. Rev. D*, 103:094501, May 2021.

[50] Thomas F. Coleman and Jorge J. Moré. Estimation of sparse jacobian matrices and graph coloring blems. *SIAM Journal on Numerical Analysis*, 20(1):187–209, 1983.

[51] Thierry Coquand and Bas Spitters. A constructive proof of the peter-weyl theorem. *MLQ*, 51(4):351–359, July 2005.

[52] Marcus Cramer, Martin B. Plenio, Steven T. Flammia, Rolando Somma, David Gross, Stephen D. Bartlett, Olivier Landon-Cardinal, David Poulin, and Yi-Kai Liu. Efficient quantum state tomography. *Nature Communications*, 1(1):149, 2010.

[53] Ophelia Crawford, Barnaby van Straaten, Daochen Wang, Thomas Parks, Earl Campbell, and Stephen Brierley. Efficient quantum measurement of Pauli operators in the presence of finite sampling error. *Quantum*, 5:385, January 2021.

[54] Ophelia Crawford, Barnaby van Straaten, Daochen Wang, Thomas Parks, Earl Campbell, and Stephen Brierley. Efficient quantum measurement of Pauli operators in the presence of finite sampling error. *arXiv e-prints*, page arXiv:1908.06942, August 2019.

[55] Michael Creutz. Gauge fixing, the transfer matrix, and confinement on a lattice. *Phys. Rev. D*, 15:1128–1136, Feb 1977.

[56] Michael Creutz. *Quarks, Gluons and Lattices*. Oxford University Press, 1983.

[57] Andrew J. Daley, Immanuel Bloch, Christian Kokail, Stuart Flannigan, Natalie

Pearson, Matthias Troyer, and Peter Zoller. Practical quantum advantage in quantum simulation. *Nature*, 607(7920):667–676, 2022.

[58] Zohreh Davoudi, Indrakshi Raychowdhury, and Andrew Shaw. Search for efficient formulations for hamiltonian simulation of non-abelian lattice gauge theories. *Phys. Rev. D*, 104:074505, Oct 2021.

[59] Zohreh Davoudi, Alexander F. Shaw, and Jesse R. Stryker. General quantum algorithms for Hamiltonian simulation with applications to a non-Abelian lattice gauge theory. *Quantum*, 7:1213, December 2023.

[60] Philippe de Forcrand. Simulating qcd at finite density, 2010.

[61] Thomas DeGrand and Carleton DeTar. *Lattice Methods for Quantum Chromodynamics*. WORLD SCIENTIFIC, September 2006.

[62] D. Deutsch. Quantum theory, the Church-Turing principle and the universal quantum computer. *Proceedings of the Royal Society of London Series A*, 400(1818):97–117, July 1985.

[63] David Deutsch and Richard Jozsa. Rapid Solution of Problems by Quantum Computation. *Proceedings of the Royal Society of London Series A*, 439(1907):553–558, December 1992.

[64] Michael Douglas and Nikita Nekrasov. Noncommutative field theory. *Reviews of Modern Physics*, 73(4):977–1029, nov 2001.

[65] Stuart E. Dreyfus. An appraisal of some shortest-path algorithms. *Operations Research*, 17(3):395–412, 1969.

[66] Léo Ducas, Eike Kiltz, Tancrède Lepoint, Vadim Lyubashevsky, Peter Schwabe, Gregor Seiler, and Damien Stehlé. Crystals-dilithium: A lattice-based digital signature

scheme. *IACR Transactions on Cryptographic Hardware and Embedded Systems*, page 238–268, February 2018.

[67] Bryan Eastin and Emanuel Knill. Restrictions on transversal encoded quantum gate sets. *Phys. Rev. Lett.*, 102:110502, Mar 2009.

[68] U. Fano. Description of states in quantum mechanics by density matrix and operator techniques. *Rev. Mod. Phys.*, 29:74–93, Jan 1957.

[69] Richard P. Feynman. Simulating physics with computers. *International Journal of Theoretical Physics*, 21(6–7):467–488, June 1982.

[70] Richard P. Feynman. Simulating physics with computers. *International Journal of Theoretical Physics*, 21(6):467–488, 1982.

[71] Richard P. Feynman. Quantum mechanical computers. *Foundations of Physics*, 16(6):507–531, 1986.

[72] Pierre-Alain Fouque, Jeffrey Hoffstein, Paul Kirchner, Vadim Lyubashevsky, Thomas Pornin, Thomas Prest, Thomas Ricosset, Gregor Seiler, William Whyte, and Zhenfei Zhang. Falcon: Fast-fourier lattice-based compact signatures over ntru. 2019.

[73] Eduardo Fradkin. *Field Theories of Condensed Matter Physics*. Cambridge University Press, 2 edition, 2013.

[74] William Fulton and Joe Harris. *Representation Theory*. Springer New York, 2004.

[75] Christof Gattringer and Christian B. Lang. *Quantum Chromodynamics on the Lattice: An Introductory Presentation*. Springer Berlin Heidelberg, 2010.

[76] Christof Gattringer and Kurt Langfeld. Approaches to the sign problem in lattice field theory. *Int. J. Mod. Phys. A*, 31(22):1643007, 2016.

[77] R.V. Gavai, F. Karsch, and H. Satz. Universality in finite temperature lattice qcd. *Nuclear Physics B*, 220(2):223–236, June 1983.

[78] Pranav Gokhale, Olivia Angiuli, Yongshan Ding, Kaiwen Gui, Teague Tomesh, Martin Suchara, Margaret Martonosi, and Frederic T. Chong. Minimizing State Preparations in Variational Quantum Eigensolver by Partitioning into Commuting Families. *arXiv e-prints*, page arXiv:1907.13623, July 2019.

[79] Pranav Gokhale, Olivia Angiuli, Yongshan Ding, Kaiwen Gui, Teague Tomesh, Martin Suchara, Margaret Martonosi, and Frederic T. Chong. $o(n^3)$ measurement cost for variational quantum eigensolver on molecular hamiltonians. *IEEE Transactions on Quantum Engineering*, 1:1–24, 2020.

[80] Daniel González-Cuadra, Torsten V. Zache, Jose Carrasco, Barbara Kraus, and Peter Zoller. Hardware Efficient Quantum Simulation of Non-Abelian Gauge Theories with Qudits on Rydberg Platforms. *Phys. Rev. Lett.*, 129(16):160501, 2022.

[81] Michael T Goodrich, Roberto Tamassia, and David M Mount. *Data structures and algorithms in C++*. John Wiley & Sons, 2011.

[82] Daniel Gottesman. *Stabilizer codes and quantum error correction*. PhD thesis, California Institute of Technology, January 1997.

[83] Daniel Gottesman. The Heisenberg representation of quantum computers. In S. P. Corney, Robert Delbourgo, and Peter D. Jarvis, editors, *Proceedings of the XXII International Colloquium on Group Theoretical Methods in Physics*, pages 32–43, Cambridge, MA, 7 1998. International Press.

[84] Daniel Gottesman. An Introduction to Quantum Error Correction and Fault-Tolerant Quantum Computation. *arXiv e-prints*, page arXiv:0904.2557, April 2009.

[85] J. Greensite and S. Olejnik. Dimensional Reduction and the Yang-Mills Vacuum State in 2+1 Dimensions. *Phys. Rev. D*, 77:065003, 2008.

[86] J. P. Greensite. Calculation of the yang-mills vacuum wave functional. *Nuclear Physics B*, 158(2):469–496, 1979.

[87] Erik J. Gustafson and Henry Lamm. Toward quantum simulations of $\mathbb{Z}_2$ gauge theory without state preparation. *Phys. Rev. D*, 103(5):054507, 2021.

[88] Erik J. Gustafson and Henry Lamm. Robustness of Gauge Digitization to Quantum Noise. 1 2023.

[89] Erik J. Gustafson, Henry Lamm, and Felicity Lovelace. Primitive quantum gates for an $su(2)$ discrete subgroup: Binary octahedral. *Phys. Rev. D*, 109:054503, Mar 2024.

[90] Erik J. Gustafson, Henry Lamm, Felicity Lovelace, and Damian Musk. Primitive quantum gates for an SU(2) discrete subgroup: Binary tetrahedral. *Phys. Rev. D*, 106(11):114501, 2022.

[91] Aric A. Hagberg, Daniel A. Schult, and Pieter J. Swart. Exploring network structure, dynamics, and function using networkx. In Gaël Varoquaux, Travis Vaught, and Jarrod Millman, editors, *Proceedings of the 7th Python in Science Conference*, pages 11 – 15, Pasadena, CA USA, 2008.

[92] F. D. M. Haldane. Nonlinear field theory of large spin Heisenberg antiferromagnets. Semiclassically quantized solitons of the one-dimensional easy Axis Neel state. *Phys. Rev. Lett.*, 50:1153–1156, 1983.

[93] C.J. Hamer. Su(2) yang-mills theory in (1 + 1) dimensions: A finite-lattice approach. *Nuclear Physics B*, 195(3):503–521, 1982.

[94] Charles R. Harris, K. Jarrod Millman, Stéfan J. van der Walt, Ralf Gommers, Pauli Virtanen, David Cournapeau, Eric Wieser, Julian Taylor, Sebastian Berg, Nathaniel J.

Smith, Robert Kern, Matti Picus, Stephan Hoyer, Marten H. van Kerkwijk, Matthew Brett, Allan Haldane, Jaime Fernández del Río, Mark Wiebe, Pearu Peterson, Pierre Gérard-Marchant, Kevin Sheppard, Tyler Reddy, Warren Weckesser, Hameer Abbasi, Christoph Gohlke, and Travis E. Oliphant. Array programming with NumPy. *Nature*, 585(7825):357–362, September 2020.

[95] Tobias Hartung, Timo Jakobs, Karl Jansen, Johann Ostmeyer, and Carsten Urbach. Digitising SU(2) gauge fields and the freezing transition. *Eur. Phys. J. C*, 82(3):237, 2022.

[96] Peter Hasenfratz and Ferenc Niedermayer. Asymptotic freedom with discrete spin variables?, 2001.

[97] M. B. Hastings, D. Wecker, B. Bauer, and M. Troyer. Improving Quantum Algorithms for Quantum Chemistry. *arXiv e-prints*, page arXiv:1403.1539, March 2014.

[98] W. K. Hastings. Monte carlo sampling methods using markov chains and their applications. *Biometrika*, 57(1):97–109, April 1970.

[99] Jens Hoppe. Membranes and matrix models, 2002.

[100] D. Horn. Finite matrix models with continuous local gauge invariance. *Physics Letters B*, 100(2):149–151, 1981.

[101] Peter Høyer and Robert Špalek. Quantum fan-out is powerful. *Theory of Computing*, 1(5):81–103, 2005.

[102] Toshihide Ibaraki. Algorithms for obtaining shortest paths visiting specified nodes. *SIAM Review*, 15(2):309–317, 1973.

[103] Timo Jakobs, Marco Garofalo, Tobias Hartung, Karl Jansen, Johann Ostmeyer, Dominik Rolfes, Simone Romiti, and Carsten Urbach. Canonical momenta in digitized

su(2) lattice gauge theory: definition and free theory. *The European Physical Journal C*, 83(7), July 2023.

[104] Daniel F. V. James, Paul G. Kwiat, William J. Munro, and Andrew G. White. Measurement of qubits. *Phys. Rev. A*, 64:052312, Oct 2001.

[105] Andrew Jena, Scott Genin, and Michele Mosca. Pauli Partitioning with Respect to Gate Sets. *arXiv e-prints*, page arXiv:1907.07859, July 2019.

[106] Pascual Jordan and Eugene P. Wigner. About the Pauli exclusion principle. *Z. Phys.*, 47:631–651, 1928.

[107] Michael Karabach, Gerhard Müller, Harvey Gould, and Jan Tobochnik. Introduction to the Bethe Ansatz I. *Computer in Physics*, 11(1):36–43, 01 1997.

[108] Dimitra Karabali, V. P. Nair, and Alexandr Yelnikov. The Hamiltonian Approach to Yang-Mills (2+1): An Expansion Scheme and Corrections to String Tension. *Nucl. Phys. B*, 824:387–414, 2010.

[109] Michael Karbach, Kun Hu, and Gerhard Müller. Introduction to the Bethe Ansatz II. *Computer in Physics*, 12(6):565–573, 11 1998.

[110] Richard M. Karp. *Reducibility among Combinatorial Problems*, page 85–103. Springer US, 1972.

[111] Frithjof Karsch. Lattice qcd at finite temperature and density. *Nuclear Physics B - Proceedings Supplements*, 83–84:14–23, April 2000.

[112] Frithjof Karsch. Lattice qcd at finite temperature and density. *Nuclear Physics B - Proceedings Supplements*, 83-84:14 – 23, 2000. Proceedings of the XVIIth International Symposium on Lattice Field Theory.

[113] Phillip Kaye, Raymond Laflamme, and Michele Mosca. *An Introduction to Quantum Computing*. Oxford University Press, Inc., USA, 2007.

[114] William Kirby, Mario Motta, and Antonio Mezzacapo. Exact and efficient Lanczos method on a quantum computer. *Quantum*, 7:1018, 2023.

[115] A.Yu. Kitaev. Fault-tolerant quantum computation by anyons. *Annals of Physics*, 303(1):2–30, January 2003.

[116] Andreas Klappenecker and Pradeep Kiran Sarvepalli. On subsystem codes beating the quantum Hamming or Singleton bound. *Proceedings of the Royal Society of London Series A*, 463(2087):2887–2905, November 2007.

[117] N. Klco, E. F. Dumitrescu, A. J. McCaskey, T. D. Morris, R. C. Pooser, M. Sanz, E. Solano, P. Lougovski, and M. J. Savage. Quantum-classical computation of schwinger model dynamics using quantum computers. *Phys. Rev. A*, 98:032331, Sep 2018.

[118] Natalie Klco, Jesse R. Stryker, and Martin J. Savage. SU(2) non-Abelian gauge field theory in one dimension on digital quantum computers. *Phys. Rev. D*, 101(7):074512, 2020.

[119] Emanuel Knill and Raymond Laflamme. Theory of quantum error-correcting codes. *Phys. Rev. A*, 55:900–911, Feb 1997.

[120] Emanuel Knill, Raymond Laflamme, and Lorenza Viola. Theory of quantum error correction for general noise. *Phys. Rev. Lett.*, 84:2525–2528, Mar 2000.

[121] Robert Koenig and John A. Smolin. How to efficiently select an arbitrary Clifford group element. *J. Math. Phys.*, 55:122202, 2014.

[122] John Kogut and Leonard Susskind. Hamiltonian formulation of wilson's lattice gauge theories. *Phys. Rev. D*, 11:395–408, Jan 1975.

[123] John Kogut and Leonard Susskind. Hamiltonian formulation of wilson's lattice gauge theories. *Phys. Rev. D*, 11:395–408, Jan 1975.

[124] John B. Kogut and Mikhail A. Stephanov. *The Phases of Quantum Chromodynamics: From Confinement to Extreme Environments*. Cambridge University Press, December 2003.

[125] Michael Kreshchuk, William M. Kirby, Gary Goldstein, Hugo Beauchemin, and Peter J. Love. Quantum simulation of quantum field theory in the light-front formulation. *Phys. Rev. A*, 105:032418, Mar 2022.

[126] Henry Lamm, Scott Lawrence, and Yukari Yamauchi. General methods for digital quantum simulation of gauge theories. *Phys. Rev. D*, 100:034518, Aug 2019.

[127] Gilbert Laporte, Hélène Mercure, and Yves Norbert. Optimal tour planning with specified nodes. *RAIRO-Oper. Res.*, 18(3):203–210, 1984.

[128] Robert G. Leigh, Djordje Minic, and Alexandr Yelnikov. On the Glueball Spectrum of Pure Yang-Mills Theory in 2+1 Dimensions. *Phys. Rev. D*, 76:065018, 2007.

[129] Gushu Li, Anbang Wu, Yunong Shi, Ali Javadi-Abhari, Yufei Ding, and Yuan Xie. Paulihedral: A Generalized Block-Wise Compiler Optimization Framework For Quantum Simulation Kernels. *arXiv e-prints*, page arXiv:2109.03371, September 2021.

[130] Hanqing Liu and Shailesh Chandrasekharan. Qubit regularization and qubit embedding algebras. *Symmetry*, 14(2):305, February 2022.

[131] Hanqing Liu and Shailesh Chandrasekharan. Qubit Regularization and Qubit Embedding Algebras. *Symmetry*, 14(2):305, 2022.

[132] C. H. Llewellyn Smith and N. J. Watson. The Shifted coupled cluster method: A New Approach to Hamiltonian lattice gauge theories. *Phys. Lett. B*, 302:463–471, 1993.

[133] Seth Lloyd. Universal quantum simulators. *Science*, 273(5278):1073–1078, 1996.

[134] J. Madore. The Fuzzy sphere. *Class. Quant. Grav.*, 9:69–88, 1992.

[135] Yuri Manin. *Computable and Uncomputable (in Russian)*. Sovetskoye Radio, Moscow, 1980.

[136] A. Mariani, S. Pradhan, and E. Ercolessi. Hamiltonians and gauge-invariant hilbert space for lattice yang-mills-like theories with finite gauge group. *Phys. Rev. D*, 107:114513, Jun 2023.

[137] D. Maslov, G. W. Dueck, D. M. Miller, and C. Negrevergne. Quantum Circuit Simplification and Level Compaction. *arXiv e-prints*, pages quant–ph/0604001, March 2006.

[138] Manu Mathur. Harmonic oscillator prepotentials in SU(2) lattice gauge theory. *J. Phys. A*, 38:10015–10026, 2005.

[139] Larry D. McLerran and Benjamin Svetitsky. Quark liberation at high temperature: A monte carlo study of su(2) gauge theory. *Phys. Rev. D*, 24:450–460, Jul 1981.

[140] Adam M. Meier, Bryan Eastin, and Emanuel Knill. Magic-state distillation with the four-qubit code. *Quantum Info. Comput.*, 13(3–4):195–209, mar 2013.

[141] P. Menotti and E. Onofri. The Action of SU($N$) Lattice Gauge Theory in Terms of the Heat Kernel on the Group Manifold. *Nucl. Phys. B*, 190:288–300, 1981.

[142] Nicholas Metropolis and S. Ulam. The monte carlo method. *Journal of the American Statistical Association*, 44(247):335–341, September 1949.

[143] Daniel Miller, Laurin E. Fischer, Igor O. Sokolov, Panagiotis Kl. Barkoutsos, and Ivano Tavernelli. Hardware-Tailored Diagonalization Circuits. *arXiv e-prints*, page arXiv:2203.03646, March 2022.

[144] Edison M. Murairi and Michael J. Cervia. Reducing circuit depth with qubitwise diagonalization. *Phys. Rev. A*, 108:062414, Dec 2023.

[145] Edison M. Murairi, Michael J. Cervia, Hersh Kumar, Paulo F. Bedaque, and Andrei Alexandru. How many quantum gates do gauge theories require? *Phys. Rev. D*, 106(9):094504, 2022.

[146] Shin Muroya, Atsushi Nakamura, Chiho Nonaka, and Tetsuya Takaishi. Lattice QCD at Finite Density*): An Introductory Review. *Progress of Theoretical Physics*, 110(4):615–668, 10 2003.

[147] Michael A. Nielsen and Isaac L. Chuang. *Quantum Computation and Quantum Information: 10th Anniversary Edition*. Cambridge University Press, 2010.

[148] Michael A. Nielsen and Isaac L. Chuang. *Quantum Computation and Quantum Information: 10th Anniversary Edition*. Cambridge University Press, USA, 10th edition, 2011.

[149] Michael A. Nielsen and Isaac L. Chuang. *Quantum Computation and Quantum Information: 10th Anniversary Edition*. Cambridge University Press, June 2012.

[150] Peter Orland. Subtleties of Non-Abelian Gauge Theories in Cold-Atomic Lattices. *PoS*, LATTICE2013:330, 2014.

[151] Peter Orland and Daniel Rohrlich. Lattice Gauge Magnets: Local Isospin From Spin. *Nucl. Phys. B*, 338:647–672, 1990.

[152] Matteo Paris and Jaroslav Řeháček. *Quantum State Estimation*. Springer Berlin, Heidelberg, Hoboken, NJ, USA, 1st ed. edition, 2004.

[153] Giorgi Parisi. Symanzik's improvement program. *Nuclear Physics B*, 254:58–70, 1985.

[154] Adrian Patrascioiu and Erhard Seiler. Is the 2d o(3) nonlinear $\sigma$ model asymptotically free? *Physics Letters B*, 430(3-4):314–319, jul 1998.

[155] Alberto Peruzzo, Jarrod McClean, Peter Shadbolt, Man-Hong Yung, Xiao-Qi Zhou, Peter J. Love, Alán Aspuru-Guzik, and Jeremy L. O'Brien. A variational eigenvalue solver on a photonic quantum processor. *Nature Communications*, 5(1):4213, 2014.

[156] Michael E. Peskin. *An Introduction To Quantum Field Theory*. CRC Press, May 2018.

[157] O. Philipsen. Lattice qcd at finite temperature and density. *The European Physical Journal Special Topics*, 152(1):29–60, 2007.

[158] John Preskill. Quantum Computing in the NISQ era and beyond. *Quantum*, 2:79, August 2018.

[159] Qiskit contributors. Qiskit: An open-source framework for quantum computing, 2023.

[160] Eric M. Rains. Nonbinary quantum codes. *IEEE Trans. Info. Theor.*, 45(6):1827–1832, 1999.

[161] Indrakshi Raychowdhury. Low energy spectrum of SU(2) lattice gauge theory: An alternate proposal via loop formulation. *Eur. Phys. J. C*, 79(3):235, 2019.

[162] Indrakshi Raychowdhury. Low energy spectrum of SU(2) lattice gauge theory: An alternate proposal via loop formulation. *Eur. Phys. J. C*, 79(3):235, 2019.

[163] Indrakshi Raychowdhury and Jesse R. Stryker. Loop, String, and Hadron Dynamics in SU(2) Hamiltonian Lattice Gauge Theories. *Phys. Rev. D*, 101(11):114502, 2020.

[164] R. L. Rivest, A. Shamir, and L. Adleman. A method for obtaining digital signatures and public-key cryptosystems. *Commun. ACM*, 21(2):120–126, feb 1978.

[165] D. Robson and D. M. Webber. Gauge Covariance in Lattice Field Theories. *Z. Phys. C*, 15:199, 1982.

[166] Jun John Sakurai. *Modern quantum mechanics; rev. ed.* Addison-Wesley, Reading, MA, 1994.

[167] J. Shigemitsu and J.B. Kogut. A study of parameters and crossover phenomena in su(n)×su(n) sigma models in two dimensions. *Nuclear Physics B*, 190(2):365–411, 1981.

[168] Peter W. Shor. Polynomial time algorithms for prime factorization and discrete logarithms on a quantum computer. *SIAM J. Sci. Statist. Comput.*, 26:1484, 1997.

[169] Daniel R. Simon. On the power of quantum computation. *SIAM Journal on Computing*, 26(5):1474–1483, October 1997.

[170] Hersh Singh. Qubit regularized O(N) nonlinear sigma models. *Phys. Rev. D*, 105(11):114509, 2022.

[171] Hersh Singh and Shailesh Chandrasekharan. Qubit regularization of the $O(3)$ sigma model. *Phys. Rev. D*, 100(5):054505, 2019.

[172] Hersh Singh and Shailesh Chandrasekharan. Qubit regularization of the $O(3)$ sigma model. *Phys. Rev. D*, 100(5):054505, 2019.

[173] Masuo Suzuki. Generalized trotter's formula and systematic approximants of exponential operators and inner derivations with applications to many-body problems. *Communications in Mathematical Physics*, 51(2):183–190, 1976.

[174] Masuo Suzuki. Fractal decomposition of exponential operators with applications to many-body theories and monte carlo simulations. *Physics Letters A*, 146(6):319–323, June 1990.

[175] K. Symanzik. Continuum Limit and Improved Action in Lattice Theories. 1. Principles and $\varphi^4$ Theory. *Nucl. Phys. B*, 226:187–204, 1983.

[176] Teague Tomesh, Kaiwen Gui, Pranav Gokhale, Yunong Shi, Frederic T. Chong, Margaret Martonosi, and Martin Suchara. Optimized Quantum Program Execution Ordering to Mitigate Errors in Simulations of Quantum Systems. In *37th International Cosmic Ray Conference*, 11 IEEE, 2021.

[177] Andrew Tranter, Peter J. Love, Florian Mintert, and Peter V. Coveney. A comparison of the Bravyi-Kitaev and Jordan-Wigner transformations for the quantum simulation of quantum chemistry. *arXiv e-prints*, page arXiv:1812.02233, December 2018.

[178] Andrew Tranter, Peter J. Love, Florian Mintert, Nathan Wiebe, and Peter V. Coveney. Ordering of Trotterization: Impact on Errors in Quantum Simulation of Electronic Structure. *Entropy*, 21(12):1218, December 2019.

[179] H. F. Trotter. On the product of semi-groups of operators. *Proceedings of the American Mathematical Society*, 10(4):545–551, 1959.

[180] Matthias Troyer and Uwe-Jens Wiese. Computational complexity and fundamental limitations to fermionic quantum monte carlo simulations. *Phys. Rev. Lett.*, 94:170201, May 2005.

[181] René van Bevern and Viktoriia A. Slugina. A historical note on the 3/2-approximation algorithm for the metric traveling salesman problem. *arXiv e-prints*, page arXiv:2004.02437, April 2020.

[182] Ewout van den Berg and Kristan Temme. Circuit optimization of Hamiltonian simulation by simultaneous diagonalization of Pauli clusters. *Quantum*, 4:322, September 2020.

[183] A. Vardy. The intractability of computing the minimum distance of a code. *IEEE Transactions on Information Theory*, 43(6):1757–1766, 1997.

[184] Vladyslav Verteletskyi, Tzu-Ching Yen, and Artur F. Izmaylov. Measurement optimization in the variational quantum eigensolver using a minimum clique cover. *The Journal of Chemical Physics*, 152(12):124114, 03 2020.

[185] Ton Volgenant and Roy Jonker. On some generalizations of the travelling-salesman problem. *The Journal of the Operational Research Society*, 38(11):1073–1079, 1987.

[186] James D. Whitfield, Jacob Biamonte, and Alán Aspuru-Guzik. Simulation of electronic structure hamiltonians using quantum computers. *Molecular Physics*, 109(5):735–750, 2011.

[187] Uwe-Jens Wiese. Towards Quantum Simulating QCD. *Nucl. Phys.*, A931:246–256, 2014.

[188] Kenneth G. Wilson. The renormalization group: Critical phenomena and the kondo problem. *Rev. Mod. Phys.*, 47:773–840, Oct 1975.

[189] C. N. Yang and R. L. Mills. Conservation of isotopic spin and isotopic gauge invariance. *Phys. Rev.*, 96:191–195, Oct 1954.

[190] Torsten V. Zache, Daniel González-Cuadra, and Peter Zoller. Quantum and classical spin-network algorithms for $q$-deformed kogut-susskind gauge theories. *Phys. Rev. Lett.*, 131:171902, Oct 2023.

[191] Alexander B. Zamolodchikov and Alexei B. Zamolodchikov. Relativistic Factorized S Matrix in Two-Dimensions Having O(N) Isotopic Symmetry. *JETP Lett.*, 26:457, 1977.

[192] Erez Zohar and Michele Burrello. Formulation of lattice gauge theories for quantum simulations. *Phys. Rev. D*, 91(5):054506, 2015.

[193] Erez Zohar, J. Ignacio Cirac, and Benni Reznik. Cold-Atom Quantum Simulator for SU(2) Yang-Mills Lattice Gauge Theory. *Phys. Rev. Lett.*, 110(12):125304, 2013.

[194] Erez Zohar, J. Ignacio Cirac, and Benni Reznik. Quantum simulations of gauge theories with ultracold atoms: local gauge invariance from angular momentum conservation. *Phys. Rev.*, A88:023617, 2013.

[195] Erez Zohar, Alessandro Farace, Benni Reznik, and J. Ignacio Cirac. Digital lattice gauge theories. *Phys. Rev.*, A95(2):023604, 2017.

[196] Çetin K. Koç and Sarath N. Arachchige. A fast algorithm for gaussian elimination over gf(2) and its implementation on the gapp. *Journal of Parallel and Distributed Computing*, 13(1):118–122, 1991.